Assessing the Impacts of Urbanization-Induced Land Use and Land Cover Changes on Urban Land Surface Temperature Using Spatial Metrics: A Case of Adama City, Central Ethiopia

Ezra Arefayne Mebratu

A thesis submitted to

The department of Geomatics Engineering

School of Civil Engineering and Architecture

Presented in Partial Fulfillment of the Requirements for the degree of Master's in Geo-Informatics

Office of Graduate Studies

Adama Science and Technology University

September 2022

Adama, Ethiopia

Assessing the Impacts of Urbanization-Induced Land Use and Land Cover Changes on Urban Land Surface Temperature Using Spatial Metrics: A Case of Adama City, Central Ethiopia

Ezra Arefayne Mebratu

Advisor: Dejene Tesema (PhD)

A thesis submitted to

The department of Geomatics Engineering

School of Civil Engineering and Architecture

Presented in Partial Fulfillment of the Requirements for the degree of Master's in Geo-Informatics

Office of Graduate Studies

Adama Science and Technology University

September 2022

Adama, Ethiopia

DECLARATION

I, Ezra Arefayne Mebratu hereby declare that this Master Thesis entitled "Assessing the Impacts of Urbanization-Induced Land Use and Land Cover Changes on Urban Land Surface Temperature Using Spatial Metrics: A Case of Adama City, Central Ethiopia" is my original work. That is, it has not been submitted for the award of any academic degree, diploma, or certificate in any other university. All sources of materials that are used for this thesis have been duly acknowledged through citation.

Ezra Arefayne Mebratu	________________	________________
Name of the student	Signature	Date

RECOMMENDATION

I, the advisor of this thesis, hereby certify that I have read the revised version of the thesis entitled "Assessing the Impacts of Urbanization-Induced Land Use and Land Cover Changes on Urban Land Surface Temperature Using Spatial Metrics: A Case of Adama City, Central Ethiopia" prepared under my guidance by Ezra Arefayne Mebratu submitted in partial fulfillment of the requirements for the degree of Masters of Science in Geoinformatics. Therefore, I recommend the submission of the revised version of the thesis to the department following the applicable procedures.

Dejene Tesema (PhD)	_______________	_______________
Advisor	Signature	Date

BOARD OF EXAMINERS APPROVAL

I, the advisor of the thesis entitled "Assessing the Impacts of Urbanization-Induced Land Use and Land Cover Changes on Urban Land Surface Temperature Using Spatial Metrics: A Case of Adama City, Central Ethiopia" and developed by Ezra Arefayne Mebratu, hereby certify that the recommendation and suggestions made by the board of examiners are appropriately incorporated into the final version of the thesis.

Dejene Tesema (PhD)	______________	______________
Advisor	Signature	Date

We, the undersigned, members of the Board of Examiners of the thesis by Ezra Arefayne Mebratu have read and evaluated the thesis entitled "Assessing the Impacts of Urbanization-Induced Land Use and Land Cover Changes on Urban Land Surface Temperature Using Spatial Metrics: A Case of Adama City, Central Ethiopia" and examined the candidate during the open defense. This is, therefore, to certify that the thesis is accepted for partial fulfillment of the requirement of the degree of Master of Science in Geoinformatics.

______________________	______________	______________
Chairperson	Signature	Date
______________________	______________	______________
Internal Examiner	Signature	Date
______________________	______________	______________
External Examiner	Signature	Date

Finally, approval and acceptance of the thesis are contingent upon the submission of its final copy to the office of Postgraduate Studies (OPGS) through the Department Graduate Council (DGC) and School Graduate Committee (SGC).

______________________	______________	______________
Head of Department	Signature	Date
______________________	______________	______________
School Dean	Signature	Date
______________________	______________	______________
Office of Postgraduate Studies, Dean	Signature	Date

ACKNOWLEDGMENT

First and foremost, I would like to praise and thank God, the Almighty and Holy Mary, Mother of God who has granted me countless blessings and opportunities, so that I have finally accomplished the thesis. Aside from my efforts, the success of this thesis is heavily reliant on the encouragement and guidelines of my advisor, many thanks to my advisor Dr. Dejene Tesema, who read my numerous revisions and helped make some sense of the confusion.

I would like to express my gratitude with due respect and love to my family, for always being there for me. Last but not least, I am grateful to Adama Science and Technology University's School of Civil Engineering and Architecture, Geomatics Engineering Department, for allowing me to complete this thesis.

TABLE OF CONTENTS

CONTENTS PAGE

LIST OF TABLES

TABLE PAGE

LIST OF FIGURES

FIGURE PAGE

LIST OF ACRONYMS

ABI	Advanced baseline imager
AI	Aggregation Index
ANN	Artificial Neural Network
ASTER	Advanced Space borne Thermal Emission and Reflection Radiometer
AVHRR	Advanced Very High-Resolution Radiometer
CSA	Central Statistical Agency
DEM	Digital Elevation Model
DN	Digital Number
ED	Edge Density
ERDAS	Earth Resources Data Analysis System
ETM+	Enhanced Thematic Mapper Plus
FLAASH	Fast Line-of-sight Atmospheric Analysis of Hypercubes
FRAC_MN	Mean Fractal Dimension Index
GOES-R	Geostationary Operational Environmental Satellite
LLHM	Localized Linear Histogram Match
LP DAAC	Land Processes Distributed Active Archive Center
LSE	Land Surface emissivity
LST	Land Surface Temperature
LULC	Land-use and land-cover
MODIS	Moderate Resolution Imaging Spectroradiometer
MWA	Mono Window Algorithm
NASA	National Aeronautics and Space Administration

NDBAI	Normalized Difference Bareness Index
NDVI	Normalized difference Vegetation index
NDVI	Normalized Difference Vegetation Index
NDWI	Normalized difference Water Index
NMA	National Meteorology Agency
NOAA	National Oceanic and Atmospheric Administration
OLI	Operational Land Imagery
PD	Patch Density
PLAND	Percentage of landscape
RMSE	Root-mean-square error
ROI	Region of interest
SLC	Scan Line Corrector
SLSTR	Sea and Land Surface Temperature Radiometer
STD	Standard deviation
SVM	Support Vector Machine
UHI	Urban Heat Island
USGS	United States Geological Survey

ABSTRACT

Changes in land use and land cover (LULC) as a result of urbanization have a substantial effect on local and regional climate. Understanding the interaction between the urbanization process and patterns of land surface temperature (LST) at both temporal and spatial scales is crucial for formulating strategies for the potential effects, but little is understood in the context of Ethiopian urban centers. The aim of this study is to examine the spatiotemporal variations in LST attributed to LULC changes due to urbanization between 1990 and 2020 in Adama City, a rapidly growing urban area. Through supervised classification using the support vector machine algorithm, decadal-scale LULC maps of the study area were prepared, and the spatiotemporal changes of LULC were investigated. Spatial metrics were utilized to analyze the dynamics of the landscape patterns. LST was extracted from the Landsat thermal band using emissivity corrected Inverted Planks Equation, and its changes over time were examined. Regression analysis was used to explore the relationship between the changes in LST and the dynamics of built-up areas and vegetation patterns. The findings show that the built-up area has undergone about 23% expansion annually in the past three decades. Furthermore, as evidenced by changes in the number of patches at the landscape level from 3248 in 1990 to 4807 in 2020, the landscape pattern structure became more fragmented. Percentage of Landscape (PLAND), Number of Patch (NP), and Patch Density (PD) of the built-up area have increased, indicating growing urbanization and aggregation with economic growth. In addition, barren land is characterized by the highest temperature followed by built-up areas, and the spatial pattern of the mean LST declined as one moved from the city center to the fringes. Moreover, the temporal changes in LST were directly correlated with the normalized difference built-up index and negatively correlated with the normalized difference vegetation index and vegetation land cover configuration. This research would assist planners in developing an effective land use plan to manage the effects of urbanization on LST, thereby supporting efforts to ensure the sustainable development of urban areas.

Keywords: Adama City, LULC change, NDVI, NDBI, LST, urbanization, Landscape Pattern

CHAPTER 1: INTRODUCTION

1.1. Background of the study

Urbanization is a phenomenon that is of major concern in both developing and developed countries. Uncontrolled urbanization leads to formal and informal settlements, industrialization, improvement of transport networks and economic growth. One of the major consequences of urbanization is the transformation of land surfaces from rural/natural environments to built-up land that supports diverse forms of human activity. These transformations impact the local geology, climate, hydrology, flora and fauna and human-life supporting ecosystem services in the region. Mapping and analysis of land use/land cover change in urban regions and tracking their environmental impact is therefore of vital importance for evaluating policy options for future growth and promoting sustainable urban development. Analyzing the dynamics of urban land-use pattern to abstract spatial process of urbanization is an important step towards the construction of spatial model in order to simulate urban land-use pattern of the past, more importantly, forecast the future condition. Spatial metrics provide good links between urban land-use pattern and process. (Magidi & Ahmed, 2019; Furberg, 2014; Yaolong & Murayama, 2006)

Land use and land cover change (LULCC) is a general term for the human modification of Earth’s terrestrial surface. These modifications come by direct and indirect activities of human actions when securing essential resources. Therefore, it is necessary to analyze these land changes for the best management of natural resources and to ensure better livelihood of the inhabitants, it is one of the challenges that aggravate environmental problems. Understanding the scope of land use change, driving forces, and consequences is very crucial. (Kullo et al., 2021; Bufebo & Elias, 2020)

Accurate information on the rate of land use pattern changes is essential for the sustainable development and management of natural resources. Land use and land cover change is driven by human actions and also drives changes that limit availability of products and services for human and livestock, and it can undermine environmental health as well. In Ethiopia, Africa, the rapid variations of LULC observed in the last decades are mainly due to population pressure, resettlement programs, climate change, and other human- and nature-induced driving forces. Anthropogenic activities are the most significant factors adversely changing the natural status of the landscape and resources, which exerts unfavorable and adverse impacts on the environment and livelihood (Regasa et al., 2021).

Impervious surfaces in urban areas will not only absorb and accumulate more solar radiation and heat but also impede long-wave sky radiation loss (Oke, 1988; RIZWAN et al., 2008) which will cause the phenomenon defined as the Urban Heat Island (UHI) effect, where atmospheric and land surface temperatures (LST) in urban areas are higher than in surrounding rural areas Different urban structures such as, buildings, concrete, asphalt and industrial activity of urban areas causes the urban heat island (Dousset & Gourmelon, 2003; L. Liu & Zhang, 2011). A number of previous studies tell that most of the earth's surface is already modified, except those areas that are peripheral in location or are fairly inaccessible. Therefore, for cities that grow at alarming rate, sustainable urban planning and development play key roles in mitigating urban heat island effects and ensure the quality of urban environment (Meyer & Turner, 1992).

changes in the land use and land cover of urban have effects on the microclimatic variable this will contribute to the decreasing property of surface reflective power, increasing of stream flow and evapotranspiration and disturbance of hydrological process. In general, from the above scholars' study one can understand when the natural land cover is replaced by pavement that takes away the natural cooling effect the surrounding land surface temperature and the airflow could be affected. This is due to building materials thermal properties, urban design geometry, and anthropogenic factors, existing land-use/land-cover and altitudes are some of the factors that contribute to UHI phenomenon. Building materials reflectance is low so they reflect less and absorb more energy, which lead to temperature increase at surface level.

Revealing the driving mechanism behind urban land use change facilitates deeper insight into the human and biophysical effects in the urbanization process and thereby supports the sustainable urban development. It has been determined that spatial metrics can have very good results in determining urban growth patterns and landscape change dynamics. (H. Wu et al., 2021; GORMUS et al., 2021)

1.2 Statement of the Problem

Urbanization induced Land use land cover change (Built-up expansion) have an impact on human health each of us requires a stable urban environment in which to live and work, as well as clean air to breathe, we also require access to open areas where we can play, exercise, and maintain mental clarity. These and other public goods connected to health are under threat from rapid urbanization. Adama City is one of Ethiopia's cities that is rapidly urbanizing, but this speedily built-up development makes the city vulnerable to issues with rising and fluctuating in land surface temperatures between urban and suburban areas. this temperature increase has an impact on energy use, air quality, and health of city residents in order to achieve sustainable and environmentally friendly city growth in Adama The factors that contribute to the increase in surface temperature in the urban areas and emergence of urban heat islands should receive primary attention.

As stated by United state environmental protection Agency (USEPA). The primary factor in urban settings that increases surface temperature is the reduction of natural landscapes, urban material properties, and land cover geometry. few studies in Ethiopia have attempted to address potential impact of land cover configuration on LST (Keno et al., 2020) however most prior studies in Ethiopia (Abel, 2018; Kidanewald, 2018; G/Michael, 2021) has only focused on presenting the synchronized correlation between built up expansion and LST. And the opposing association between NDVI and NDWI with LST this signifies the impact of compositional land cover changes on LST were the primary focus of earlier studies. However, in addition to compositional change, the geometry and Fragmentation of the land cover also have an impact on the thermal climate of the urban landscape. Moreover, the goal of prior studies (Belete Tafesse and Suryabhagavan, 2019; Moisa et al., 2021) in Adama City was to solely give information on the effects of urbanization-related changes in land use and land cover composition on land surface temperature. Thus, due to a lack of studies regarding the impact of land cover configuration on LST. Adama City is less able to lower the rise in land surface temperature in urban areas as a result of a change in land cover configuration.

The purpose of this study was to assess Adama City's Multidirectional and Multitemporal LST profile and statistically ascertain how built-up dynamics and vegetation land cover configuration affect land surface temperature in Adama City. In earlier studies, there is enough evidence to confirm that land cover fragmentation and shape have an impact on land surface temperature. However, more research is needed to demonstrate how vegetation land cover configuration affects the thermal climate of adama city.

1.3 Objectives

1.3.1 General objective

The general objective of this study is to analyze the impacts of urbanization-induced land use land cover change on spatiotemporal distribution of land surface temperature in Adama City.

1.3.2 Specific objectives

- To analyze the changes in land use land cover in the study area from 1990 to 2020
- To examine the dynamics of landscape structure in the study area from 1990 to 2020
- To assess spatiotemporal variations of LST in the study area from 1990 to 2020
- To ascertain the relationship of LST with the patterns of vegetation and built-up land cover dynamics in the study area from 1990 to 2020.

1.4 Research questions

1. How has the land cover in Adama City changed between 1990 and 2020?
2. What changes occurred in Adama City's landscape structure between 1990 and 2020?
3. How has Adama City's Multidirectional and Multitemporal LST profile changed between 1990 and 2020?
4. What effect does the configuration of vegetation land cover and built-up dynamics have on LST?

1.5 Significance of the study

Cities' urbanization causes a slew of obstacles including overcrowding, garbage disposal issues, a lack of green space, air pollution, and excessive energy usage, all of which contribute to global warming. In this study impact of urbanization-induced land use land cover dynamics and vegetation cover spatial pattern on land surface temperature, as well as multidirectional and multitemporal LST profiles of Adama city, is examined. The study will be used by Adama City municipality, land use planning and land administration officials as a working document to depict the trend of fast urbanization and to plan remedies for the city's continued rise in land surface temperature through optimal land cover composition and vegetation cover configurations. Furthermore, the approaches and procedures employed in this study will be used as a reference material for anybody or individual interested in further studying the impact of land cove spatial pattern on land surface temperature.

1.6 Scope of the study

This study's geographic focus was within Adama City Administrative Boundary in the Oromia Regional State, the contextual scope on the other hand looked at how LULC composition and configuration patterns have changed over the study period (1990 to 2020), notably concerning Vegetation land cover configuration, and assessed the multidirectional and multitemporal LST profile of Adama city moreover, assessed impact of vegetation land cover configuration and built-up dynamics on Land surface temperature in Adama city.

1.7 Limitation of the study

The data for this study was collected, processed, interpreted, and analyzed in an effort to obtain all the essential information. However, there have been certain limitations on the thesis work one of the difficulties in the study's Land surface temperature inversion is correction for atmospheric error of Landsat thermal band, and lack of time series satellite LST product to validate the 1990 Landsat retrieved LST, However, to help with the solution of this issue, On the research region, it is assumed that the atmosphere is uniform and in suite LST for 1990 collected from weather station is used for validation. Another limitation of the study was the lack of cloud-free wet season Landsat imageries and the time-consuming process required to obtain data from several governmental agencies.

1.8 Organization of the Study

The study has organized in to five chapters. The first chapter contains brief description of introduction, the second chapter deals with literature review and addresses the relevant literature that was associated with the study, the third chapter has described the materials and methods, the fourth chapter was concerned with results and discussion of the study finally, the fifth chapter covers the conclusion and recommendations.

CHAPTER 2: LITERATURE REVIEW

2.1 Urbanization

Urbanization is the process of growth in a country’s urban population accompanied with an increasing importance of the cities relative to rural areas across the economic, political, and cultural aspects. The process comprises aspects of urbanization itself and urban concentration or the degree of urban resource concentration in one or two cities (Davis & Vernon Henderson, 2003). According to United Nations (UN) world population prospect 2018 more than half of the world’s population now live in urban areas (4.3 billion) increasingly in highly-dense cities. However, urban settings are a relatively new phenomenon in human history this transition has transformed the way we live, work, travel and build networks.

Africa's rate of urbanization and urban population growth has substantially changed across the whole continent as well as within its various regions, says a recent report by the Organization for Economic Co-operation and Development (OECD, 2020). According to the report (OECD, 2020), Africa is one of the least urbanized regions of the globe, and its urbanization pace will continue to be among the quickest in the world in the future years. Indeed, the urban population of Africa in 1950 was 27 million people, a tiny fraction of today's urban population of about 567 million people notably, the (OECD) report contends that since 1990, Africa's fast urbanization has been driven mostly by high population growth and the reclassification of rural settlements, it also estimates that Africa's population will double between now and 2050, with urban areas absorbing two-thirds of the increase.

2.1.1 Urbanization in Ethiopia

Ethiopia, has a very low level of urbanization, even by African standards 21.2% in 2019, is among the least urbanized but fast urbanizing countries in sub-Saharan Africa (Gebrekristos Mezgebo, 2021). Urbanization in Ethiopia has been growing at a rate of 4.5%, faster than 4% of Sub-Saharan Africa, (World Bank, 2016) and is expected to urbanize at rate of 5.4% (World Bank, 2015). The rapid increase in urban populations has meant that peri-urban areas are growing much more quickly than formal urban centers. Peri-urban areas are those areas immediately around a city. They are areas in transition from countryside to city (rural to urban), often with undeveloped infrastructure, where health and sanitation services are under pressure and where the natural environment is at risk of degradation.

Ethiopia's rapid urbanization has been accompanied with gradual structural transformation. Agriculture remains the largest employment, employing over 69% of the labor force in 2019 (Gebrekristos Mezgebo, 2021) despite its declining contribution to Gross domestic product (GDP), the low level of employment in industry (about 10%) shows that urbanization is most likely related to the rise of consuming cities and has minimal positive externalities in terms of job creation and productive investments.

2.2 Urban heat island

Urban heat islands are urbanized areas that experience higher temperatures than outlying areas. Structures such as buildings, roads, and other infrastructure absorb and re-emit the sun's heat more than natural landscapes such as forests and water bodies. Urban areas, where these structures are highly concentrated and greenery is limited, become "islands" of higher temperatures relative to outlying areas (Yang et al., 2016) in all of its manifestations, urban heat island is a ubiquitous outcome of urbanization, as the vegetation is replaced with the built-up area during urban development. This process leads to changes in the physical properties of the surface structure which modifies the thermal environment of urban areas.

Heat islands can be categorized into two groups: atmospheric and surface-based since they can both be found in the air and on the ground. Surface UHIs are characterized as situations where the surface temperature of an urban region is higher than that of nearby rural areas. Atmospheric temperatures in metropolitan areas that are greater than those in neighboring rural areas are known as atmospheric urban heat islands. Again, there are two distinct types of atmospheric UHI: canopy layer UHI and boundary layer UHI. (Voogt & Oke, 2003). CL-UHI is based on the near-surface air temperature measured below roof height and is typically presented as a temperature difference between the air within the UCL and that measured in a rural area outside the settlement, Boundary layer urban heat islands are those that begin on roofs and in the tops of trees and continue upward until the atmosphere is no longer influenced by urban landscapes. The normal distance from the surface of this region is no more than one mile.

Anthropogenic activities that generate heat from different sources, such as traffic, residential structures, industries, and densely built mass buildings, exacerbate the UHI impact. As a result, the increasing trend of UHI and its effects are being paid attention to in many studies of urban climatology. (Yuan & Bauer, 2007)

Magee et al., (1999) used data from two stations and determined that the UHI in Fairbanks, Alaska, grew by 0.4°C in annual mean value, over the 49-year period 1949-1997, whereas winter months experienced a more significant increase of 1.0°C due to surface inversions which are frequent during this season of the year. It is pointed out that the Fairbanks station moved twice and used three different types of thermometers during the measurement period.

(J. X. L. Wang & Gaffen, 2001) used surface observations (hourly data) from 196 stations in China for 30-year period (1961-1990). They argued that the highest temperature was in southeastern China, where the monsoon system dominated. Surface temperature increased during this 30-year period, with stronger trends in nighttime and in winter. Interestingly, an analysis of a map by Portman revealed that 38% of the rural stations were within 15 km of the Yellow Sea and 63% of them within 50 km, while only 19% and 29%, respectively, of the urban stations were that close

Winkler et al., (1981) analyzed spatially the UHI in Minneapolis-St. Paul, Minnesota, in Midwest USA, using 10 years of data (1967-1976), both unadjusted and adjusted, from 21 stations in an area of 18000 km2. According to their research, the mean annual urban-rural difference was 0.5°C (unadjusted data) and 1.0°C (adjusted data). They proceeded on time of observation and latitude adjustment. Todhunter, (1996) also investigated the Minneapolis-St. Paul mean UHII from 1950-1990 and found it to be 2.1°C, as determined by data of a local National Weather Service (NWS) forecast office, a university station, a cooperative network stations and 13 weather stations (26 stations in total) with the greatest difference in elevation be-tween two stations being equal to 119 m.

According to various research, vegetation helps to lessen the impact of UHI. Result from study on parks' effectiveness at reducing the urban heat island effect in Addis Abeba, planting trees in urban areas has a considerable cooling effect. It's crucial to examine how changes in land use and land cover affect the urban heat island, which deteriorates daily due to a variety of factors, including natural ones like climate variability or climate change, which can result in floods and droughts, or anthropogenic ones like industrialization and urbanization, among many others.

2.3 Land use land cover change

Land cover changes are a conversion of land cover from one category to another and modification of the conditions within a category. Whereas land-use change occurs when land experts decide that an alteration to another land utilization category is desirable (Patel et al., 2019) The understanding of land-use/land-cover change has moved from simplicity to realism and complexity over the last decades. In the beginning, the studies were concerned mostly with the physical aspect of the change, but later, in the research agenda on global environmental change. Scientists realized that land surface processes influence climate because of the land use/cover change. In mid1970s, it was recognized that land cover change modifies surface albedo and thus surface atmosphere energy exchanges, which have an impact on regional climate.(Otterman, 1974; Charney et al., 1977; Sagan et al., 1979). Much broader range of impacts of land-use/cover change on ecosystem, goods and services were further identified. Of primary concern are impacts on biotic diversity worldwide (Sala et al., 2001), soil degradation (Stanley et al., 2015) and the ability of biological systems to support human needs (Vitousek et al., 1997);

Human populations and their use of land have transformed most of the terrestrial biosphere into anthropogenic biomes. Such transformation has caused a variety of new ecological patterns and processes to emerge and has been significant for more than 8000 years (Ellis, 2011). Recently, issues related to LULC change have gained interest among a wide variety of researchers, ranging from those who favor modeling spatiotemporal patterns of land conversion to those who try to understand the causes, impacts and consequences. Land use affects land cover and changes in land cover affect land use. A change in either however is not necessarily the result of the other. Changes in land cover by land use do not necessarily imply degradation of the land. However, many shifting lands use patterns driven by a variety of social causes, result in land cover changes. These changes affects biodiversity, water and radiation budgets and other processes that come together to affect climate and biosphere (Riebsame et al., 1994)

Human activities which are mainly driven by socio-economic factors bring out changes in non-built-up and built-up land despite restrictions by physical conditions. Land use change, including land transformation from one type to another and land cover modification through land use management, has altered a large proportion of the earth’s land surface. The aim is to satisfy mankind’s immediate demands from natural resources (Patel et al., 2019). The worldwide changes to forests, farmlands and waterways are being driven by the need to provide food, fiber, water, and shelter to more than six billion people. Global croplands, pastures, plantations and urban areas have expanded in recent decades. This expansion is accompanied by large increases in energy, water, and fertilizer consumption, along with considerable losses of biodiversity(Foley et al., 2005)

More recent changes in land use have been dominated by losses of agricultural land. Similar to the rest of the world, East Africa is not an exception to these land use land cover change in particular, very rapid changes are clearly recognizable in Ethiopia (Regasa et al., 2021) due to the population pressure, resettlement programs, climate change, and other human and nature-induced driving forces. Similar to other countries, anthropogenic activities are the most significant factors adversely changing the natural status of the Ethiopian landscape. (Regasa et al., 2021) In the past decade in Ethiopian lands changed from natural to agricultural land use, waterbody, commercial farmland, and built-up/settlement. Some parts of forest land, grazing land, swamp/wetland, shrubland, rangeland, and bare/ rock out cropland cover class changed to other LULC class types, mainly as a consequence of the increasing anthropogenic pressure.

Abdul Athick & Shankar, (2019) in the study in adama woreda revealed interesting aspect that build up, dense vegetation and sparse vegetation increased in area of approximately 160%, 30% and 78% respectively at the expense of barren land which decreased at 8.5%, but there is not much change in the water bodies.

Different land use changes may affect one another. Most of the ecological consequences of land use change reflect interactive effects under different land use changes. For example, deforestation has led to the degradation of freshwater and exchange of earth energy balance which leads to the siltation of Global warming as a result of interactive effects of different land use along their change trajectories represent a challenge for a better understanding of the land use change issue. Changes in land and ecosystems and their implications for global environmental change and sustainability are a research challenge for the human environmental sciences.

2.4 The Driving forces of Land use and Land cover Change

Land use and land cover changes are influenced by different factors related to human population growth, economic development, and technology changes. Human-induced (Anthropogenic) factors are the major driving forces of land use and land cover changes (G. Shi et al., 2018) even though there is also a contribution from the natural processes. Nowadays, the human-related causes of LULC changes are very serious (Agarwal et al., 2002). There are several types of anthropogenic problems for LULC changes. Urban expansion due to rapid population growth is one factor for LULC change subsequently it brings a dramatic change of landscape patterns and types. These changes have been changing the availability of different biophysical resources and lead to decreased availability of different products and services for humans, livestock, and damage to the environment. Therefore, urban expansion in and around urban areas has great impacts on the environment. For example, it causes an increase in the temperature of urban areas (Xie & Zhou, 2015)

Land cover can be altered by forces other than anthropogenic. For instance, Natural events such as weather, flooding, fire, climate fluctuations and ecosystem changes may also initiate modifications upon land cover. There are also incidental impacts on land cover from other human activities such as forest and lakes damaged by acid rain from fossil fuel combustion and crops near cities damaged by tropospheric ozone resulting from automobile exhaust (Kuemmerle et al., 2009) observed the conversion of cropland to grassland in Arges¸ County in Romania which he related to the rapid changes in socio-economic, demographic and institutional conditions after 1989, According to USEPA, (2004) the general causes of LULC changes are:

- Natural procedures, such as climate and atmospheric variations, wildfire, and pest infestation.
- The direct effect of human activity such as road and illegal house construction and deforestation.
- An indirect effect of human activity such as water diversion leading to the lowering of the water table and contamination of groundwater.

2.5 Types of land use land cover change

When quantifying variation in land use and land cover across the landscape, pattern can arise from variation in composition and/or in configuration (Gustafson, 1998). composition focus on questions regarding “how much” and “what variety” (Fahrig, 2001). In contrast, configuration focuses on questions of “where” and “under what context” (Lookingbill et al., 2010). Composition emphasizes the amount and variety of different land-use or land-cover types, without explicit consideration of land-use or land-cover arrangement. In contrast, configuration focuses on the arrangement and/or position of land uses or land covers across landscapes. changing the composition of land uses may alter Land cover abundance. In contrast, altering the configuration leads to change in structure of Land cover.

Distinguishing the effects of landscape composition versus configuration is highly relevant to many problems in Ecosystem. Based on this distinction, change in Land cover composition focuses on changes in the amount and verity of land cover types in the landscapes, whereas change in Land cove Configuration focuses on changes in the structure and fragmentation of the landscape (Fahrig, 2003). Understanding the role of compositional versus configurational in this way is essential for promoting Environmental sustainability.

2.6 Supervised image Classification algorithms

Supervised image classification is a classification method in which a user selects sample pixels in an image that are representative of specific classes and then instructs the image processing software to utilize these training sites as references for the categorization of all other pixels in the picture. It is well established that the selection of a suitable classifier is essential for improved classification accuracies (Lu and Weng, 2007). A number Supervised classification Classifier/Algorithms have been developed in the past decades some of them are parallelepiped, minimum distance, maximum likelihood, non-parametric classifiers and machine learning techniques as decision tree method, support vector machine and Artificial neural networks.

2.6.1 Parallelepiped classifiers algorithm

Parallelepiped classification is a simple classification based on a decision rule for multispectral data (Perumal & Bhaskaran, 2010). Decision boundaries for the parallelepiped algorithm are formed based on a standard deviation threshold which is chosen from the mean of each selected class in the training set. The decision boundaries form an interval between two-pixel values with a hyper rectangle region in feature space. A pixel is classified based on whether the value of that pixel lies above the lower threshold value and below the higher threshold value of the interval. Merits of Parallelepiped classifiers is uses simple decision rule to classify Multispectral data which makes computational efficient and fast for executions. however, misclassify a pixel (if the digital value of the pixel lies inside the parallelepiped decision boundaries.). also, Pixels will be not classified if the digital value of the pixel is not lie inside the parallelepiped decision boundaries

2.6.2 Minimum distance classifiers algorithm

This is also a simple supervised classifier which uses the center point (average of all pixels of sample class) to represent a class in training set. This technique uses the distance measure, where the Euclidean distance is considered between the pixel values and the centroid value of the sample class (Abbas & Jaber, 2020) The pixel with the shortest distance with the class is assigned with that class. The classifier is fast in execution, computation time is minimum as it depends mainly on the training dataset and all pixels will be classified, but the algorithm may be prone to errors resulting in misclassification of pixels as it will classify a pixel even if the shortest distance is far away. Spectral distance is calculated for all values of a class mean; the unclassified pixel is assigned to the class with the lowest spectral distance resulting in classification of all pixels.

2.6.3 Maximum Likelihood classifiers algorithm

This method of classification calculates the probability for a given pixel to each class and then the pixel will be allocated to a particular class with the highest probability (Otukei & Blaschke, 2010) It calculates the mean and covariance matrix for the training samples and assumes that the pixel values are normally distributed. A class can be characterized by the mean value and the covariance matrix. A probability density function is defined and the input pixels are mapped based on the likelihood that the pixel belongs to that particular class. This classifier is a sophisticated classifier with good separation of classes, but the training set should be strong to sufficiently describe mean and covariance structure. Also, the algorithm is computationally intensive

2.6.4 Decision Tree classifiers algorithm

In this method of classification, a tree structure is built with root node and leaf nodes. The leaf nodes represent the classes of the features. Every interior node in the tree consists of a decision criterion. The attributes are partitioned based on spectral characteristics. The partition takes place based on the homogeneity (similarity of pixel values) until a leaf node is assigned with a particular class (Otukei & Blaschke, 2010). A group of pixel values will be classified into two groups based on the separability with respect to a feature. This method uses the hierarchical rule and use non-Parametric approach. This method does not require any extensive design or training. Computational efficiency is good but requires complex calculations and the accuracy may depend fully on the design and selection of features

2.6.5 Support Vector Machines classifiers algorithm

SVM classifier is based on decision planes that define decision boundaries. It builds a hyperplane from the training data which separates pixels with different class membership (Otukei & Blaschke, 2010). The hyperplane gives the largest minimum distance to the training samples. Larger the margin, lower will be the generalization error. The method gives a good separation achieved by the hyperplane. Here the computational complexity is reduced also can be used with small training datasets and high-dimensional data (Pal & Mather, 2005) but training is time consuming as selection of optimum hyperplane is necessary for improved classification.

2.6.6 Artificial Neural Network classifiers algorithm

The algorithms with artificial neural network approach simulate the human learning process for assigning meaningful labels to images. ANN imitates few functions of a person's mind (Mahmon & Ya'acob, 2014). It consists of a sequence of layers with a set of neurons in each layer and the preceding and succeeding layers are joined by weighted connections. The accuracy and performance of artificial neural network highly depend on the network structure (Kaur, 2015). ANN networks are data driven and self-adaptive technique. The computation rate is high and handles noisy input. But ANN training is time taking and the network type architecture is difficult to choose.

2.7 Land cover spectral indices

Spectral indices are combinations of the pixel values from two or more spectral bands in a multispectral image to obtain considerable evidence (Prasad et al., 2022) Spectral indices are designed to highlight pixels showing the relative abundance or lack of a land-cover type of interest in an image. the most common mathematical formulas that are used in spectral indices are the normalized difference.

2.7.1 Normalized difference vegetation index (NDVI)

NDVI is a dimensionless index that describes the difference between visible and near-infrared reflectance of vegetation cover and can be used to estimate the density of green on an area of land (Weier, J. and Herring, 2000). In the simplest terms possible, the Normalized Difference Vegetation Index (NDVI) measures the greenness and the density of the vegetation captured in a satellite image. It drives from NIR and Read infrared and the value lies between -1 and 1. Higher NDVI value indicate healthiness of vegetation and how dense is the vegetation where negative values are mainly formed from clouds, water and snow and values close to zero are primarily formed from rocks and bare soil   Vegetation coverage is one of the most important indicators of a regional ecological situation. Vegetation growth conditions determine the land surface temperature of a specific area because high NDVI value indicates low land surface temperature (LST) by the latent heat flux from the surface to atmosphere via evapotranspiration. Lower LSTs usually are found in areas with high NDVI (Y. Liu et al., 2015). NDVI value and LST have an inverse relationship as shown in different studies. findings forward that there is need to be greenery area or urban vegetation cover in order to maintain urban climate, minimize urban heat island (UHI) effect and sustain of the urban ecosystem (Faqe Ibrahim, 2017)

2.7.2 Normalized difference Built-up index (NDBI)

The Normalized Difference Built-up Index (NDBI) is another vital urban climate indicator for environmental monitoring this serves as an effective method of mapping and analyzing land-uses by providing information on the spatial extent of built-up areas and impervious surfaces (Zha et al., 2003). NDBI uses the NIR and SWIR bands to emphasize manufactured built-up areas with values ranging from positive 1 to negative 1. The negative values often signify vegetation, while the positive denotes built-up urban/impervious surfaces.

2.7.3 Normalized difference Water Index (NDWI)

The Normalized Difference Water Index (NDWI) is a satellite-derived index from the Near-Infrared (NIR) and Short-Wave Infrared (SWIR) channels. It refers to one of at least two remote sensing-derived indexes related to liquid water one is used to monitor changes in water content of leaves using near-infrared (NIR) and short-wave infrared (SWIR) wavelengths, proposed by (Gao, 1996) and another one is used to monitor changes related to water content in water bodies, using green and NIR wavelengths, defined by (McFEETERS, 1996). NDWI concept as formulated by Gao combining reflectance of NIR and SWIR is more common and has wider range of application. It can be used for exploring water content at single leaf level. The SWIR reflectance reflects changes in both the vegetation water content and the spongy mesophyll structure in vegetation canopies, while the NIR reflectance is affected by leaf internal structure and leaf dry matter content but not by water content. The combination of the NIR with the SWIR removes variations induced by leaf internal structure and leaf dry matter content, improving the accuracy in retrieving the vegetation water content (Ceccato et al., 2001).

2.7.4 Normalized Difference Bareness Index (NDBAI)

A normalized difference bareness index (NDBAI) was proposed by (X. L. Chen et al., 2006) to distinguish bare land from other land use classes using Landsat data. This index is based on higher radiation of bare soil on the thermal band. NDBAI was an option to monitor bare soil, land conversion, impervious surface, and its relation to surface temperature (H.-M. Zhao & Chen, 2005) the value of NDBAI ranges between −1 and +1. Generally, the positive value of NDBAI indicates the bare land. The bareness increases with the increase of the positive NDBAI.

2.8 Land surface temperature

LST is a measure of how hot land surface at a particular location and it define as the skin temperature of the surface.(Latif, 2014) It is an essential factor in many areas like global climate change studies, urban land use/land cover and geo-/biophysical.(Jeevalakshmi et al., 2017). it derives from thermal band which is located in the thermal infrared region in Landsat (TM) Thermal Infrared (TIR) band 6 and Landsat 8 thermal infrared (TIR) band 10 and 11. LST is a mixture of vegetation and bare soil temperatures. This quality makes LST a good indicator of energy partitioning at the land surface–atmosphere boundary and sensitive to changing surface conditions (Z. L. Li & Duan, 2018). the knowledge LST provides on the redistribution of energy into latent and sensible heat fluxes makes it one of the most important parameters in the physical processes of surface energy and water balances (Teskey et al., 2014). Its retrieval from remotely sensed thermal infrared (TIR) data provides spatially continuous LST measurements with global coverage to examine the thermal heterogeneity of the earth's surface and the impact on surface temperatures resulting from natural and human-induced changes (Y. Liu et al., 2015). LST is a basic determinant of the terrestrial thermal behavior, as it controls the effective radiating temperature of the earth's surface.

2.9 Land surface temperature retrieval methods and Algorithms

Many LST retrieval algorithms based on remotely sensed images have been introduced so far to enable the extraction of LST from Visible, Near Infrared (VNIR) and TIR imagery (Jiménez-Muñoz & Sobrino, 2010) These algorithms can be categorized in two main groups: algorithms based on one thermal channel (single channel algorithms) and algorithms based on more than one TIR channel (split window algorithms). Accurate LST retrieval from TIR data depends on atmospheric effects, sensor parameters, spectral range, viewing angle, and surface parameters such as emissivity and geometry (Sattari & Hashim, 2014; Dash et al., 2001). Whereas emissivity and atmospheric effects are two fundamental factors to derive LST from thermal data.

2.9.1 Inverted plank equation

The Planck Function is used frequently to compute the radiance emitted from objects that radiate like a perfect “Black Body”. The inverse of the Planck Function is used to find the “brightness temperature” of an object whose emitted radiance has been measured. The Planck function is used to compute the intensity of the thermal radiation. It is a function that shows the amount of thermal electromagnetic radiation which can be emitted by a blackbody under thermal equilibrium conditions at a known temperature. With the LSE of an area known, the LST of an area can be estimated through the inversion of the Planck function. The brightness temperature recorded by a sensor in space is calculated under the assumption that the land surface is a black body, i.e., an object with an emissivity of 1 however perfectly black body is ideal object. Therefore, non-black body will emit less that the Planck Function predicts. The Planck function enables the emissivity correction of brightness temperature. Its derivation is one of the triumphs of 20th Century physics

2.9.2 Radiative transfer equation

The RTE is a direct method for LST retrieval using a single TIR band. also known as the atmospheric correction method, based on the principle of subtracting the atmospheric influence on surface radiation from the total amount of thermal radiation observed by the satellite sensors in order to obtain the surface thermal radiation intensity, subsequently converting it to the corresponding LST. This approach requires parameters, upwelling (L_{up}) and downwelling (L_{down}) radiance and average atmospheric transmittance(τ_i).

2.9.3 Mono window algorithm

Qin et al. proposed the Mono-Window Algorithm (MWA) based on the radiative transfer equation for the Landsat TM band 6 data, which can avoid real-time dependence data. The method requires three main parameters, i.e., emissivity, atmospheric transmittance, and effective mean atmospheric temperature.

2.9.4 Single channel Algorithm

The single-channel (SC) algorithm was developed by Jimenez-Munoz and Sobrino it has been widely used to retrieve land surface temperature from Landsat series data for its simplicity and requirement of only one thermal infrared channel. it uses estimated atmospheric parameters (or atmospheric functions, i.e., combination of atmospheric parameters) to correct the atmospheric effect in a single channel toward retrieving LST (Cristóbal et al., 2009; Jimenez-Munoz et al., 2009; Jiménez-Munoz & Sobrino, 2003; Qin et al., 2010) the final retrieval error due to effective mean atmospheric temperature can be reduced because it requires few real-time atmospheric parameters and only the LSE and the atmospheric water vapor contents.

2.9.5 Split-Window Algorithm

McMillin, (1975). initially proposed a split-window algorithm for observing ocean surface temperature based on AVHRR thermal infrared data. Rozenstein et al., (2014) and Qin et al., (2001) improved the SWA based on the work of previous scholars. SWA was developed to enabling the extraction of LST from instruments that are equipped with more than one TIR channel. The algorithm takes advantage of the differences in absorption between two thermal infrared channels in the atmospheric window between 10.5 and 12.5 µm. (Weng et al., 2019). Many SWA equations have been derived by numerous researchers for LST estimation (BECKER & LI, 1990; Price, 1984). With an exception of the way these algorithms calculate their parameters, they operate in the same manner (Jin et al., 2015).

From the above mentioned LST Inversion methods except Split window Algorithm all methods used for Estimating land surface temperature for all Landsat sensors which have one or more thermal infrared band while SWA applicable only for Landsat 8 and 9 due to their requirement of at least two thermal infrared band.

2.10 Validations of retrieved Landsat LST

Multiple validation methods and activities are necessary. to assess LST compliance with specifications two common methods that have been widely used to validate and determine the uncertainties in LST products derived from satellite measurements (Schneider et al., 2012; Guillevic et al., 2014) are ground-based validation and satellite products inter-comparison.

2.10.1 Ground-based validation

This approach involves comparisons with ground-based measurements of LST, and has been frequently used to validate LST products retrieved from MODIS (Bosilovich, 2006; Coll et al., 2005; Kabsch et al., 2008) and Advanced Very High Resoluion Radiometer (AVHRR)

(Prata, 1994), The two main limitations of this approach are the spatial representativeness of the in-situ reference measurements and directional effects (Guillevic et al., 2013; Ermida et al., 2014). For most mixed vegetated landscapes composed of various land cover types or soils, the LST measured by a station does not represent the surrounding area that is part of the coarser satellite sensor footprint (Göttsche et al., 2016). The method is particularly suited for studies over inland water bodies which provide large spatially homogenous targets and can be used to both evaluate and improve the performance of retrieval algorithms. To validate through this approach in situ reference data must be selected based on the following criteria: networks with high quality instrumentation and maintenance, and good spatial representativeness for the satellite sensor footprint.

2.10.2 Satellite product Inter-Comparison

This approach involves comparing a new satellite LST product with a heritage LST product (Martin et al., 2019; Hulley & Hook, 2009; Trigo et al., 2008). The method is particularly valuable for finding spatial disagreements between LST products over large areas and for a wide range in cover types. However, the approach does not yield absolute validation results and satellite LST inter-comparisons alone are insufficient to validate a new product, i.e. different retrieval algorithms based on similar assumptions and formulations (e.g. split-window) can be highly consistent with each other but biased when compared to ground reference LST (Guillevic et al., 2014). The intercomparison approach requires accounting for differences in spatial resolution, view angle and overpass time between the satellite datasets. Different observations are never strictly simultaneous and the differences in sensor footprint increase with differences in viewing geometry. Some of common Satellite based LST products were MODIS, GOES-R, ABI, SLSTR, VIIRS, SEVIRI & ASTER

Table 2.1 Common Satellite Based LST product

Satellite	Launch date	Spatial resolution
Moderate Resolution Imaging Spectroradiometer (MODIS)	1999	1km
Geostationary Operational Environmental Satellite (GOES-R)	2016	0.5-2km

Advanced baseline imager (ABI)	2018	0.5-2 Km
(SLSTR) Sea and Land Surface Temperature Radiometer	2016	1-3 km
Visible Infrared Imaging Radiometer Suite (VIIRS)	2011	500 m, 1 km
Spinning Enhanced Visible and InfraRed Imager (SEVIRI)	2001	0.5-1 km
Advanced Spaceborne Thermal Emission and Reflection Radiometer (ASTER)	2000	90 m

2.11 Methods of Estimating Land surface Emissivity from satellite data

LSE is defined as the ratio of the power radiated by a surface with a given temperature to the power radiated by the ideal black surface with the same temperature, simply stands for the surface ability that transforms heat energy into radiant energy, LSE (ε) is one of the key parameters to retrieve accurate LST from remotely sensed imagery different techniques have been developed to estimate the LSE from satellite passive sensors Some of the more well-known techniques include temperature independent spectral indices (TISI)-based method (Becker & Li, 1990), Day/Night method (Watson, 1992 and Wan & Li, 1997), Normalized Difference Vegetation Index (NDVI)-based emissivity calculation method (J. A. Sobrino & Raissouni, 2000) and classification based emissivity estimation method (Peres & DaCamara, 2004) when using a single thermal channel, only semi empirical methods(*NDVI and Classification method*) can be applicable in practice for the estimation of surface emissivity (F. Chen et al., 2016).

2.11.1 The temperature-independent spectral indices-based method

(TISI)-based method of LSE estimation was proposed by Becker & Li (1995) for spectral analysis in the infrared region. In this method, LSE is estimated based on a temperature-independent index that is generated by calculating the ratio of approximated function in two different bands, which means at least two thermal bands are certainly required.

2.11.2 The Day/Night (D/N) method

Day/Night method was proposed by (Wan & Li, 1997) for LSE estimation based on a pair of day and night measurement. This method is based on the assumption that the LSE does not change with time unless there is a change in environmental parameters. The primary drawback of day/night method is sensitivity to measurement noise. Another weakness of this technique is the need for highly accurate geometric registration and radiometric correction of image pairs

2.11.3 NDVI-based method

The NDVI-based emissivity estimation method was introduced by van de griend & owe, (1993) and was further developed by Valor & Caselles (1996) and Sobrino & Raissouni, (2000). This method assumes that (1) the surface classes are soil, vegetation, or their mixture (2) there is a relationship between the LSE and the NDVI of each class and (3) the LSE can be derived using the spectral library. The fact that this approach does not need accurate atmospheric correction and that it has high performance for single thermal band sensors may be regarded as its advantages. However, this method is not suitable for areas with special cover.

2.11.4 Classification-based method

classification-based emissivity estimation method, the model of this method provides a range of LSE values for each class based on structural properties and spectral measurements (Snyder et al., 1998). The classes for which LSE is calculated are in fact a subset of the standard international geosphere–biosphere program classes (Gillespie et al., 1998). The fact that this approach does not need atmospheric correction and multitude of thermal bands may be regarded as its advantages. However, this method is ill-suited for low-resolution data, and its accuracy depends on classification accuracy.

2.12 Effect of land use land cover change on Land surface temperature.

Land use land cover (LULC) change has a great impact on the regional environment and climate change (F. Zhang et al., 2016). The rapid change in LULC is a major environmental issue in recent times because it affects environmental settings and landscape structure (Yee et al., 2016). LULC is influenced by urbanization which affects the thermal environment in the city centers (Mumtaz et al., 2020). Unplanned urban expansion is one of the main LULC changes, The changed LULC pattern to impermeable surfaces resulted in a change in thermal environments and the formation of surface urban heat islands in urban areas (Effati et al., 2021).

Spatial and temporal change of Land surface temperature offers details on the variance of the earth's surface energy change from time to time. That is the main factor for monitoring climate and vegetation in impermeable area. Land surface temperature is an important climate variable associated with environment change and is an indication of the surface energy balance as it is a central parameter in the physics of land surface processes (Mumina & Mundia, 2014). The methods of remote sensing and GIS are used to detect changes in land use and its effect on the temperature of the land surface (Buyadi et al., 2013). Rapid urbanization causes numerous environmental problems such as extreme change of Land use /Land cover. Urbanization changes the natural surface into an impervious area.

2.13 Land Use/Land Cover Studies Using Remote Sensing and GIS

Remotely sensed imageries provide an efficient means of obtaining information on temporal trends and spatial distribution of urban areas needed for understanding, modeling and projecting land changes. (Elvidge et al., 2004) In case of inaccessible regions, this technique is perhaps the only method of obtaining the required data on a cost and time effective basis. Satellite imagery is able to provide more frequent data collection on a regular basis unlike aerial photographs. Although aerial photographs may provide more geometrically accurate maps but is limited in respect to its extent of coverage and expenses. The importance of remote sensing technique was realized by while using traditional method of surveying i.e., aerial photographic approach to monitor urban land use in developing countries with Ilorin in Nigeria as the case study.

Land use/land cover change detection is a process which identifies the differences in the state of an object or phenomenon by observing it at different times Change detection is an important process in monitoring and managing natural resources and urban development because it provides quantitative analysis of the spatial distribution of the population of interest. (Macleod & Congalton, 1998) list four aspects of change detection which are important when monitoring natural resources. They include; firstly, detecting the changes that have occurred; secondly, identifying the nature of the change; thirdly, measuring the area extent of the change and lastly, assessing the spatial pattern of the change. The basis of using remote sensing data for change detection is that changes in land cover result in changes in radiance values which can be remotely sensed. Techniques to perform change detection with satellite imagery have become numerous as a result of increasing versatility in manipulating digital data and increasing computer power

Conventional ground methods of land use mapping are labor intensive, time consuming and are done infrequently. These maps soon become outdated with the passage of time in a rapid changing environment. In recent years, satellite remote sensing techniques have been developed, which have proved to be of immense value for preparing accurate land use/land cover maps and monitoring changes at regular intervals of time. Despite spatial and spectral heterogeneity challenges of urban environments, remote sensing seems to be a suitable source of reliable information about the multiple facets of urban environment (Federico Moran, 2010) and local levels and further to explore the extent of future changes, the current geospatial information on patterns and trends in land use/land cover are playing an important role.

2.14 Land surface temperature variation study using Remote sensing

Meteorological data from weather stations or thermometers mounted on vehicles have generated statistical data used to investigate UHI (Wang et al., 2007; Wong & Yu, 2005). This has been considered as limited in space and biased, since the readings are made on the spot where the equipment is situated. These limitations have been overcome by the use of satellite data which provide more uniform spatial sets of observations and wider coverage to the UHI. However, satellite imagery is also guided by sensor characteristics and image resolution. Image resolution is usually considered through three aspects which include spectral, spatial and radiometric resolutions. The temporal resolution which is an indication of the revisiting frequency of a sensor over a particular place is also an important guide for satellite imagery. Remote sensing is extremely useful for understanding the spatiotemporal land cover change in relation to the basic physical property of materials used on urban structures. These properties related with the surface radiance and emissivity data (Patel et al., 2017). The electro-magnetic wavelength region of 3 –35 micro meter is called thermal-infrared (TIR) region. The useful spectral bands in this range are limited by the intensity of radiation emitted and the atmospheric windows. An excellent atmospheric window lies between 8 and 14 micro meter, in which most remote sensors are set up to detect the thermal radiative properties of the ground materials (Gupta, 2018). Currently available satellite TIR sensors provide different spatial resolution and temporal coverage data that can be used to estimate LST. The Geostationary Operational Environmental Satellite has a 4-km resolution in the TIR, while National Oceanic and Atmospheric Administration (NOAA), Advanced Very High-Resolution Radiometer (AVHRR) and Terra and Aqua Moderate Resolution Imaging Spectroradiometer (MODIS) have 1-km spatial resolutions. Significantly, better-resolution data come from the Terra-Advanced Space borne Thermal Emission and Reflection Radiometer (ASTER), which has a 90-m spatial resolution, meanwhile the Landsat 5 Thematic Mapper (TM) has a 120-m resolution, and Landsat 7 ETM þ has a 60-m resolution in the TIR bands. Better resolution and less frequent TIR observations from Landsat might be used to understand the spatial variation within coarser-resolution observations made by MODIS and AVHRR, which provide more frequent measurements. Recent satellite systems, e.g., MODIS and ASTER, include features to allow easier calibration and provide LST as standard products. This is not true for the Landsat data (F. Li et al., 2004). The first research conducted on urban heat island investigation using satellite remote sensing was performed by Rao, (1972). VHRR thermal data acquired at night were used to examine urban and rural surface temperature differences.

2.15 Spatial metrics

Spatial metrics are indicators describing land use patterns in an urban area. They are defined as mathematical expressions of patch characteristics, such as the area, the perimeter, the geometry (shape), the relative position in the urban area and others. There are numerous types of spatial metrics that are found in the existing literature, such as area/density/edge metrics, shape metrics, core area metrics, isolation/proximity metrics, contrast metrics, contagion/interspersion metrics, connectivity metrics, and diversity metrics. The commonly used metrics can be subdivided into two broad categories (Hardin, 2000) measurement of individual patch characteristics (e.g. size, shape, perimeter), and measurement of whole landscape characteristics (e.g. richness, evenness, dispersion, contagion), or into three categories (Bhatta, 2010) – patch, class, and landscape metrics. Patch metrics are computed for every patch in the landscape, Class metrics for every class and landscape metrics are computed for the entire patch mosaic. The metrics are usually computed with Fragstats, (Mcgarigal, 2015) a public domain software available since 1995 current version 4.2. Fragstats contains a large library of metrics that can be estimated at the class and landscape level. Spatial metrics have been used for different purposes, such as characterizing urban patterns in order to support planning policy; comparing physical patterns of different cities or regions; or understanding the spatial-temporal patterns of urban development. They have also been increasingly used together with other methods, such as remote sensing techniques or imbedded in urban growth models (Banzhaf et al., 2009; Van de Voorde et al., 2009).Based up on previous classification by several authors. metrics which aim at analyzing different characteristics of urban pattern and its spatiotemporal development (Aguilera et al., 2011; Frenkel & Ashkenazi; 2008; Lu, 2007) can be divided into the following three categories: shape irregularity and fragmentation, diversity.

2.15.1 Shape irregularity metrics

Shape irregularity includes the metrics that assess whether an urban settlement has a regular or even shape or if, on the contrary, it has a complex shape with a ragged edge. They can be used to characterize a single patch (e.g., fractal dimension or shape index) or at the landscape level (e.g., Landscape shape index, or area weighted mean patch fractal dimension). The metrics most often used to analyze shape irregularity are area weighted mean patch fractal dimension, area weighted mean shape index and landscape shape index.

2.15.2 Fragmentation metrics

Fragmentation metrics measure the extent to which urban settlements – or patches – are close together (aggregated) or dispersed (fragmented). These metrics are used at the landscape level. A fragmented landscape is normally characterized by a higher number of patches, with a smaller average size and located further away from each other. The metrics mostly used to measure fragmentation are mean patch size, number of patches, patch density and contagion index.

2.15.3 Diversity metrics

Diversity metrics focus more on the composition of the urban landscape rather than on its shape. The most used metrics are Shannon's diversity and evenness indexes, which measure the distribution of different patch types (for instance land use types) throughout the urban area. Other metrics include the largest patch index, measuring the relative importance of the largest patch (which may be useful to study for instance the importance of the urban center), and the compactness index, which uses a concept of compactness based on both fragmentation and shape irregularity.

2.16 Moving Window Analysis

A moving window is a rectangular arrangement of cells that applies an operation to each cell in a raster dataset while shifting in position entirely. Moving window analysis is a prominent means of analyzing the spatial variability of landscape patterns at multiple scales. results of a landscape analysis are scale dependent. One approach to deal with this is by using a moving window (Hagen-Zanker, 2016) Moving window analysis is a common approach to multi-scale analysis. A "window" of defined size and shape is moved over the data, the moving distance is equal to the width of the window. All data located within the window section are statistically summarized the number and average of all points inside the window, the minimum/maximum values, the standard deviation, the coefficient of variation, etc. The results are again points to the centers of the moving windows and as their attributes the statistical indicators of these windows.

In moving window analysis, each location is associated with the landscape patterns present in the spatial window surrounding it. The size of the window determines the scale of the analysis For each focal cell in the landscape, a matrix is used to specify the neighborhood and the metric value of this local neighborhood is assigned to each focal cell (Fletcher, 2017). Thereby, the windows are allowed to overlap (McGarigal et al 2012). The result of a moving window analysis is a raster with an identical extent as the input, however, each cell now describes the neighborhood in regard to the variability of the chosen metric (Hagen-Zanker, 2016).

2.17 Urban Rural Gradient

Urban-rural gradient paradigm is an analysis methodology, coming from landscape ecology, which enables to investigate how urbanization provokes changes in ecological patterns and processes into landscape. Also used to describe how Anthropogenic effects. affect their surroundings and how they compare to areas less affected by Anthropogenic effects (Ae & Hahs, 2007). Generally speaking, the urban-to-rural gradient mediates between the poles of 'the urban' and 'the rural'. There are two main urban–rural gradient analysis methods that have been developed and applied in the literature. The first one is the use of directional transects running across the city center with their ends both extending to the rural areas (L. Zhang et al., 2004) . The second one applies concentric rings or zones around the city center with standard distance intervals extending to the rural areas (X. Zhang et al., 2017). The concentric ring or zones around the city center with standard distance intervals extending to the rural areas. The concentric ring gradient analysis method is effective in cities exhibiting single-core urban growth patterns around the city center (Ranagalage et al., 2017) . A wide range of social, economic, demographic, administrative or political indicators have been used to define urban areas, but there is no consensus on how to construct a consistent definition based on any single set of attributes (Montgomery et al., 2013). The terms ‘urban area’ or ‘urban footprint’ are widely used to basically refer to the spatial extent of urbanized areas on a regional scale; a definition which is both fuzzy and inconsistent (Isikdag et al., 2011; Taubenb et al., 2019). As such, defining the urban area based on the physical extent of the built-up land (impervious surface), as adopted in most remote sensing urban studies (Herold et al., 2005; Van de Voorde et al., 2009). is the best option.

2.18 Empirical Review

Land use land cover change brought significant change in the ecosystem. Since change in land use land cover also bring change in surface albedo characteristics. (Choudhury et al., 2019; Belete, 2017; Haylemariyam, 2018) rapid urbanization brought fast transformation of LULC pattern which in turn significantly affect LST. Barren land and built-up area exhibit highest mean value of land surface temperature. While vegetation class exhibit lowest mean land surface temperature. Moreover, Hereher (2017) as stated in the transformation from agriculture to urban land increased the LST by 1.7 °C and the transformation of bare land to agriculture, which decreased the LST by 0.52 °C for the same period.

Supposing to hydrological process. (Dejene & Abebe, 2019) assessed the spatiotemporal changes of runoff at the adama city watershed and its sub-watersheds and noted that in city built-up expanded by 22% annually from 1995 to 2019. Similarly, the runoff depth is increased by 9.5% in the City and 12.9% and 6.9% within the two sub-watersheds, likewise (Mango et al., 2011) conducted research over the Upper Mara River basin in Kenya and reported that if forest cover were converted to grass land, then surface runoff increased by 20%. Furthermore, (Garg et al., 2019) studied LULC change in Pennar River Basin located in Southern part of India. showed that there is human induced alteration to LULC pattern, as the area under urban landscape is increasing (0.14%) and natural forest is declining (0.7%). These changes resulted in increase of runoff potential by around 45%.

In the case of the green space. (Gashu & Gebre-Egziabher, 2018) studied urban land use/land cover and green infrastructure change in Bahir Dar and Hawassa city. in accordance with their study vegetation decreased by 30% and 14% in Bahir Dar and Hawassa respectively for the period 1973–2015, while built-up areas expanded by 10% and 24% respectively in the two cities. To sum up the study key findings land use land cover change modify reflective power, runoff depth and Vegetation cover of the natural earth surface, however the study focused on the impact of change in land use land cover composition and disclosed a Gap in the categories of configuration thus, assessing the impact of change in LULC configuration on the environment is important in reducing the impact of change in land cover configurations and provide opportunity for preparing adequate mitigation strategies.

Taking in to consideration the influence of land cover configuration on land surface temperature is significant. in view of the fact that land cover configuration besides composition have impact on Land surface temperature. Green infrastructure arrangement has substantial advantage, it has been shown that in the hot desert climate, clustered greenspaces enhance the cooling effect at a local scale, such as in small urban parks, but dispersed greenspaces show a better local cooling effect (P. Shi et al., 2017; Z. Zhao et al., 2018) showed that both clustered and evenly arranged trees provide significant cooling benefits to the entire residential area. Furthermore, (Masoudi & Tan, 2019) reveal that more, simpler shape, less fragmented, and more connected urban green space patches had lower LST and higher cooling effect. Thus, supposing to urban green space, the finding from the study emphasizes that size and the shape of vegetation are important factors in determining its cooling effect.

B. Yang & Ke, (2015) reveal proportion of water body, average water body size, the isolation and fragmentation of water have high correlation with the LST. Furthermore, (Cai et al., 2018) publish that Water bodies have an obvious impact on the relationships between the urban form factors and the LST, particularly at a distance less than 250 meters. In general, large area, low degree of landscape fragmentation, and complex outlines lead to low LST (Du et al., 2019). As reported in the studies land cover configuration significantly affect land surface temperature. land cover patch size, shape and distribution highly correlate with Land surface temperature. Therefore, it was appropriate considering impact of land cover Configuration on Land surface temperature. To effectively analyze and mitigate its effect. However, researches in local level focused mainly on the impact of land cover composition on Land surface temperature.

Studying Surface urban heat island is important. for the reason of its impact in health-related issue and energy consumption rate. It has been shown that in Delhi metropolitan city change in the minimum, maximum and mean SUHII has increased by 1.26 ◦C, 4.6 ◦ C and 1.18 ◦ C during 1991 to 2018 and hence, the thermal comfort has declined in the city. (Shahfahad et al., 2022). likewise, (X. Li et al., 2019) found that UHI could result in a median increase of 19.0% in cooling energy consumption and a median decrease of 18.7% in heating energy consumption. furthermore, (Liao et al., 2017) studied the relationship between land surface temperature and electricity consumption in 32 major cities in China the study found that there is a positive correlation between electricity consumption and land surface temperature at night and no correlation during the daytime. besides (Akbari et al., 2016) also found area which shows increase in UHI has shown increase in energy consumption. Prior study confirms that increase surface urban heat island intensity disturbs thermal comfort of the city and energy consumption for cooling purpose. Even-though in Ethiopia studies concerned about SUHI is less.

2.19 Research and knowledge gaps

The UHI is a thermal anomaly with horizontal, vertical and temporal dimensions. Although it may be observed in almost all settlements, large and small, its characteristics appear to be related both to the intrinsic nature of cities (such as size, building density and land-use distribution) as well as to external influences (e.g., climate, prevailing weather circumstances and seasons) (Angel et al., 2005). it has been proved to occur as a result of the introduction of artificial surfaces, such as buildings and roads made of dry and impervious construction materials, along with human activities that radically alter the energy balance in cities and the atmospheric layers above (Erell et al., 2011; Roth, 2007). It exacerbates impacts by affecting rainfall patterns, interacting with and worsening air pollution, increasing flood risk and decreasing water quality (Hester & Bauman, 2013). However, the most direct impact of the UHI on human health is through exposure to increased temperature, which can be particularly problematic during heat waves.

Since urban heat islands are a global phenomenon, their examination has increased exponentially in the past few decades, reflected in the remarkably rapid growth of available literature on the subject (Arnfield, 2003). Similarly, UHI studies shows increment in Ethiopia (Chaka & Oda, 2021; Degefu et al., 2021; Feyisa et al., 2014; Warkaye et al., 2018). Despite research on urban heat island (UHI) has increased, Ethiopian literatures majorly focused on the detection of UHI and the influence of land cover composition change on UHI. However, studies regarding multidirectional profile of LST in different urban landscape structure and more-importantly contribution of land cover configurations to UHI under city scale has scarcely been reported in the literature.

Given that the LULC change brought about by urbanization is the most significant, it is crucial to investigate the LST profile of the urban landscape using a multidirectional approach in order to examine the Various impacts of urbanization on the pattern, functioning, and dynamics of landscapes. Previous research found that the composition of land cover elements, rather than their arrangement, orientation and shape, was more important in defining LST. The configuration of land cover features, on the other hand, is critical. The findings also suggest that, in addition to balancing the relative amounts of different land cover types, changing the spatial arrangement of various land cover aspects can mitigate the negative effects of urbanization on UHI. Moreover, impact of land cover configuration in urban areas varies with landscape and climate.

The utilization of findings from urban environment research in planning policy is crucial to inform sustainable development in the context of growing urbanization. since urban studies are intended to develop planning policies that take into account the needs of space users in consideration of their social, psychological, environmental comfort, financial, physical, and other characteristics and needs. As a result, research-informed design or redesign of the urban terrain in cities is required.

Understanding the impacts of various changes in land cover composition and configuration on Land Surface Temperature at the City Scale is necessary to control or reduce the harm caused by land use and land cover change on the thermal environment of cities. Due to Adama city's unique spatial location, spatial planning, level of urbanizations and level of management previous research conducted in various country urban areas was unable to present a complete picture of the situation, leaving it unclear how to stop a rise in land surface temperature in Adama city caused by the change in configuration of land cover.

2.20 Conceptual framework of the study

All decision-makers, including urban planners and environmentalists, must take urbanization-induced changes in land use and land cover into account (Jat et al., 2008). Major neighborhood changes are brought about by urban expansion. Urban areas are created when agricultural fields are lost (Rimal, 2012). In other words, the surface of the ground is dominated by man-made structures, and less and less of the natural land features, such as vegetation and water bodies, are present. Cities grow, changing the surface characteristics of the land, such as its thermal capacity, surface albedo, and soil moisture. Due to the different surface materials used in urban and suburban settings, such as the asphalt used for roads, there are temperature disparities between these two types of locales.

The difference in surface temperature between urban and rural locations is often influenced by three main determinants. Urban Material Properties, Urban Land Cover Geometry, and Reduced Natural Landscapes in Urban Environments (United state environmental protection Agency). The conceptual model shown in (Figure 2.1) below outlines the key factors that affect LST and the variation in land surface temperature between urban and rural set

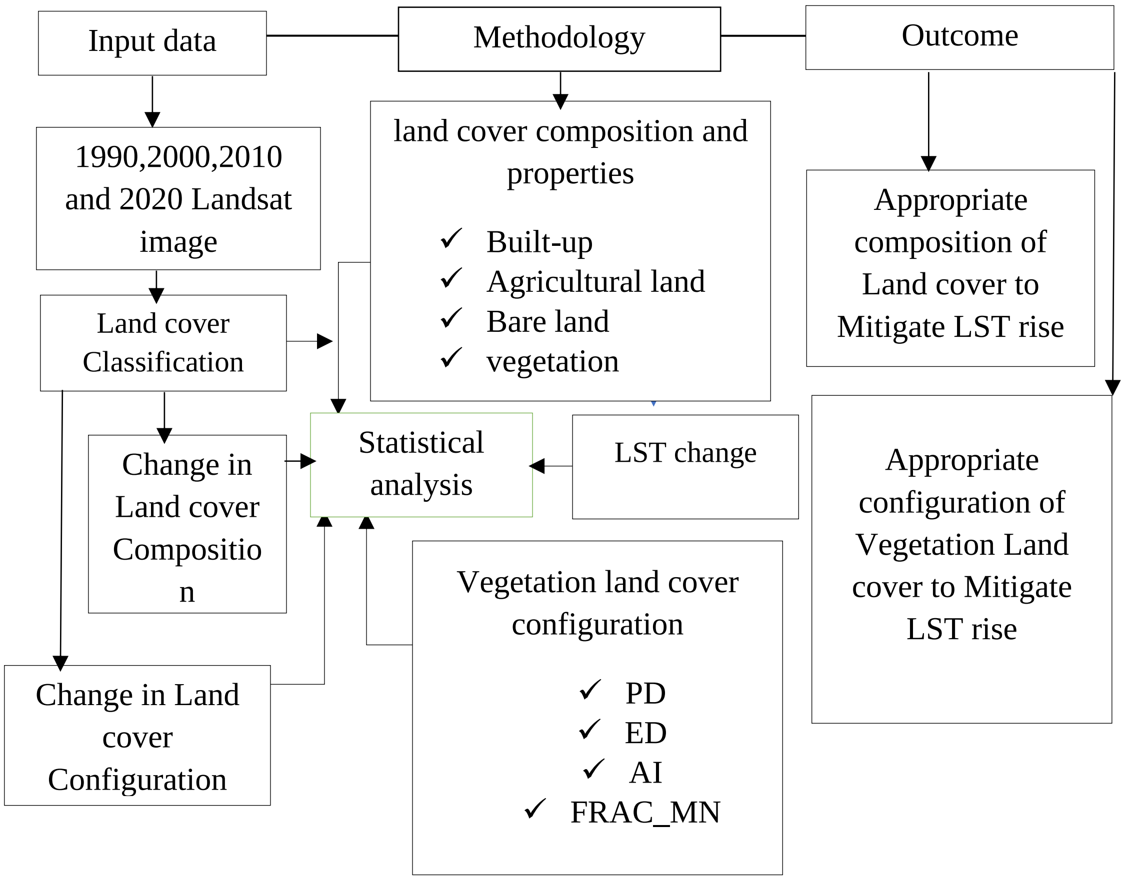

Figure 2.1 Conceptual framework of the study

CHAPTER 3: MATERIALS AND METHODS

3.1 Description of the study area

3.1.1 Geographic location

Adama is a city in the central Oromia Region of Ethiopia (Figure 3.1) located in the east Shewa Zone 99 km southeast of the capital Addis Ababa the city sits between the base of an escarpment to the west, and the Great Rift Valley to the east. enclosing between 8° 26`35``N to 8° 38`46``N latitude and 39° 9`20``E to 39° 21`30``E longitude covering an area extent of new proposed boundary about 313.04 km^2. Adama city is one of the railway urban centers founded as a railway depot in 1916 along Addis Ababa Djibouti railway line the construction of Addis Ababa-Djibouti railway line was a major factor for the emergence.

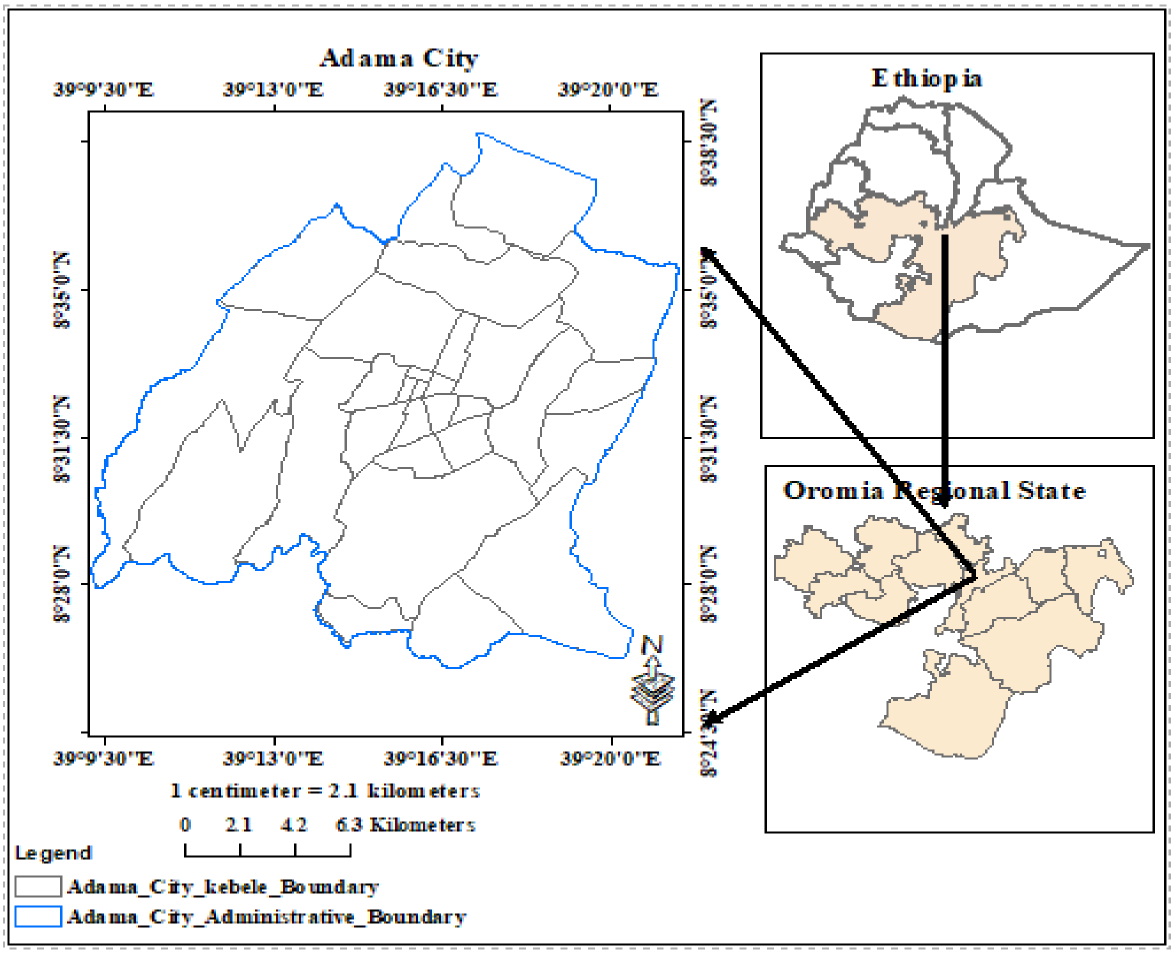

Figure 3.1 Location Map of Study Area

3.1.2 Demographic

Adama city is the fourth largest urban center in Ethiopia regarding population size (Central Statistical Authority, 2021) population projection. Moreover, it is the first largest urban center in Oromia Region and one of few cities in the country with a threshold population of over 300,000 the city has long population survey trends which have been covered by most demographic and housing censuses and surveys since 1965 G.C when the first baseline urban demographic survey was conducted in the country (Socio Economic Profile of Adama, 2018). According to the last three consecutive censuses conducted in the country Adama city showed a large increase in population in the first Ethiopian population and housing census, which was held in May 1984 Adama had a population of 77,237, The following population and housing census conducted in 1994 reported that Adama had a total population of 127, 842, in the third base Ethiopian population and housing census which was conducted in 2007 (the most recent year for which data are available) 220,212 people were inhabited in Adama. According to Oromia Urban Planning Institution (OUPI) four *Gandas/kebeles* namely Daka Adi, Dabe Soloke, Boku Shenen and Melka Adama with about 11,940 populations excluded from total population of adama city in the third population and housing senses that makes population of adama city 232,152 in 2007. In the new structural plan 11 new rural *Gandas/kebeles* are delineated under the city administrative boundary based on (Central Statistical Authority, 2021) population projection in 2021 adama city have 435,222 populations of whom male 212,991 and female 222,231.

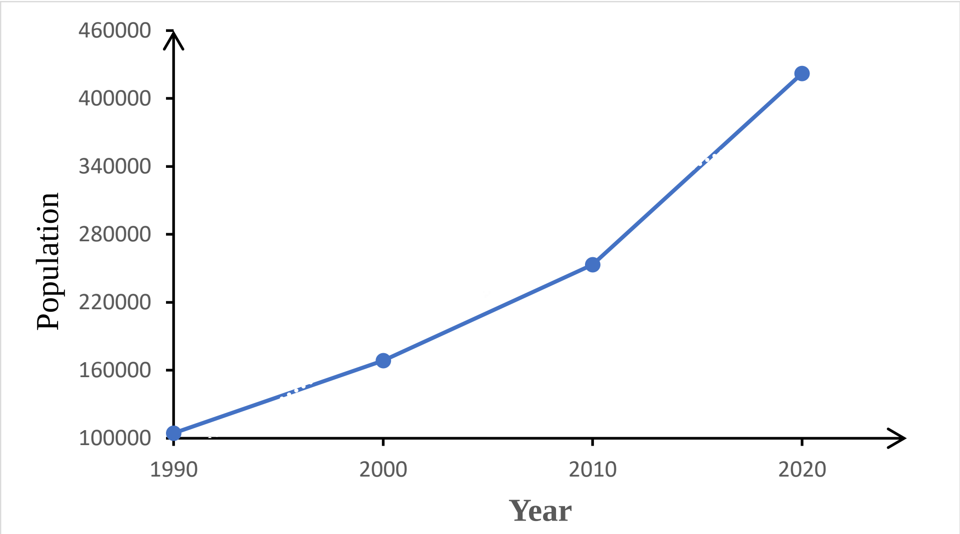

Figure 3.2 Population of Adama City from 1990 - 2020 (Projected, CSA)

3.1.3 Urban growth

Adama is one of Ethiopia's fastest-growing cities in terms of population, urban built-up area, and economic function. The population of the city has grown at the rate of 9% from 2004 to 2016 (Tesema & Assefa, 2019) with the total population predicted to reach almost 435,222 by 2021 (Central Statistical Authority,2021). Adama city growth is supported by both natural urbanization and rural-to-urban migration. Indeed, the city's population is primarily made up of migrants from adjacent rural areas, rural areas in other regions, and other urban areas. Adama city is one of in the regions and in the countries that experiences a high influx of migrants each year migrants made up 53.7 % of the city's population, according to the census in 1984, Similarly, the second census in 1994 found that the proportion of migrants was 52.9 % after a decade, and it was estimated that around 59.2 % of the total population was counted as migrant in 2007 (CSA, 1984, 1994, 2007), As previously stated, a major proportion of Adama city population is made up of migrants, who are mostly drawn to the city in search of work which demonstrates a city's ability to recruit residents from other cities or rural areas.

Adama City's built-up area rose by 293 % between 1984 and 2015 (Sinha et al., 2016) Similarly (Dejene & Abebe, 2019) reported that the city's built-up territory has more than doubled, with a 22 % annual urban expansion from 1995 to 2019. Adama is a thriving and expanding city that is providing an increasing economic contribution to the region and the country. In Adama city top three job sectors are wholesale trade, manufacturing, and construction, which represent for 23.2 %, 19.0 %, and 9.4 % of total employment, respectively. Nonetheless, other industries, including as transportation and storage, the service industry (real estate, hotels, food and services), retail, and construction, contribute significantly to the city's economy (Dube & Mulugeta, 2015). To summarize, Adama City's urban growth during the previous few decades can be attributed to both geographical and socio-demographic reasons.

3.1.4 Climate condition

3.1.4.1 Rainfall

Rainfall record from 2001 to 2020 at the Adama Meteorological Station shows that Adama city falls within summer maximum rainfall region of the country. The mean annual rainfall of Adama city was 1035.217 mm and the maximum monthly average rainfall was 240.227mm in the month of July (Figure 3.3). The two months that acquire maximum rainfall are July and August, whereas the minimum rainfall acquired was during December–February.

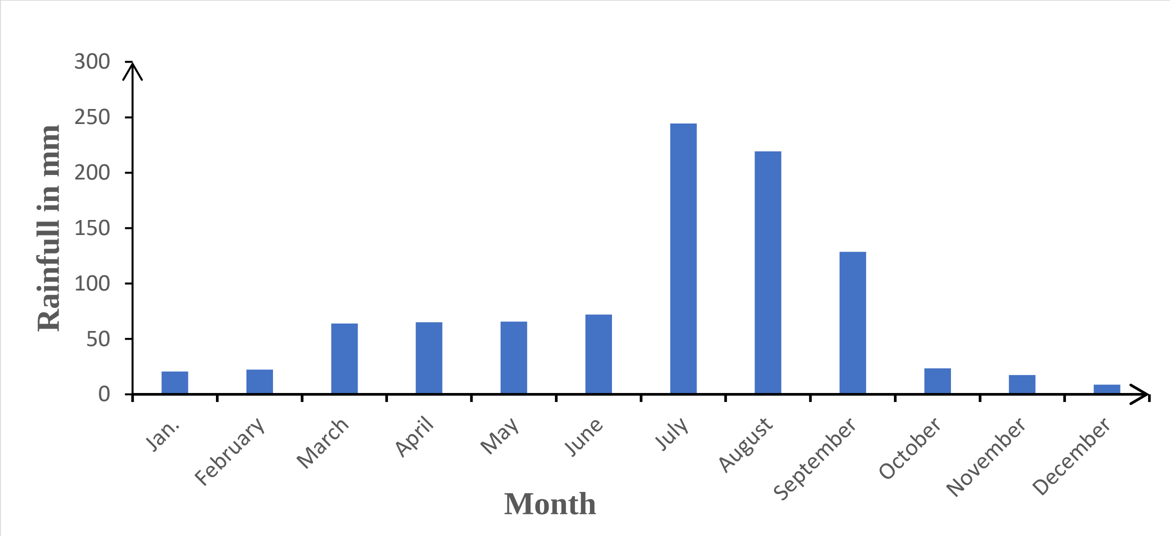

Figure 3.3 Adama City Monthly Average Rainfall from 2001-2020

3.1.4.2 Temperature

According to the Ethiopian Meteorology Agency, Adama station data (1990–2020), the mean annual temperature of the city is 22.87°C. It is classified as semi-humid to semi-arid climate, In Adama, march to June is the hottest month with the maximum mean temperature of above 32°C in May (figure 3.4). The monthly minimum mean temperature was November-December and January-February. The maximum temperature varies between 27.36°C and 32.24°C while the minimum monthly humidity varies between 14.01°C and 18.56°C.

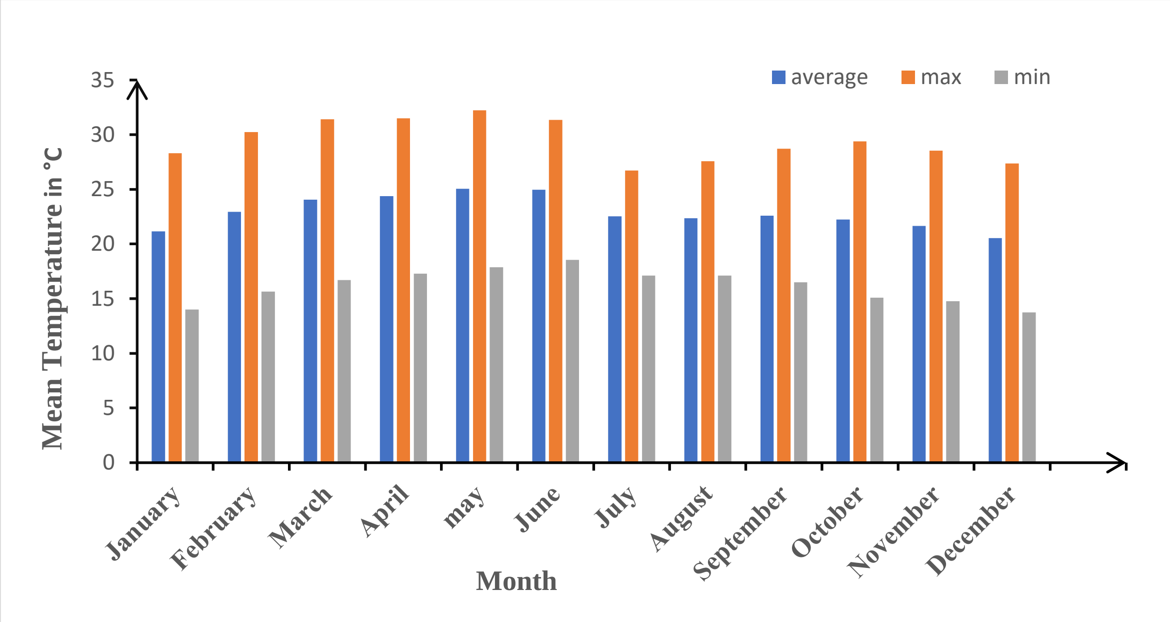

Figure 3.4 Adama City Monthly mean Max, Min and Average Temperature from 1990 - 2020

Temperature data (1990–2020), which have been obtained from Ethiopian Meteorology Agency, Adama station, As illustrated in (Figure 3.5), there has been a mild increase in mean average maximum and minimum (kiremit) season temperatures.

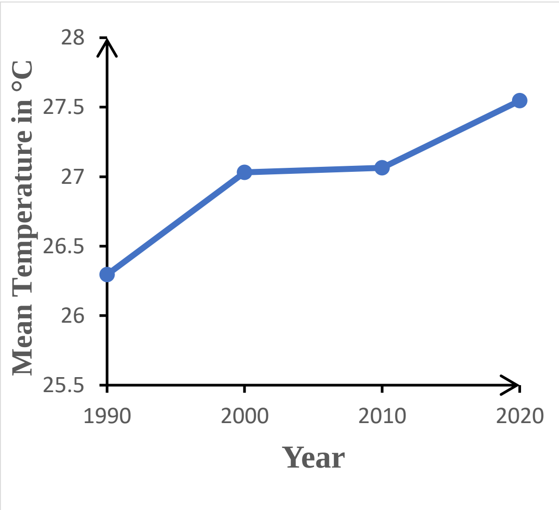

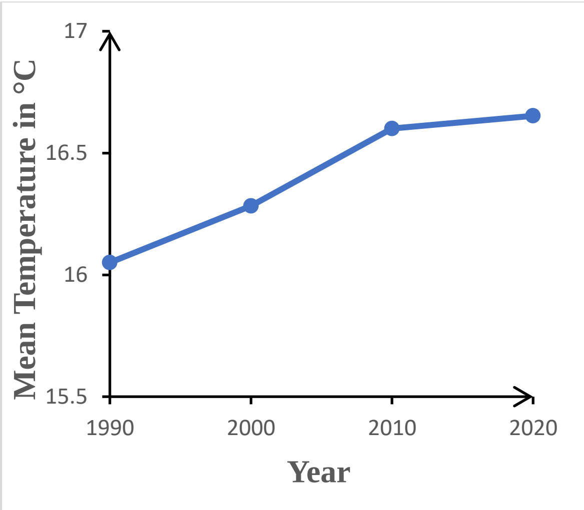

Figure 3.5 Adama City summer (Kiremet) season mean max(left) and min(right) temperature

Adama city enjoys favorable climatic conditions due to its geographical locations surrounded by plateaus that experiences moderate temperature and rainfall which is favorable for life, rainfall mostly occurs in the summer season it receives abundant and heavy rainfall every year during this season adama city have single meteorology station.

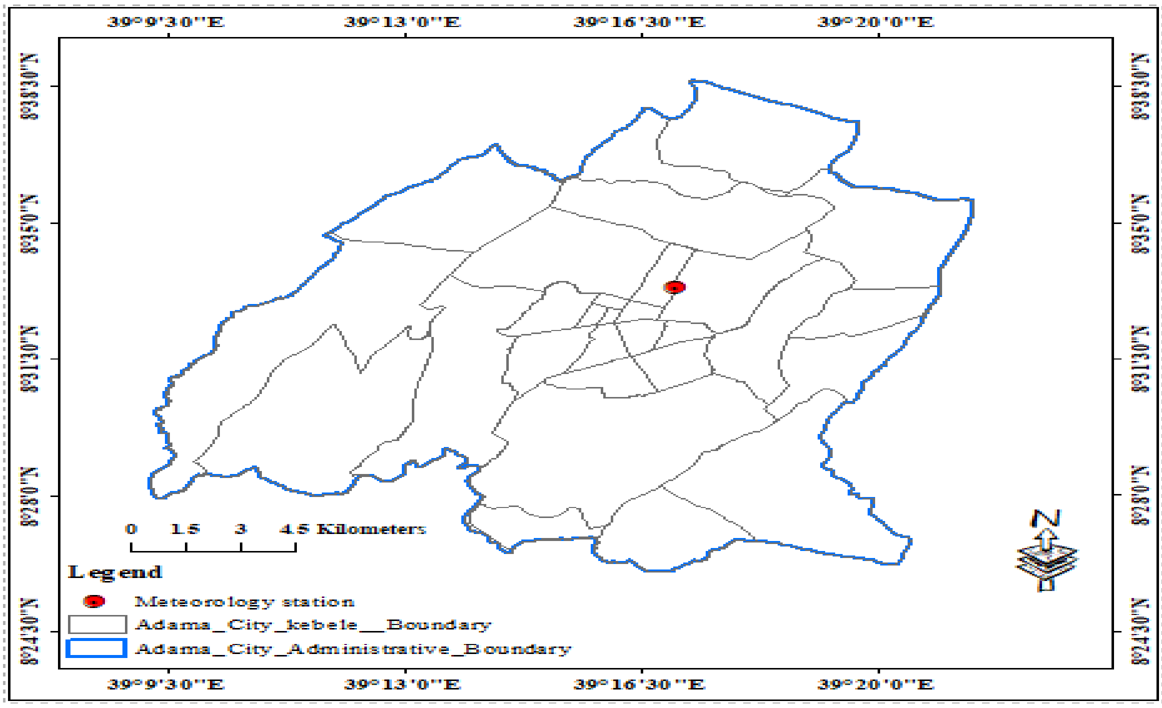

Figure 3.6 Adama City Meteorology Station Map

3.1.5 Topography

The existing built-up area of Adama city, is in between 'Kechema' and 'Boriticha' uplands, with a flat topography (figure 3.6), this topography generally rolls down from north (Dhaka Adi) to south direction up to the expressway that runs from Addis Ababa to Adama. The western and eastern parts of the built-up areas that are adjacent to Kechema and Boriticha uplands are affecting by flood from the dissected uplands during the rainy season. Adama city lies in the Great Ethiopian Rift Valley. Within this major landform, there are plateau and plain landscapes. Within these landscapes, there are also smaller, wider, shallower and deeper gullies. The elevation ranges from 1,452 to 2055 m above sea level. The lowest and highest points are located at the extreme east and northwest part of the expansion areas.

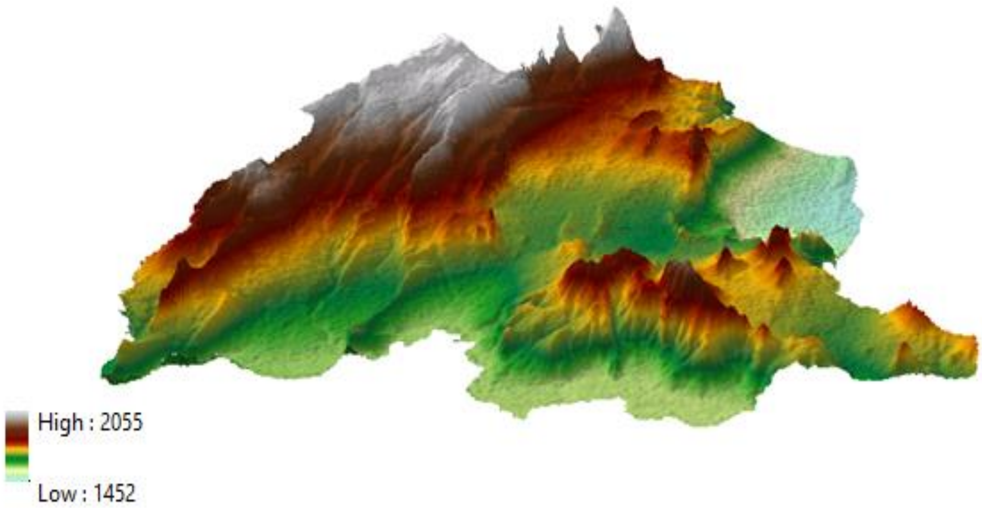

Figure 3.7 3D Elevation Map of Adama City

Aspect map of Adama City was classified according to the angles; Flat (-1−0°), North (0-22.5°), North−east (22.5−67.5°), East (67.5−112.5°), South−east (112.5−157.5°), South (157.5−202.5°), South−west (202.5−247.5°), West (247.5−292.5°), North−west (292.5−337.5°) and North (337.5−360°). The distribution of various aspect classes in the present study area is presented in (Figure 3.7 and Table 3.1).

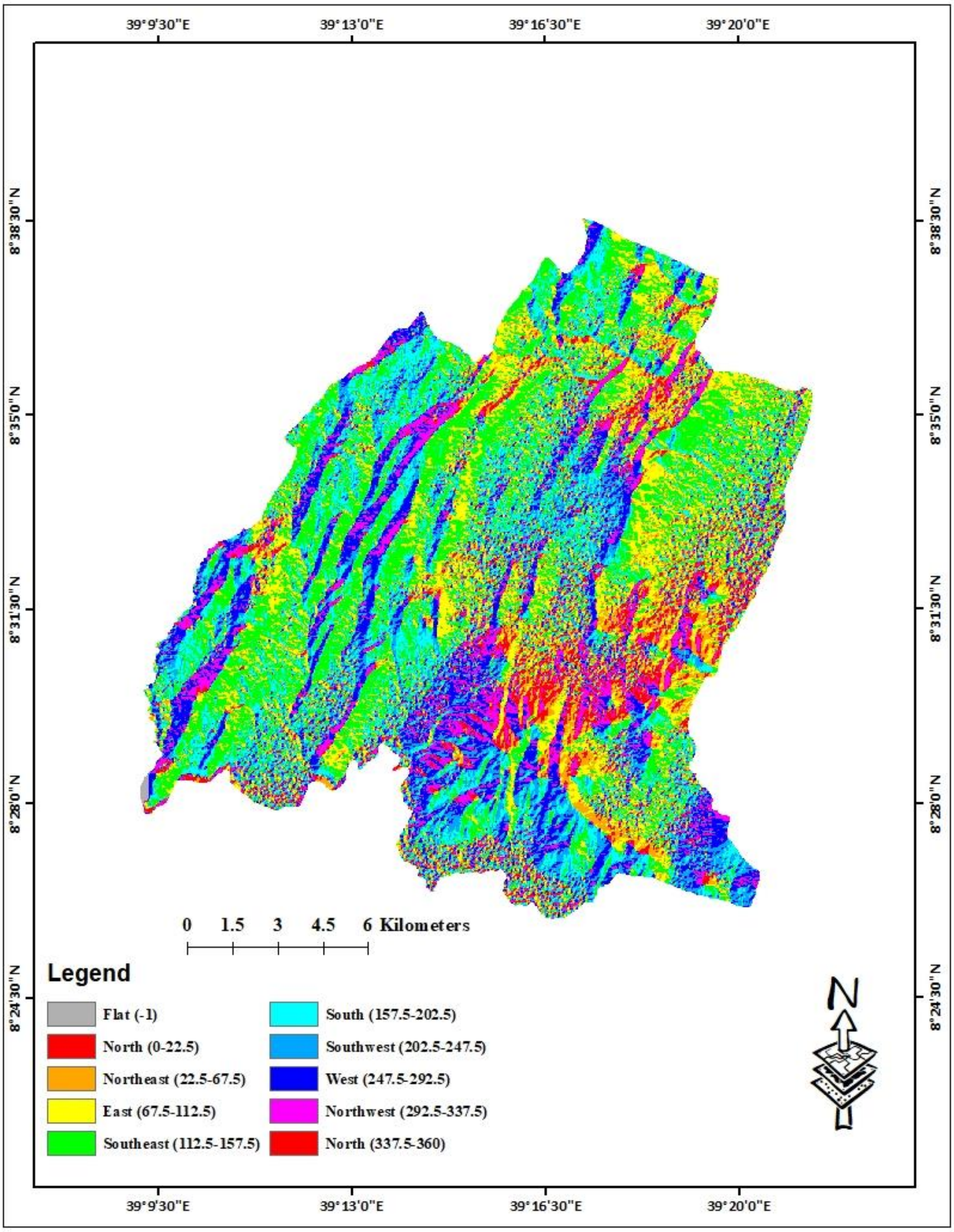

Figure 3.8 Aspect Map of Adama City

Table 3.1 Aspect sub-classes and their coverage area

Aspect classes	Area (km^2)	%
-1 - 0	1.413	0.454826
0 - 22.5°	11.277	3.629917
22.5 − 67.5°	23.3217	7.506946
67.5 − 112.5°	47.4741	15.28128
112.5 − 157.5°	76.1004	24.49571
157.5 − 202.5°	47.1969	15.19206
202.5 − 247.5°	32.5854	10.48881
247.5 − 292.5°	36.2097	11.65542
292.5 − 337.5°	27.2178	8.761048
337.5 − 360°	7.8723	2.533989

3.1.6 Land use land cover

In Adama city, there is a wide range of land use categories, including residential, commercial, business administrative, open spaces and environmentally sensitive areas with graveyards, sports and recreational, manufacturing, and storage, among others.

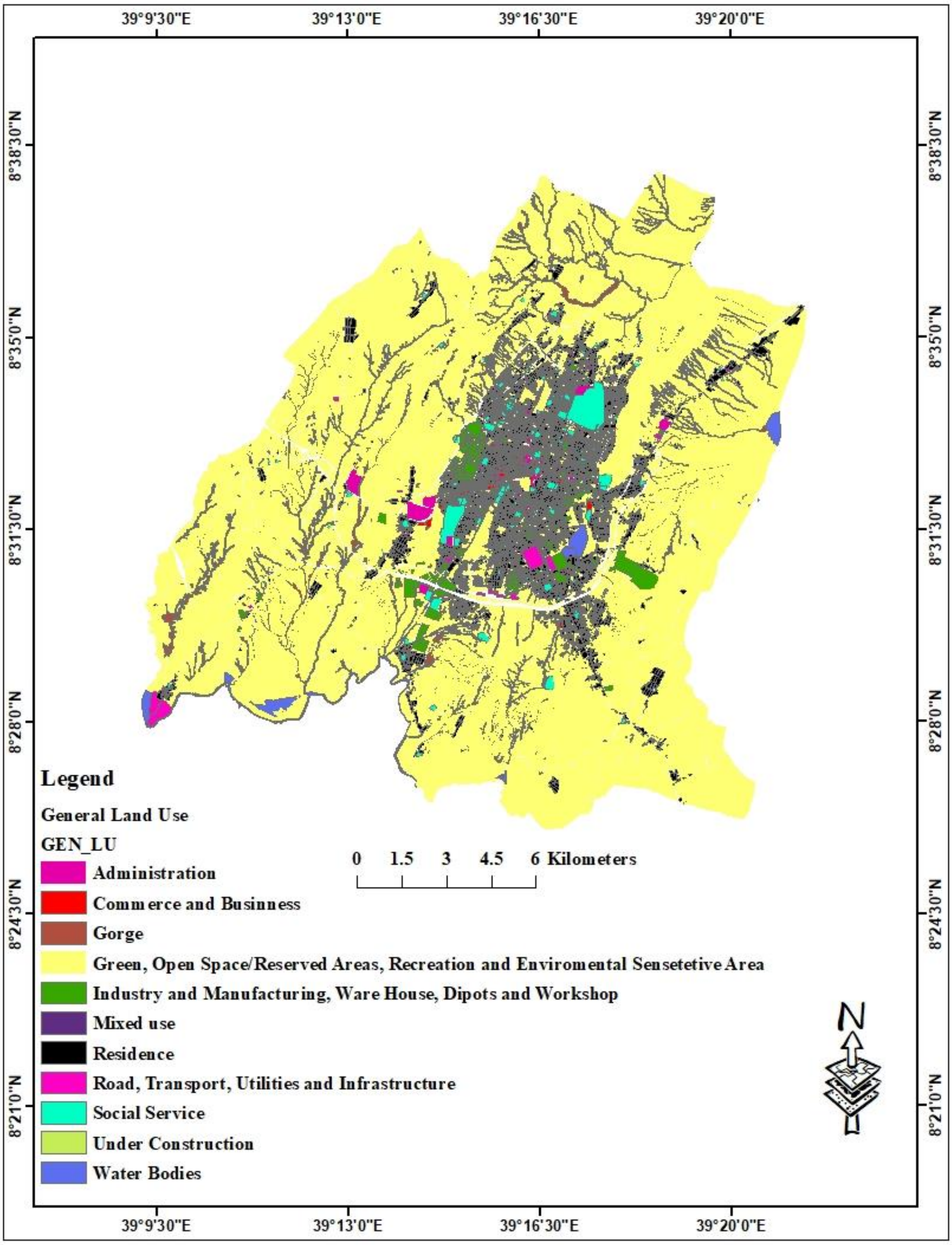

Figure 3.9 Land use category map of adama city

3.2 Data source

Land-use/land-cover change analysis is essential for determining the impact LULC compositional and configurational change on the LST. For this propose in this study data from secondary source employed. Different remote sensing satellite imagery (Landsat, MODIS and ASTER) and aerial photograph used. All chosen Landsat Satellite imagery was classed as Landsat 7 and 5 due to the absence of cloud-free Landsat 8 satellite images during the wet season in the study area all image are radiometrically calibrated and projected to Adindan UTM zone 37N projection systems, NASA's MOD11A2 Eight-day LST Product with a spatial resolution of 1km*1km and a temporal resolution of eight days was downloaded for the purpose of validating the retrieved Land surface temperature from the Landsat satellite. It was then resampled to 30m. Likewise, 30 m Advanced Spaceborne Thermal Emission and Reflection Radiometer (ASTGTM-DEM) was collected from Earth Explorer Characteristics of all satellite imagery used in this study are presented in the (Table 3.2)

Table 3.2 Data Source

Sensor	Scene Date	SCENE_CENTER TIME In GMT	Cloud coverage %	Scene Type	Spatial-Resolution
Landsat					
Landsat 5	1990-09-13	"07:00:14.7290690Z"	15	Maine	30 m
Landsat 7	2000-09-16	"07:30:57.5111704Z"	24	Maine	30 m
Landsat 7	2010-09-28	"07:32:40.0353533Z"	12	Maine	30 m
Landsat 7	2010-10-14	"07:32:45.9485909Z"	6	Fill	30 m
Landsat 7	2020-10-09	"07:04:45.0100953Z"	1	Maine	30 m
Landsat 7	2020-10-25	"07:03:42.4346669Z"	3	Fill	30 m
MODIS					

	Day of pixel composite in Julian		Temporal Resolution	Spatial-Resolution
MOD11A2-V6	2000-260/ (2000-09-17)	-	8 days	1000 m
MOD11A2-V6	2010-265/ (2010-09-22)	-	8 days	1000 m
MOD11A2-V6	2020-281/ (2020-10-08)	-	8 days	1000 m
ASTER				
			Spatial-Resolution	
AST(GTM)V003	-	-	-	30 m (1 arc-second)

Administrative boundary, road network, existing LULC, structure plan of the city, population, and climatic data were acquired from their respective sources, as specified in the (Table 3.3)

Table 3.3 Ancillary Data Source

Data	Data source
New Adama city Administrative Boundary	Oromia Urban Planning Institute
Population data	Central Statistical Authority (CSA) and Oromia Urban Planning Institute
Climate data	(NMA) adama station
Road	Adama City administration urban land sectors office
Existing land use	Adama City administration urban land sectors office
Reference data (Validation)	Aerial imagery and Google image

3.3 Software used

Software used in this study were selected based on the capability to work on the existing problems in achieving the predetermined objectives. In order to achieve the objective of the study different software were used. Hence software package like ENVI 5.3 was used for image processing and classification activities on satellite images, Fragstats 4.2 used for

Analyzing the spatial pattern, Moreover, Google Earth Pro was used to check the accuracy of land use/land cover class. Also, SPSS for statical analysis and ArcGIS 10.8 for LST inversion, spatial analysis, and map preparations as stated in the (Table 3.4)

Table 3.4 Material and Software used

Software	Version	Purpose
ENVI	5.3	Preprocessing and classification
FRAGSTSATS	4.2	Analyzing the dynamics of Landscape pattern
ArcGIS	10.8	LST retrieval, spatial Analysis and Mapping
SPSS	26	Statical analysis, tabulation and graphical representation.
Google Earth Pro	7.3.4.8642	visual image interpretation and validation of the result

3.4 Data collection method

As a part of this study, interdecadal time frame from 1990 to 2020 was selected to analyze urbanization induced LULC change in Adama city a major reason for this time frame can be attributed to two main factors First, Ethiopia has maintained a legacy of a centralist government structure until 1991(Ferdissa, 2019) cities and towns throughout the country have been regarded extensions of central authorities thus, this period illustrates the trend of urbanization in Adama city before and after the abolition of centralized government Structure Secondly, Adama city growth rate was moderate until 1991. Adama city had 1.2 km^2 in 1937, but it expanded slowly over 54 years to 34.20 km^2 in 1991 (1937-1991), compared to the intensified expansion after 1991, which is roughly four times in 2004 and nine times in 2017 the size of the city in 1991, Furthermore, there is no ground truth available for the study area prior to 1990 in the decadal range

With regard to the short research periods, LULC changes and urban expansion were investigated in detail. However, In the wet season, the study area is characterized by a significant amount of cloud cover Consequently, it was difficult to perform a multitemporal analysis over a short period of time as a result the study time frame being conducted over a period of 10 years.

As “time series analysis” This study require data acquired at different time period on the same space. In the light of this Landsat imagery was downloaded starting from 1990 up to 2020 within 10-year interval during accusation of Landsat time series data The following quality criteria were assumed for the data.

- **Landsat Sensor**

Since 1972, the Landsat series of Earth-observing satellites has been imaging Earth’s land areas. Landsat represents the world longest continuously acquired collection of space-based moderate resolution land remote sensing data. Currently three Landsat satellites are operating thus are Landsat 7, Landsat 8 and the newly launched one Landsat 9. For this study one Landsat 5 TM and five (including the fill scene) Landsat 7 ETM+ image is collected from the USGS public domain website based on availability of the sensor (for example only Landsat TM is available in 1990) and less cloud covered image in September month one of the rainy seasons in Ethiopia (locally kiremit) in this case also only Landsat 7 ETM+ image is available as less cloud covered image.

- **Phenology/Season**

Restricting imagery to a particular season can minimize reflectance discrepancies caused by phenology, haze, and sun angle differences. Reflectance variation due to Seasonal characteristics of vegetation have impact in the accuracy of classified LULC map. (J. Liu et al., 2015). images close to the peak of the growing season or time of maximum vegetation “greenness” have been preferred. Moreover, image acquired from the direst season (specifically harvesting period) increase LST of farmland land cover type. (Belete, 2017; Balew & Korme, 2020) which is not suitable for urban heat island (UHI) study in regarding to this all image are downloaded from the end of Summer locally (kiremt) up to the beginning of Winter locally (bega) which comprises the growing period for Meher (one of grain growing seasons in Ethiopia) clearly (September-October).

- **Single Data Runs**

Obtaining consecutive scenes within a path collected on the same date increases the ease with which information can be derived from the scenes, because atmospheric conditions and solar zenith angle variations will change gradually for the block of data in question. However due to the acquisition schedule of Landsat satellite which is every 16 day the satellite repeats the same place which is not available in decadal range. A priority was given to acquire scenes from the same month (September) to compensate this atmospheric and zenith angle variations

- **Cloud cover**

Cloud free imagery is one of the good criteria for image quality. Previously researchers would reject partly cloud-affected scenes in favors of cloud-free scenes. in this study cloud cover up to 24% is used since cloud cover percentage clarify total cloud coverage with in the scene not with in the study area. For example, in this study the study area only accounts about less than 1% of the entire scene just about (0.95489%) or 313.243 km^2 out of (185km * 180km) the entire scene in addition Quality Assessment (QA) band in Landsat collection one level one product is used to musk out the cloud and shadow of cloud. To reduce the impact of cloud and cloud shadow all the images were cloud masked.

- **Collection level**

Radiometric and geometric quality of satellite image is the most important properties for time series analysis their consistency ensure that measured change is due to earth surface change and not due to sensor changes in view of this all-Landsat images for the study grouped under L1TP (precision and terrain correction) collection 1 level 1 and tier1 products and which accounts the highest accuracy, precision terrain processing and suitable for time series analysis. L1TP data product are radiometrically calibrated and orthorectified using ground control point and digital elevation model (DEM) data to control for relief displacement, however LITP only accounts geometric corrections and are not corrected for atmospheric conditions which is the most important part of preprocessing of satellite imagery (specifically for spectral indices)

3.5 Methods of Data processing

3.5.1 Pre-processing

Landsat collection one level one L1TP Tier one data have the highest geometric and radiometric accuracy precisely the geo-registration/geo-referencing of Tier 1 scenes is consistent and within prescribed image-to-image tolerances of ≦ 12-meter radial root mean square error (RMSE). (https://www.usgs.gov/landsat-missions/landsat-collection-1) as a result of this geometric correction is not necessary. Yet the image has not been corrected for atmospheric condition different atmospheric condition like effects of clouds and aerosols had influence on the accuracy of time series analysis across space and time. therefore, atmospheric correction should be executed. besides to this each band DN should have to be converted to the actual surface reflectance and TOP of atmosphere brightest temperature (thermal case).

- **Radiometric Calibration**

Radiometric Calibration refers to the ability to convert the digital numbers recorded by satellite imaging systems into physical units. Those units are either radiance (W/m^2/sr/μm) or apparent top-of-atmosphere reflectance. It is required to improve the quality of image pixel values and provide a measurable physical unit of each pixel and to determine the true reflectance value of the earth surface. radiometric calibration was performed in ENVI software using Radiometric calibration tool and all the image were converted to radiance.

- **Atmospheric correction**

Irradiance is the downwelling radiation from the sun. Radiance is the upwelling radiation from the Earth to the sensor. Absorption reduces the intensity with a haziness effect. Scattering redirects EM energy in the atmosphere causing an adjacent effect where neighboring pixels are shared. These two processes affect the quality of an image and are the main driver for atmospheric correction. atmospheric correction may not be important for certain applications like, when conducting land cover classification for a single year, relative temperature difference. it is absolutely necessary when performing a time-series analysis for example, in comparing spectral characteristics of a pixel or group of pixels (an object) acquired on different dates, removal of the influence of atmospheric conditions prior to comparison is crucial. In the light of this all image is corrected for atmospheric condition through ENVI by means of FLAASH atmospheric correction using input from its metadata text file (MTL.txt) and scaled from 0 up to 1using the band math tool in ENVI. In FLAASH atmospheric correction require Radiometrically calibrated image as input. then produce atmospherically corrected surface reflectance image this atmospheric correction is only applicable for spectral band.

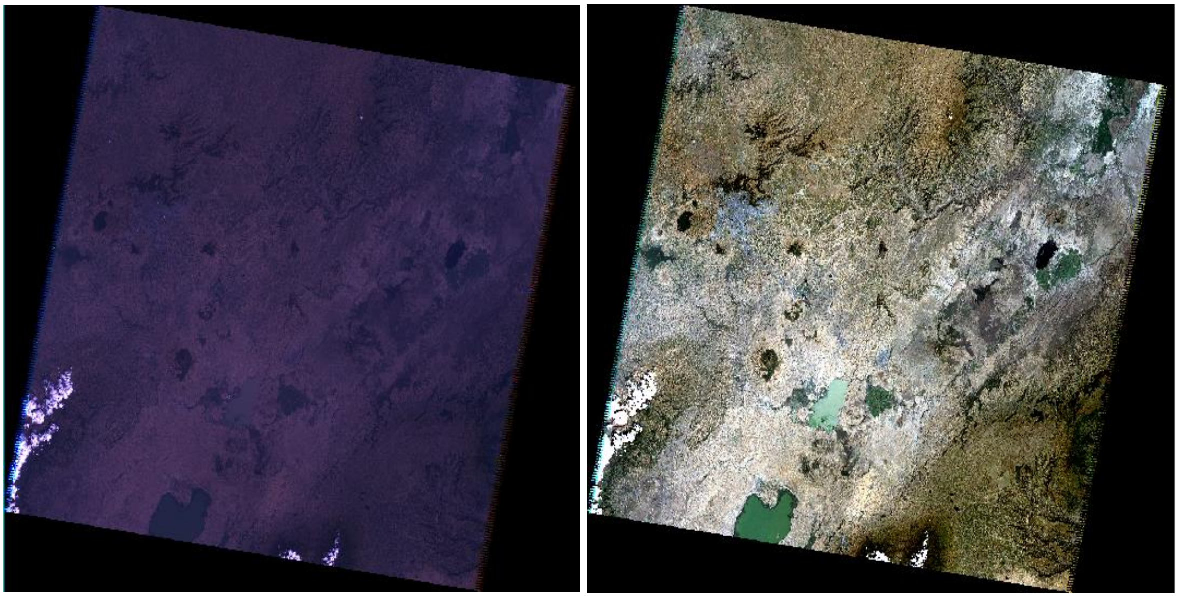

Figure 3.10 2010 Landsat image before atmospheric correction on the left and after atmospheric correction on the right

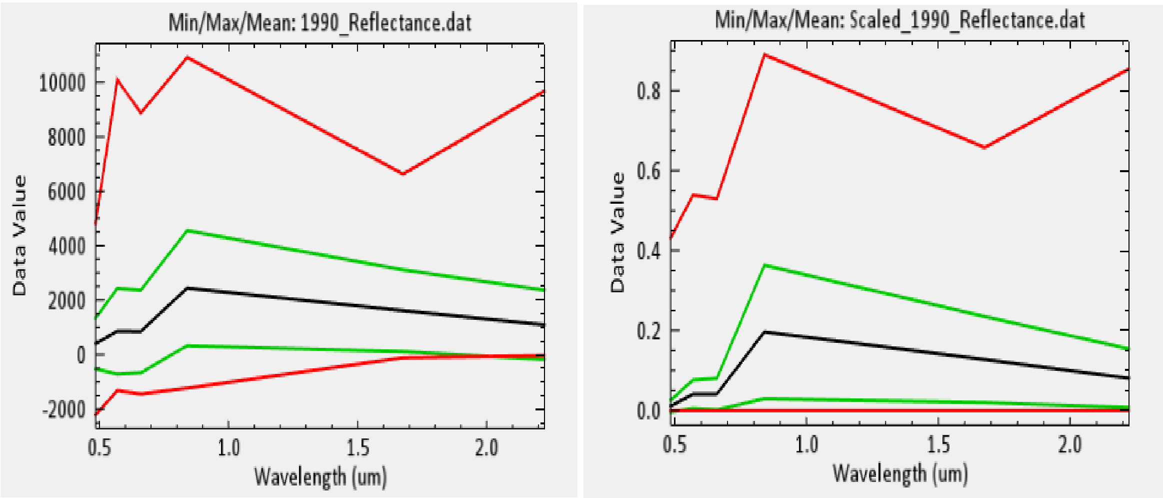

Figure 3.11 Un-scaled 1990 reflectance TM image on the left and Scaled (0-1) reflectance image of 1990 on the right

- **Scan line correction**

On May 2003 Landsat 7 ETM+ had a failure of scan line corrector which compensate the forward motion of Landsat as a result, imaged area is duplicated and causing the scanning pattern to exhibit wedge-shaped scan-to-scan gaps that range from a single pixel near the center of the image to about 14 pixels along the east and west edges of each scene on average (Maxwell et al., 2007). image in the third and fourth epoch have Scan line error, each scene losses about 22% of the image data. Nevertheless, the spatial and spectral quality of the remaining portion of the image is not diminished. (Wulder et al., 2008).

- **Gap filling method (**Scan line error correction**)**

A number of gap filling methods have been developed from the simple one for display purpose which is focal analysis. This method is designed to modify neighboring pixels in a single Landsat 7 SLC-off scene, creating a final aesthetic image only - no scientific analysis accuracy is guaranteed using this method (https://landsat.usgs.gov) up to the complex one for scientific analysis such as localized linear histogram match (LLHM), and adaptive window linear histogram match (AWLHM) (Scaramuzza et al., 2004), neighborhood similar pixel interpolator (NSPI) (J. Chen et al., 2011), Geostatistical Neighborhood Similar Pixel Interpolator (GNSPI) (J. Chen et al., 2011; M.J. Pringle & Muir, 2009; C. Zhang et al., 2007), Weighted Linear Regression (WLR) (Zeng et al., 2013) and Geographically Weighted Regression (GWR) method each of the above mentioned method have their own merits and flaws seeing that for this study the one developed by USGS which termed as Local linear histogram match is selected based on its simplicity and easy of rapid implementation.

- **Local Linear Histogram Match**

The U.S. Geological Survey (USGS) Earth Resources Observation Systems (EROS) Data Center (EDC) has developed multi-scene (same path/row) gap-filled products to improve the usability of Enhanced Thematic Mapper Plus (ETM+) data acquired after the May 31, 2003 Scan Line Corrector (SLC) failure. The initial gap-fill capability employs a histogram-based compositing algorithm designed to combine an SLC-off image with one or more SLC-off and/or SLC-on scenes. SLC-off gap-filled products were released in two phases. Phase 1 involved a local linear histogram matching technique. It allowed the user to choose one SLC-on scene for the fill image and was used for gap-filled products generated between 6/1/2004 to 11/18/2004 phase 2 is an enhancement of the Phase 1 algorithm that allows users to choose multiple scenes and to combine SLC-off scenes Phase 2 processing is used on all gap-filled products processed on or after 11/18/2004. (USGS Phase 2 Gap-Fill Algorithm).

Local histogram match applies a transfer function which converts the radiometric values of the fill scene into equivalent radiometric values of a primary scene. Then this transformed data is used to fill the gaps. The scene that the user selects to be used for the bulk of the data is defined as the primary scene. All valid data within the primary will be retained. The scenes the user selects to fill in the gaps in the primary scene are referred to as the fill scenes SLC off scene also used as fill scene for the primary scene because location of SLC off vary in each scene. In this study image acquired in 2010 and 2020 have both primary and fill scenes. Significant aspect for quality in LLHM method are selection of appropriate image to fill gap of the primary scene these images must be accurately co-registered with the primary scene, date and season must be near and same season as primary scene to avoid phenology impact. By considering this fill scene selected as much as near to the primary seen besides to this both the primary scene and fill scene are L1TP product having the same geometric accuracy so co-registration will not be an issue. SLC off is corrected in ENVI using an add-on module which is called as ***landsat_gapfill.***

Table 3.5 Primary and full scene Landsat Image

Scene type	Landsat Image ID	Date
Primary scene	LE07_L1TP_168054_20100928_20161212_01_T1	2010-09-28
Fill scene	LE07_L1TP_168054_20101014_20161212_01_T1	2010-10-14
Primary scene	LE07_L1TP_168054_20201009_20201104_01_T1	2020-10-09
Fill scene	LE07_L1TP_168054_20201025_20201120_01_T1	2020-10-25

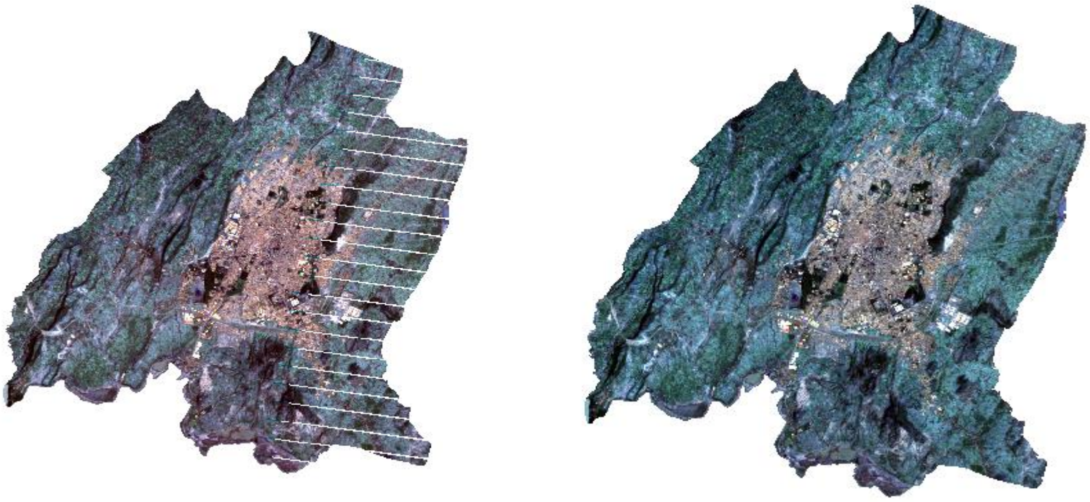

Figure 3.12 Adama city 2020 Landsat SLC off image on the left and corrected one image on the right using LLHM Method

- **Layer stacking and Reprojection**

Landsat satellite provide multispectral imagery: an image produced by a sensor that measure the reflected energy with in several specific section/band Separately each band have unique functions and characteristics. for the purpose of time series analysis this sections/band have to be combined/stacked as one in order to use the image in typical manner and to produce single multi band image. Besides to this each Landsat image should have to projected to the local reference Datum. Adindan in our study case. ENVI layer stacking tool and Reproject raster tool used for stacking individual band as one multispectral image and to project in to the local Datum system.

- **Subset/resizing of the study area**

The study area is Adama city so the recent structural plan of the city is used as a boundary to subset the study area section from the imagery.

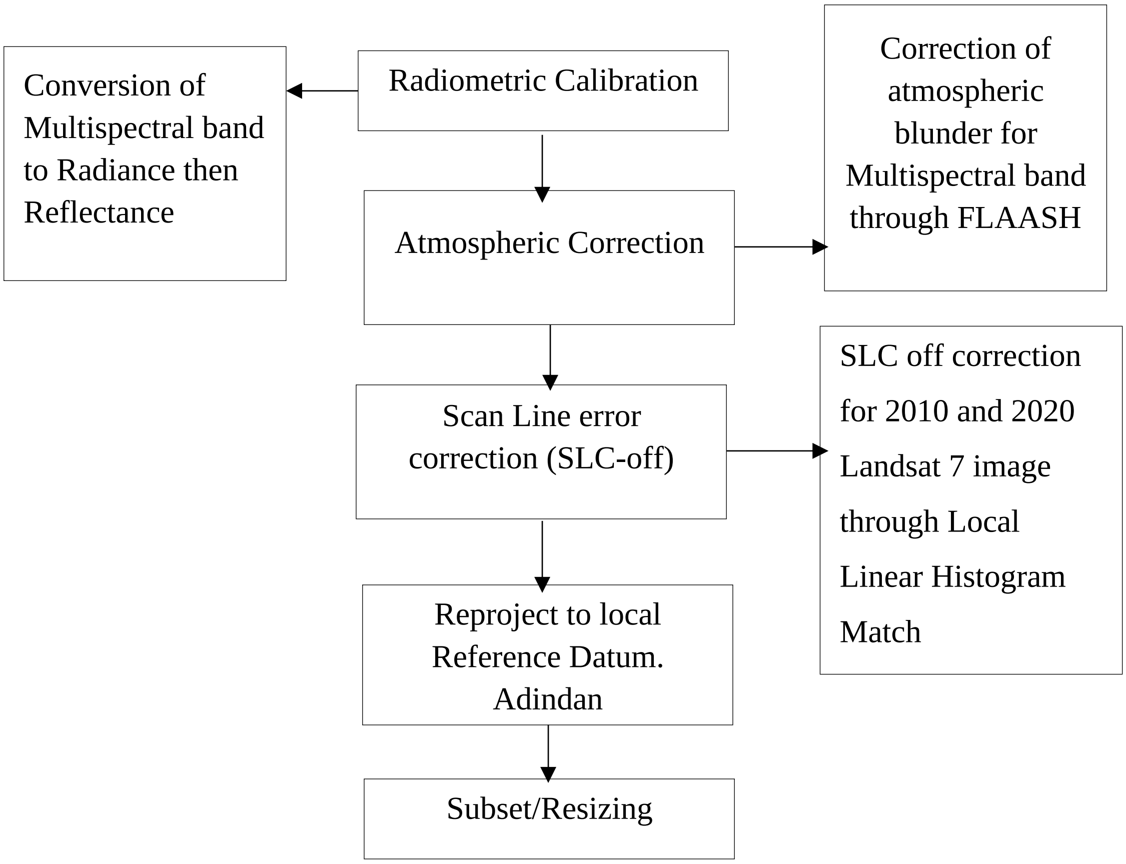

Figure 3.13 Image pre-processing

3.6 Methods of data analysis

3.6.1 Analysis of land use land cover dynamics

3.6.1.1 Land Use land cover Mapping

- **Defining Classification schema**

After carrying out review of previous literature, visual inspection (survey) of existed land cover type in the study area and on their significant impact on LST the following four LULC types were assigned to classify the study area land use land cover classes thus are Bare land, Vegetation, Built up and Agricultural Land. Their description is within the next (Table 3.6)

Table 3.6 Land Use land cover classes

LULC classes	Descriptions
Bare land	land which has very few plants and no trees
Vegetation	Encompasses plants (trees and shrubs) considered collectively, especially those found in a particular area
Agricultural land	land devoted for agricultural purposes
Built up	Land under houses, large building, industrial sites, warehouses, roads, and parking lot

Supervised image classification

For classifying the study area land use land cover supervised classification method is selected in the view of Errors can be detected by operators and they often remedy them and Expertise knowledge of the area is required, so this method will give the accurate result. In this classification, analyst(user) identifies examples of the Information classes (i.e., land cover type) of interest in the image. These are called "training sites". The image processing software system is then used to develop a statistical characterization of the reflectance for each information class. This stage is often called "signature analysis" and may involve developing a characterization as simple as the mean or the rage of reflectance on each band, or as complex as detailed analyses of the mean, variances and covariance over all bands. Once a statistical characterization has been achieved for each information class, the image is then classified by examining the reflectance for each pixel and making a decision about which of the signatures it resembles most.

- ***Training sample selection***

Good quality training data are needed to 'teach' the classifying software to recognize similar patterns in the imagery These represent only a small sample of the entire image/region to be classified

Evaluating Training data

Collected signature (Sample) should have to be tested before used for the classification purpose and There are tests to perform that can help determine whether the signature data are a true representation of the pixels to be classified for each class. There are number of methods for evaluation of the signatures for this study total sum of pixel in each ROI (class) and ROI separability are selected. based on rule of thumb the number of pixels in each training class at least should not be less than 100 times the number of spectral bands used. (Dr. Michael Govorov, Malaspina University College, with attribution to IDRISI) and ROI separability was determined by using the “Jeffries-Matusita and Transformed Divergence separability” measures, and a separability index was computed between each pair of training samples The values of ROI separability range from 0 to 2, and the value greater than 1.8 is often considered to be a high-quality training sample. Number of training sample (pixel in ENVI) and separability of Training sample is an important quality for the training sample in this study All the training sample satisfies Dr. Michael Govorov Minimum number of sample and Jeffries-Matusita and Transformed Divergence separability” measures, and a separability index.

Table 3.7 Number of training Pixel for classification

Pixel in (ROI)	1990	2000	2010	2010
Built up	2318	2816	4529	7943
Agricultural Land	14600	14600	14875	13045
Bare land	5749	4389	5173	9787
Vegetation	2864	3030	2851	5240

According to Dr. Michael Govorov rule of thumb number of pixels in each training class at least should not be less than 100 times the number of spectral bands used in the image for this study for Landsat 7 all band used except band 8 panchromatic and band 6 thermal band 6 similarly for Landsat 5 all band used except band 6 which is thermal band

Table 3.8 Separability of Training sample

Training (ROI) Separability	Maximum	Minimum
1990	1.89758557	1.80105339
2000	1.90164425	1.84796114
2010	1.91072337	1.85103832
2020	1.96265034	1.79953870

Likewise-separability of training sample evaluated through “Jeffries-Matusita and Transformed Divergence separability” measures, and a separability index was computed between each pair of training samples all training sample have separability index above 1.8.

- ***SVM Classification Algorithms***

For this study Support Vector Machine classification (SVM) algorithm is selected in the view of SVM algorithm doesn’t affect by training sample size and their distribution which is the most important in supervised image classification. moreover, it’s important for the problem of mixed pixel problem in urban area. Support Vector Machine (SVM) is a supervised classification method derived from statistical learning theory that often yields good classification results from complex and noisy data. It separates the classes with a decision surface that maximizes the margin between the classes. The surface is often called the optimal hyperplane, and the data points closest to the hyperplane are called support vectors. The support vectors are the critical elements of the training set.

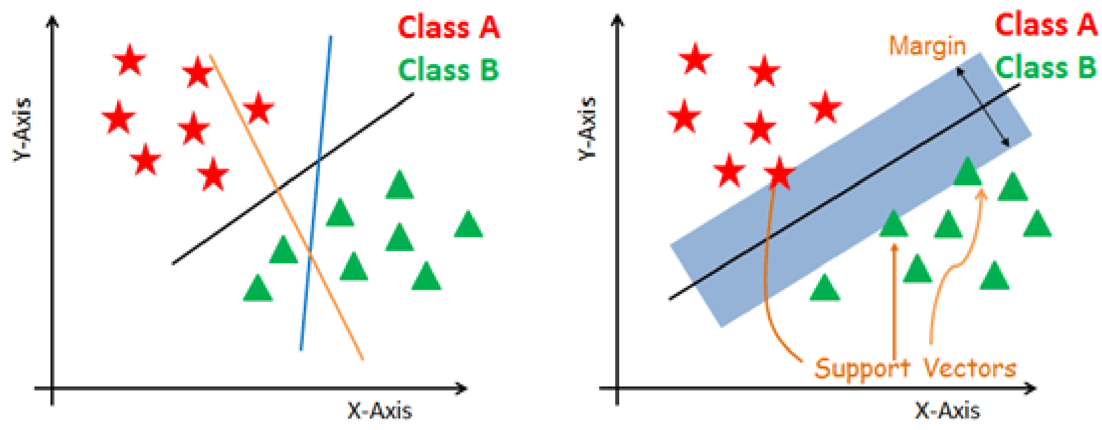

Figure 3.14 SVM classification (source scikit-learn)

SVM draws a decision boundary which is a hyperplane between any two classes in order to separate them or classify them

- ***Accuracy assessment***

Accuracy assessments determine the quality of the information derived from remotely sensed data The goal is to quantitatively determine how effectively pixels were grouped into the correct feature classes in the area under investigation. The accuracy assessment assesses how well a classification worked and understands how to interpret. The most common error estimate is the overall accuracy, while Kappa coefficient (K) is the measure of agreement of accuracy. It provides a difference measurement between the observed agreement of two maps and agreement that is contributed by chance alone. In this study accuracy assessment has performed in ENVI using Random Generated ground truth from ROIs while generating random sample point (Table 3.9) stratified random sampling type is used to control biased in sampling. ground truth ROIs is created using Google image as Reference. Then confusion matrix is created between the classified image and ground truth ROIs. To assess the accuracy of classified image. According to Rwanga & Ndambuki, (2017) kapa statistics that ranges between (0.81--1) are perfectly agreed between the refence and classified image.

Table 3.9 Number of Random sample points Generated for Accuracy assessment

LULC classes	Random sample point			
	1990	2000	2010	2020
Agricultural land	535	640	834	850
Bare land	353	488	754	582
Built-up	243	243	550	553
Vegetation cover	213	129	315	382

Producer's Accuracy measures the percentage of correctly classified pixels from a sample data or indirectly indicates errors of omission for a particular class. The number of correct sample units in a category was divided by the total number of sample units of that category from the reference data (i.e., the column total).

$$\textbf{Producer's Accuracy} = \frac{(Ci)}{(Ct)} \times 100 \text{.............. equation (1)}$$

Where, Ci = correctly classified sample locations of the reference data or column and Ct = total number of sample locations of the column.

User's Accuracy measures the total number of correct sample units in a category is divided by the total number of sample units that were classified into that category on the map (i.e., the row total). This result is a measure of commission error. It is calculated as:

$$\textbf{User's Accuracy} = \frac{(Ri)}{(Rt)} \times 100 \text{...................... equation (2)}$$

Where, Ri = correctly classified samples in the row and Rt = total number of samples in the row

Overall Accuracy was computed by dividing the total correctly (i.e., the sum of the correctly classified sample units) by the total number of sample units in the error matrix. This value is the most commonly reported accuracy assessment statistic.

$$\textbf{Overall Accuracy} = \frac{(Sd)}{(n)} \times 100 \text{....................equation (3)}$$

Where, Sd = sum of values along diagonal and, n = total number of samples.

Kappa statistics was used to measure the agreement or accuracy between the remote sensing derived classification map and the reference data.

$$\textbf{Kappa statistics} = \frac{N\sum_{I=1}^{K} nii - \sum_{i=1}^{k} ni+n+i}{N^2 - \sum_{i=1}^{K} ni-n-i} \text{................equation (4)}$$

Where K = number of rows in the error matrix; nii = number of observations in row i and column i (on the major diagonal); ni+ = total of observations in row i (shown as marginal total to right of the matrix); n+i = total of observations in column i (shown as marginal total at bottom of the matrix) and N = total number of observations included in matrix

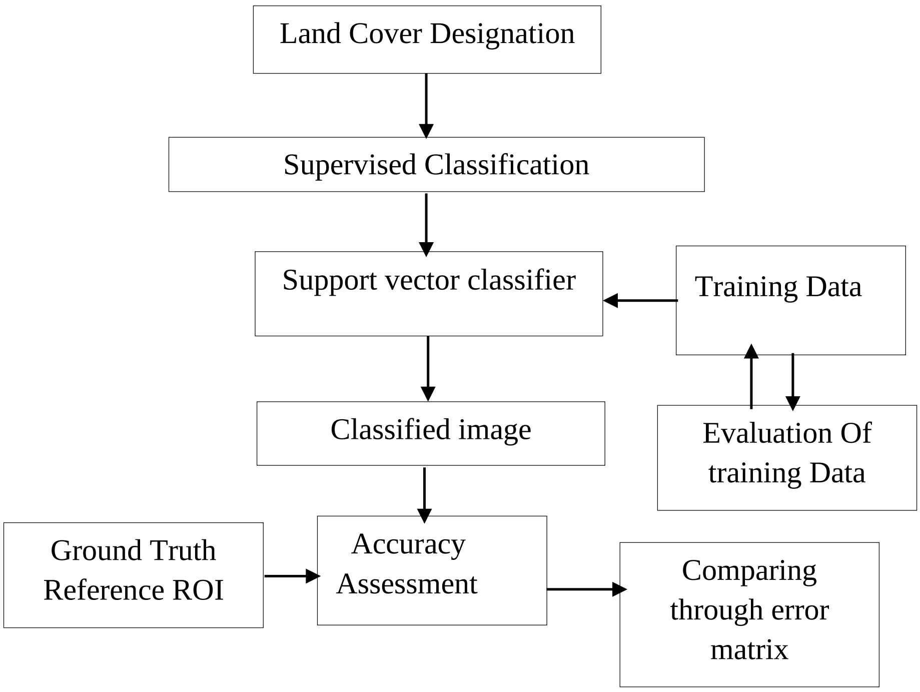

Figure 3.15 Land cover Classification schema

3.6.1.2 Land Use Land Cover Change detection

Remote sensing change detection technique is a set of basic operations applied on the analysis units of two or more remote sensing data sets representing the same geographic area at different times. Spectral Change analysis were conducted using post classification image comparison technique (thematic change in ENVI). Post classification change analysis assumes we are given two images covering the same scene, taken at two different times with the same acquisition conditions. The Already stated method selected in order to minimize possible effects of atmospheric variations and sensor differences and it was found to be the most suitable for detecting land use/land cover change. Change statistics were computed by comparing values of area of one data set with the corresponding value of the second data set in each period. As stated in Butt et al (2015) change and percentages of change detection of LULCC were calculated using the following equations.

$$Observed\ Change\ (\Delta) = A_2 - A_1 \text{……………………equation(5)}$$

$$Percentage\ of\ change\ (\Delta\ \%) = \frac{A_2 - A_1}{A_1} \times 100 \text{…………..….. equation(6)}$$

Persistence, swap and Net change (Gain/loss)

Persistence is the land-use class that does not change from time T_1 to time T_2. (Shaded diagonal in table 4.3,4.4 and 4.5) Swap is the simultaneous loss and gain of land use class in a landscape. Gain is the amount of land use/cover Class added to specific class of land use/cover type between the change time (T_1 and time T_2). it is residual from the difference between total class in T_2 and Persistence, whereas loss is the amount of land use/cover class loosed by specific land use/cover type Between the change time (T_1 and time T_2). The remaining from the difference between total class in T_1 with persistence. (Tesfaye et al., 2021), All of the above mention persistence, swap, loos, gain and net change are calculated based on changes on class level.

3.6.2 Analysis of Landscape pattern and its dynamics

Spatial/configuration change were analyzed using spatial metrics: which are numerical indices that give a good indication of urban sprawl and used to describe structure and pattern of landscape. Spatial metrics use patches as a basic unit or element to measure landscape structure and pattern. Patches are defined as discreet areas of homogeneous environmental conditions in a landscape (McGarigal, 2015; Reis et al., 2016). The shape, size and division or isolation of patches are important characteristics to measure a landscape under investigation. the study sought to examine the change in configuration of land cover and their impact on land surface temperature.

3.6.2.1 Selection of Spatial metrics

Spatial metrics come from the concept of landscape metrics which were developed in the late 1980s and incorporated measures from both information theory and fractal geometry based on a categorical, patch-based representation of the landscape. Patches are defined as homogenous regions for a specific landscape property of interest, such as “industrial land”, “park” or “high-density residential area”. Landscape metrics are used to quantify the spatial heterogeneity of individual patches, all patches belonging to a common class, and the landscape as a collection of patches. When applied to multi-scale or multi-temporal datasets, the metrics can be used to analyze and describe the changes in the degree of spatial heterogeneity (Dunn et al, 1991; J. Wu et al., 2000) In the application to urban domain, Herold et al., (2003) pointed out that the approaches and assumptions might be more generally described as “spatial metrics”.

In general, pattern metrics should fulfill the following criteria they should not be correlated with other pattern metrics, they should be capable of capturing changes in landscape pattern over space and time, be insensitive towards the spatial resolution of remote sensing data, and be insensitive towards the number of land cover classes used. (Sinha et al., 2016). in considering this 9 metrics selected (Table 3.10) regarding their usability for change in both composition and configuration and structure of land cover and their impact on LST.

Table 3.10 Selected spatial metrics

Characteristics		Metrics	Range	Unit
Composition	1	PLAND	0 < % LAND ≤ 100	Percent
Configuration/fragmentation	1	ND	ND > 0	Meter
	2	ED	ED >= 0	Meters per hectare
	3	AI	0 <= AI <= 100	Percent
	4	PD	PD>0	Number per 100 hectares
	5	NP	NP≥1	None
Structure/Shape	1	PAFRAC	$1 \leq PAFRAC \leq 2$	None
	2	FRAC_MN	1≤MPFD≤2	None
	3	Core area index MN	0≤CAI<100	Percent

- **Description of metrics**

Percentage of Landscape (PLAND) quantifies the proportional ratio of each patch type in the landscape. It equals the sum of the area (m^2) of all patches of the corresponding patch type, divided by the total landscape area (m^2), and multiplied by 100 (to convert to percentage)

Edge density (ED): this metric describes the configuration of the landscape because an overall aggregation of classes will result in a low edge density. ED = 0 if only one patch is present and increases, without limit, as the landscapes becomes more patchy

Aggregation index (AI): the number of like adjacencies divided by the theoretical maximum possible number of like adjacencies for that class summed over each class for the entire landscape. Equals 0 for maximally disaggregated and 100 for maximally aggregated classes

Patch density (PD): describes It describes the fragmentation the landscape. PD Increases as the landscape gets patchier.

Number of Patch (NP); number of patches is a simple measure of the extent of subdivision or fragmentation of the landscape pattern it's the number of patches of the corresponding class type

FRAC_MN; the mean of the fractal dimension index of all patches in the class/landscape FRAC_MN = 1 if all patches are squared and FRAC_MN = 2 if all patches are irregular, it overcomes one of the major limitations of the perimeter-area ratio (holding shape constant an increase in patch size will cause a decrease in the perimeter-area ratio.)

PAFRAC; PAFRAC is a 'Shape metric'. It describes the patch complexity of specific class while being scale independent (Limitation of perimeter-area ratio). This means that increasing the patch size while not changing the patch form will not change the metric.

Core area index; CAI is a 'Core area metric'. It equals the percentage of a patch that is core area. A cell is defined as core area if the cell has no neighbor with a different value than itself more core area when the patch is large and the shape is rather compact, i.e., a square

3.6.2.2 Changes in landscape composition and configuration

To understand change in composition and configuration of LULC in the study area at the landscape and class level, FRAGSTATS (v. 4.2.1) was used (Zeller et al., 2012). It calculates a large set of landscape metrics for an area into elements such as patch density, shape, core area, diversity, contagion, and interspersion (Dewan et al., 2012). for these section spatial metrics are computed without sampling strategies using 8-cell neighborhood rule Because of this particular section concerned only about analyzing change in configuration and composition of landscape.

Nearest Distance (ND)

Like as previously stated, nearest distance is not spatial metrics but shows the change in the Configuration of specific land cover in the landscape through some temporal ranges. For this study nearest distance is used to assess the change in mean distance between 100 random generated point and nearest available vegetation patch (change in configuration of Vegetation) in the study area from 1990 to 2020.

Near Distance is Calculated in ArcGIS environment through near analysis tool. To do these 100 random points was generated in ArcGIS then the nearest distance between this Randomly generated points and vegetation land cover patch was calculated using near tool for each epoch then mean nearest distance was used to assess the trend. of configuration of vegetation land cover in Adama city in the past 30 years.

Spatial pattern of vegetation land cover

FRAGSTATS is a program designed to compute a wide variety of landscape metrics for categorical map patterns (McGarigal et al., 2002). To figural materialize spatial pattern of vegetation cover of adama city the study employed Moving window analysis in FRAGSTATS Software with a window shape square and size 300 m, also the study used 8-cell rule which considers all eight adjacent cells that share a side with the focal cell in moving window analysis the window moves over the landscape one cell at a time, calculating the selected metric within the window and returning that value to the center cell and output a new continuous surface grid map for each selected metric (McGarigal et al., 2002) and generating the results as a new grid for each selected metric. four class level spatial metrics including aggregation index, patch density, FRAC_MN and Edge density were used to depict the spatial pattern of Vegetation cover in adama city. metrics were selected due to their potential impact in LST.

3.6.2.3 Computation of indices

NDVI and NDBI were used to characterize land cover class associated with LST. NDVI was used in the previous study for monitoring drought, agricultural production and vegetation density (X. L. Chen et al., 2006; Faqe Ibrahim 2017), while NDBI is sensitive to the built-up area and used as an indicator of built-up extent (Sruthi & Aslam, 2015; Lopresti et al., 2015; Gandhi et al., 2015).

Normalized Difference Vegetation Index (NDVI)

One of the most commonly used urban climate indicators in environmental studies is the Normalized Difference Vegetation Index (NDVI), which serves as a reliable index for extracting vegetation conditions of remotely sensed data. the study employed NDVI to examine the city vegetation distribution and extract emissivity values. NDVI was calculated following Townshend and Justice (1986) equation. NDVI value varies from−1 to+1:

$$NDVI = \frac{(NIR-RED)}{(NIR+RED)} \text{……..……………………………. equation (7)}$$

where NIR is near infrared band of the image (band 4) and RED is red band of the image (band 3)

Normalized Difference Built-Up Index (NDBI)

The Normalized Difference Built-up Index (NDBI) is another vital urban climate indicator for environmental monitoring This serves as an effective method of mapping and analyzing land uses by providing information on the spatial extent of built-up areas and impervious surfaces. The NDBI designates built-up area's density in unit pixel, with values ranging from positive 1 to negative 1. The negative values often signify vegetation, while the positive denotes built-up urban/impervious surfaces

$$NDBI = \frac{(SWIR-NIR)}{(SWIR+NIR)} \text{……..…………………….……..…. equation (8)}$$

where SWIR is shortwave infrared band of the image (band 5) NIR is near infrared band of the image (TM band 4)

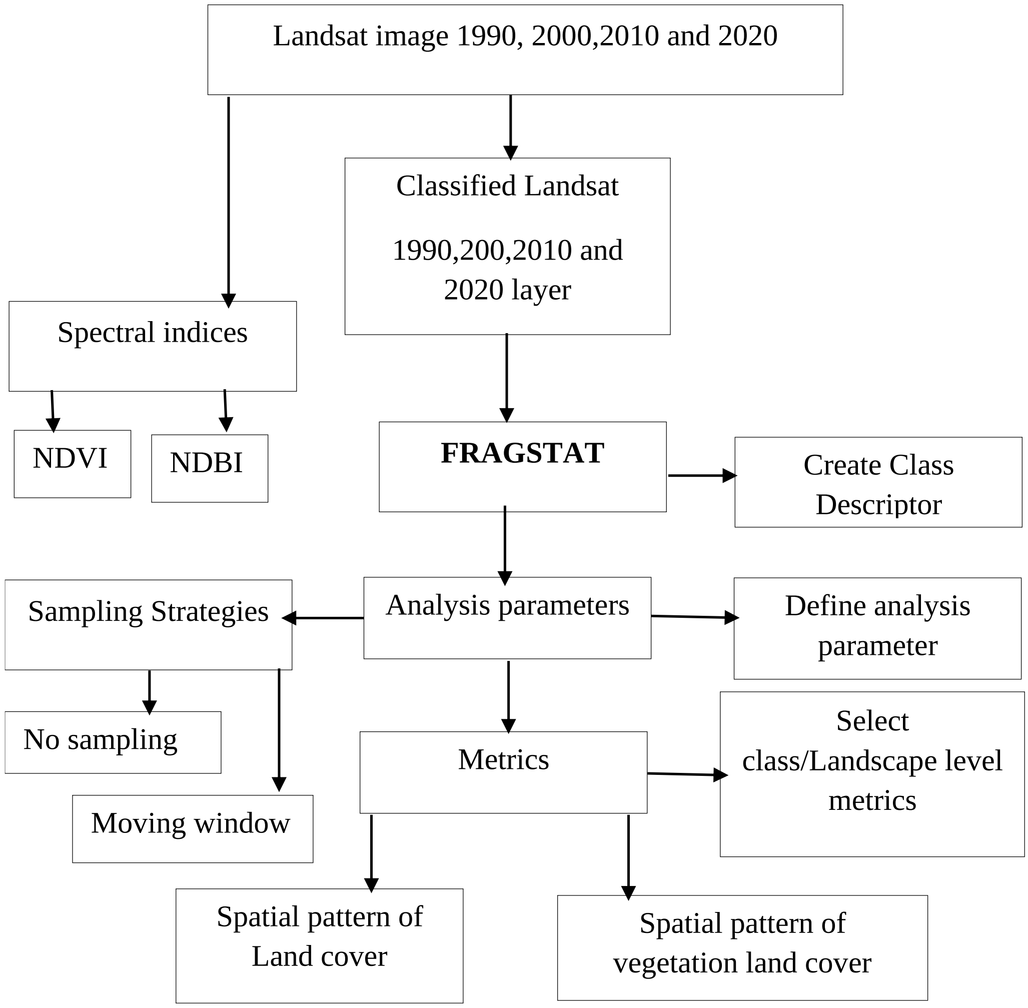

Figure 3.16 landscape pattern Dynamics

3.6.3 Spatiotemporal variations of LST

Land surface temperature (LST) is a fundamental parameter closely associated to many lands surface processes and surface-atmosphere interactions. Analysis of spatiotemporal variation of LST may provide important information to understand eco-climatic properties. the spatiotemporal pattern of LST in Adam city were analyzed based on Landsat Retrieved LST products from 1990 to 2020.

3.6.3.1 Land surface temperature (LST) derivation

Land surface temperature (LST) has a significant role in the land surface characters on local and global scale. The most important task in estimation of LST from satellite thermal data is removing the effects of atmospheric attenuations, topographic and land surface emissivity (Sattari & Hashim, 2014). the study employed Landsat 5 and 7 thermal infrared (TIR) bands to retrieve and map the study area's LST. In this study Emissivity corrected Plank's equation Land Surface Temperature Retrieval Method is selected because of the scheme doesn't require real time atmospheric parameters to compute land surface temperature the method comprises four main procedures Conversion of DN to at sensor radiance, Conversion of at sensor radiance to Top of atmosphere Brightest temperature, Estimation of Emissivity and Estimation of Emissivity corrected LST.

Accurate' LST is mostly dependent on two factors, namely atmospheric correction and emissivity however in this study Atmospheric correction for thermal band is not considered. In fact, the error due to an error in the emissivity correction is two times larger than that due to an error in the atmospheric correction (Prata et al., 1995), and more importantly the study is concerned about impact of land use/cover dynamics on land surface temperature and the relative surface temperature differences between urban center and the surrounding area not about the absolute values of Land surface Temperature besides to these Since the SUHI effect is studied in a spatial extent of a few kilometers around the city center (local scale) it is reasonable to assume the homogeneity of the atmosphere over the urban area

Conversion of DN to TOP of Atmosphere (TOA) Radiance.

Digital number (DNs) store thermal data in the Landsat sensor and deliver a manner of representing signifying pixels that have not yet been calibrated and converted into radiance units (How Jin Aik et al., 2020). The metadata file included within the satellite imagery bundle is used to convert the digital number (DN) values into radiance

Converting DN values to a measure of radiance is an important step toward using remote sensing data in a quantitative way – in which the values in each cell have actual physical meaning pixels are converted from DN to units of absolute radiance using 32-bit floating-point calculations. The following equation is used to convert DNs in a Level 1 product back to radiance units:

$$I_\lambda = Grescale \cdot QCAL + Brescale \text{ ....equation (9)}$$

Which is also expressed as:

$$I_\lambda = \left(\frac{LMAX_\lambda - LMIN_\lambda}{QCALMAX - QCALMIN} \right) \cdot \left(QCAL - QCALMIN \right) + LMIN_\lambda \text{ . equation (10)}$$

Where L_λ is Spectral radiance at the sensor's aperture in (Watts/(m² * sr * µm)), *Grescale* is Rescaled gain (the data product "gain" contained in the Level 1 product header or ancillary data record) in (Watts/(m² * sr * µm))/DN, *Brescale* is Rescaled bias (the data product "offset" contained in the Level 1 product header or ancillary data record) in (Watts/(m² * sr * µm)),

QCAL is Quantized calibrated pixel value in DN, $LMIN_\lambda$ is Spectral radiance scaled to QCALMIN in (Watts/ (m² * sr * µm)), $LMAX_\lambda$ is Spectral radiance scaled to QCALMAX in (Watts/ (m² * sr * µm)), QCALMIN is Minimum quantized calibrated pixel value (corresponding to $LMIN_\lambda$)

DN:

- = 1 for LPGS products
- = 1 for NLAPS products processed after 4/4/2004
- = 0 for NLAPS products processed before 4/5/2004

QCALMAX = Maximum quantized calibrated pixel value (corresponding to $LMAX_\lambda$) in DN = 255). (*Landsat 7 Data Users Handbook*, 2019).

Conversion to TOP of Atmosphere Brightest temperature.

Thermal data can also be converted from spectral radiance (as described above) to brightness temperature, which is the effective temperature viewed by the satellite under an assumption of unity emissivity.

$$B_{top}(^\circ K) = \frac{K_2}{\ln(\frac{K_1}{I_\lambda}+1)} \quad \text{……………………………...equation (11)}$$

Where B_{top} = Top of atmosphere brightness temperature (K), I_λ = Top of Atmosphere spectral radiance (Watts/(m^2 * srad * µm)), K1 = Band-specific thermal conversion constant from the metadata (K1_CONSTANT_BAND_x, where x is the thermal band number) and K2 = Band-specific thermal conversion constant from the metadata (K2_CONSTANT_BAND_x, where x is the thermal band number)

Estimating Land surface Emissivity.

LSE is defined as the ratio of the power radiated by a surface with a given temperature to the power radiated by the ideal black surface with the same temperature, simply stands for the surface ability that transforms heat energy into radiant energy. LSE (ε) is one of the key parameters to retrieve accurate LST from remotely sensed imagery. correctly estimating of LST is crucial. For this study NDVI based semi empirical method was employed to estimate the emissivity from the imagery. Since Classification based emissivity method Requires a priori knowledge of emissivity database for classes, as well as the corresponding classification map (Gillespie, 1996)

NDVI Thresholds Method

The method proposed obtains the emissivity values from the NDVI considering different cases. (J. Sobrino et al., 2004). However, this method has some flaws such as lack of continuity for emissivity values at NDVI since they are calculated in different ways. In spite of those drawbacks still the method is operative.

(a) NDVI < 0.2

In this case, the pixel is considered as bare soil and the emissivity is obtained from reflectivity

values in the red region.

(b) NDVI >0.5

Pixels with NDVI values higher than 0.5 are considered as fully vegetated, and then a constant

value for the emissivity is assumed, typically of 0.99

(c) 0.2≤ NDVI ≤ 0.5

In this case, the pixel is composed by a mixture of bare soil and vegetation, and the emissivity is calculated according to the following equation:

$$\varepsilon = \varepsilon_v + p_v + \varepsilon_s(1 - p_v) + d_\varepsilon \text{ ....equation (12)}$$

Where εv is the vegetation emissivity and εs is the soil emissivity, P_v is the vegetation proportion obtained according to (Carlson & Ripley, 1997):

$$P_v = \left[\frac{NDVI - NDVI_{min}}{NDVI_{max} - NDVI_{min}} \right]^2 \text{ …………………… equation (13)}$$

The term $d\varepsilon$ in includes the effect of the geometrical distribution of the natural surfaces and also the internal reflections. For plain surfaces, this term is negligible, but for heterogeneous and rough surfaces, as forest, this term can reach a value of 2%. A good approximation for this term can be given by

$$d_\varepsilon = (1-\varepsilon_s)(1-p_v)F\varepsilon_v \text{ …………………………equation (14)}$$

where F is a shape factor (J. Sobrino et al., 1990) whose mean value, assuming different geometrical distributions, is 0.55. Taking into account Equations and, the LSE can be obtained as

$$\varepsilon = mP_v + n \text{ …………………………………… equation (15)}$$

Where $m = \varepsilon_v - \varepsilon_s - (1-\varepsilon_s)F\varepsilon_v$ and $n = \varepsilon_s + (1-\varepsilon_s)F\varepsilon_v$ ………… equation (16)

In order to apply this methodology, values of soil and vegetation emissivity’s are needed. To this end, a typical emissivity value of 0.99 for vegetation has been chosen.

The choice of a typical value for soil is a more critical question, due to the higher emissivity values variation for soils in comparison with vegetation ones. A possible solution is to use the mean value for the emissivity’s of soils included in the ASTER spectral library (http://asterweb.jpl.nasa.gov). In this way considering a total of 49 soils spectra, a mean value of 0.973 (with a standard deviation of 0.004) is obtained. Using these data soil and vegetation emissivity’s of 0.97 and 0.99, respectively. (J. A. Sobrino et al., 2004).

$$\varepsilon = 0.004P_v + 0.986 \text{ ……………………………equation (17)}$$

Modified threshold NDVI method of estimation is further modified and called as simplified-$NDVI^{TMH}$ In this method the problem of lack of continuity for emissivity values at NDVI for both $NDVI_S$ and $NDVI_V$ since they are calculated in different ways. not any more a problem because the cavity term is not considered (for the case of $NDVI_V$ since the cavity term given by $NDVI^{TMH}$ is not applicable when NDVI > NDVIv), and the expression for the surface emissivity when NDVI < NDVIs is just reduced to the soil emissivity. These simplifications, hereinafter referred to as $SNDVI^{THM}$ (simplified $NDVI^{THM}$). (J. Sobrino et al., 2008). However, it is only applicable for Landsat 5.

Emissivity corrected LST

To retrieve the LST values, the at-satellite TBs need to be scaled using land surface emissivity values. After creating the emissivity images, the emissivity-corrected LST values were extracted as follows

$$LST(^{\circ}C) = \frac{K_2}{\ln(\frac{\varepsilon_\lambda K_1}{I_\lambda}+1)} - 273.15 \quad \text{equation (18)}$$

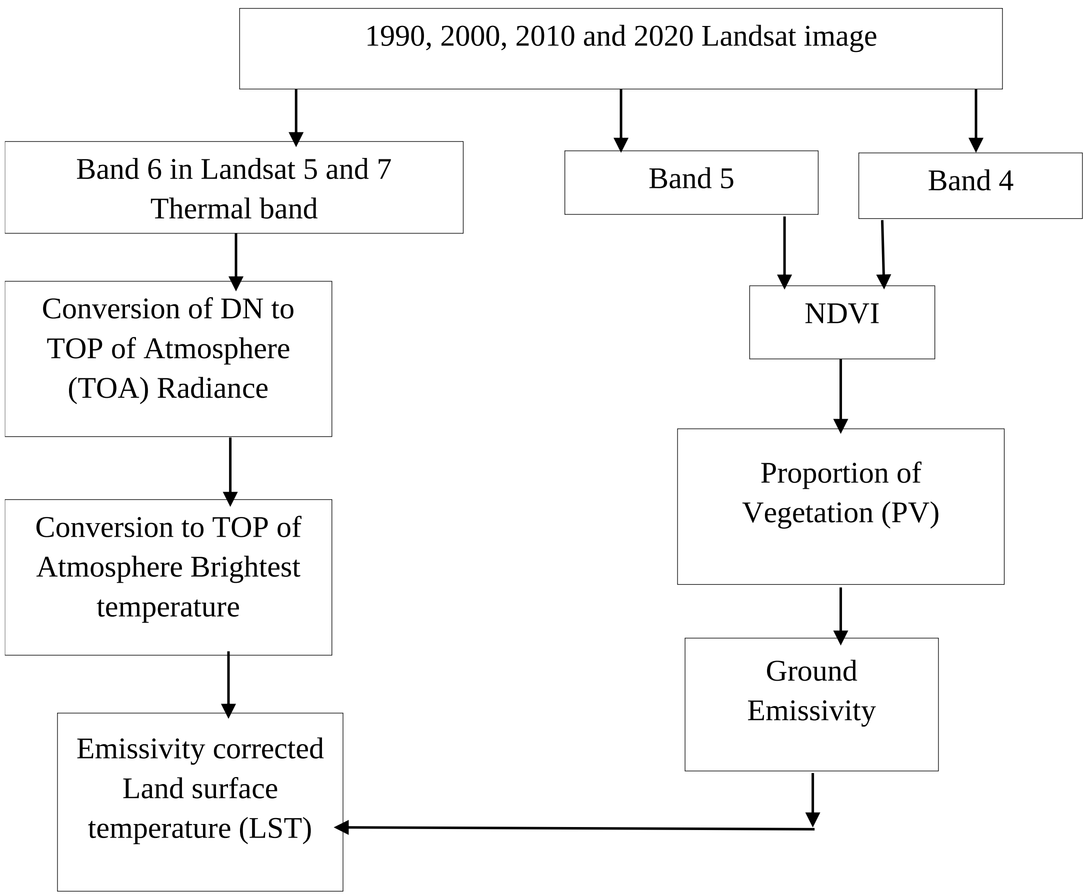

Figure 3.17 Land Surface Temperature Derivation

Validation of the retrieved LST

Validation of the retrieved LST is important which substantially assure the quality of the retrieved LST product. For this study ground based and satellite base validation approached were used to assess the validation of retrieved LST using in suite data collected with Adama station and MODIS Land surface product.

ASTER data have better spatial resolutions than MODIS but data are acquired when tasked and the telescopes on the ASTER sensor can be pointed to each side to expand data collection opportunities. As a result, ASTER images do not have regular and repeating path and row footprints as many other sensors have. As result of this ASTER is not suitable/challenge for time series analysis.

Ground based validation is conducted using descriptive Statistics while satellite based intercomparison conducted using accuracy indicators Root Mean Square Error (RMSE) and precision indicator Standard deviation (STD). MODIS LST product obtained from the Earth Data website was downscaled multiplying by 0.02 then, a total of 50 random points were generated in ArcGIS with Buffer radius of 100 then LST values of both MODIS and Landsat were extracted to the generated buffered point of each study year. Then, for the sake of comparison and validation with the original Landsat 7 ETM^+ and Landsat 5 TM LST result MODIS is resampled to 30m spatial resolution to match with Landsat LST product using bilinear interpolation on ArcGIS because It is suitable for continuous data. Eventually, the difference between the MODIS LST product and retrieved LST was computed for each of the generated points. MODIS data were available starting from the year 1999 as a result of this satellite-based validation for the year of 1990 is not available. to avoid impact of seasonal variations MODIS image area acquired with similar season as Landsat.

3.6.3.2 Change in Land surface temperature

Descriptive statistics, such as percentage, range, and mean were used to analyze the changes in land surface temperature of the study area from 1990-2020 mean, range, and standard deviation of each LST change were calculated using ArcGIS software then spatial distribution of LST with classified temperature range was derived from the retrieved LST of summer seasons in order to analyze the change and proportion of LST coverage

3.6.3.3 Urban rural gradient analysis

The ideal choice is to define the urban area based on the physical extent of the built-up land (impervious surface), as done in the majority of remote sensing urban studies. Urban development patterns of Adama city are based on single-core concept therefore, the study used the concentric ring gradient analysis method to study the spatial patterns of LST along the urban–rural landscape of the city. considering this, Deraritu roundabout around “postabet” is selected as city center because of all of the three main gate to and from Adama meet at this roundabout besides to this most old building of the city found around this core center. then multiple concentric rings created around the city center with a distance intervals of 300 m. Subsequently, Built-up Coverage is calculated in each concentric ring then zones which contained Built-up coverage more than 15% of the total ring area considered as urban zone while those covered less than 15% considered as rural zone therefore 6 buffer zone form image 1990, 8 buffer zone form image 2000, 12 buffer zone from image 2010 and 18 Buffer zone from image 2020 became urban zone out of the total 47 urban-rural buffer zones. (Figure 4.12) similarly the Mean LST determined in each ring and plotted across the urban–rural gradient.

3.6.3.4 Surface urban heat island

Surface urban heat island is the variation in surface temperature between urban area and suburban area. It is among the most evident aspects of human impacts on the earth system. the study assesses the variation of surface temperature in Adama city using the following Formulas.

$$SUHI = LST\mathrm{u} - \mathrm{L}ST_{\mathrm{r}} \ldots\ldots\ldots\ldots\ldots\ldots\ldots\ldots \text{ equation (19)}$$

where LSTu is the mean land surface temperature of an urban zone, and LSTr is the mean Land surface temperature of the neighboring rural zone

However, to understand the variation in the distribution of Land surface temperature with in the city it is important to analyze the intensity of SUHI with in each buffer rings along the urban and as well as rural setting Instead of simple describing the discrepancy in surface temperature between urban and rural zone.

SUHI intensity is a well-known measure of the SUHI effect across the urban–rural landscape. It is generally defined as the difference in temperature between each urban concentric zone and rural concentric zones. The SUHI intensity is calculated using either air temperature from meteorological data (Levermore et al., 2018) or mean surface temperatures using satellite images (Estoque et al., 2016). Analyzing SUHI intensity patterns and their urban and rural area variations has remained an imperative part of SUHI studies (Martin-Vide et al., 2015).

Using zonal statistics mean LST of each ring calculated. Then SUHI intensity calculated by calculating the difference between the mean LST at the city center (i.e., the kilometer 0) and the mean LST in each of the 300 m concentric zones across the urban–rural landscape. The following Equation was used to calculate the SUHI intensity of Adama city:

$$\text{SUHI intensity} = \mu LST0 - \mu LSTi \ldots\ldots\ldots\ldots\ldots\ldots\ldots\ldots \text{ equation (20)}$$

where μLST_0 is the meter 0 mean LST at the city center and μLST_i is the mean LST in each buffer zone, where i = 1,2,3…. n and n are the total number of buffer zones.

3.6.4 Statistical analysis

3.6.4.1 Correlation Analysis

The relationship between LST and the spatial patterns of vegetation land cover (PD, ED, AI and FRAC MN) and land cover spectral indices (NDVI and NDBI) was evaluated using Pearson correlation analysis. To avoid Miscorrelation between NDBI and LST due to lower ability of NDBI to separate Bare land cover over Built-up, random sample point sites on bare land cove were replaced by repeatedly performing the random sample point generation from NDBI

A sample of 100 randomly generated point with Buffer radius of 200 meter for spectral indices and 300 meters for vegetation land cover configuration metrics were used to investigate the Linear relationship between LST with Vegetation land cover configuration metrics and Land cover of Spectral indices. The mean Value of spectral indices, Vegetation land cover configuration metrics and LST were extracted with in each buffer ring then Pearson correlation analysis was implemented using SPSS software package. The study compares the **p**-value to the established significance level in order to reasonably conclude that changes in land cover and vegetation land cover spatial pattern effect variations in land surface temperature, positive and negative numbers suggest a direct and indirect association, respectively. Furthermore, like Bulti & Assefa, (2019) the correlation intensity was characterized using the absolute value of the correlation coefficient: very weak (|r| 0.19), weak (|r| 0.39), moderate (|r| 0.59), strong (|r| 0.79), and very strong (|r| 1). A **p**-value is a statistical measurement used to validate a hypothesis against observed data. for engineering studies, a significance level (also known as alpha or α) of 0.05 was typically acceptable. An α of 0.05 indicates that the risk of concluding that a correlation exists—when, actually, no correlation exists—is 5%.

3.6.4.2 Regression Analysis

Regression analysis is a set of statistical methods used for the estimation of relationships between a dependent variable and one or more independent variables. It can be utilized to assess the strength of the relationship between variables. Simple and Multiple linear regression models were built to select the best model that describes the highest variance in LST due to spatial pattern of Vegetation land cover. in the regressions LST was used as the dependent variable, and area and edge of vegetation cover, shape of Vegetation Cover and Aggregation were used as independent variables. 7 Models were constructed and compared. The models describe LST as a function (1), Each individual configuration metrics (2), in paired (3) and in threefold the model examines the explanatory power of configuration variables on LST, as well as their relative predictive importance and whether a combination of different configuration variables could yield better predictions of LST. particular, the study investigated whether adding configuration variables could significantly improve the model to predict LST. Before multiple linear regression analysis performed determinant factors (Vegetation land cover configuration Metrics) had to fulfill criteria of Normality and collinearity

Normality Test

Normal distribution, is a probability distribution that is symmetric about the mean, showing that data near the mean are more frequent in occurrence than data far from the mean for the continuous data, data that definitely does not meet the assumption of normality is going to give poor results Normality of the independent/predictor variable assessed using SPSS Kolmogorov-smirnov test, according to the test if P(**sig)** value < o.o5 the variable doesn't follow normal distributions.

Collinearity Test

Multicollinearity refers to a situation in which more than two explanatory variables in a regression model is highly linearly related. happens when independent variables in the regression model are highly correlated to each other the study used Variance Inflation Factor (VIF) in SPSS to check multi-collinearity. It is a measure of multicollinearity in the set of multiple regression variables. The higher the value of VIF the higher correlation between this variable and the rest. If the VIF value is higher than 10 and tolerance < 0.1, it is usually considered to have a high correlation with other independent variables

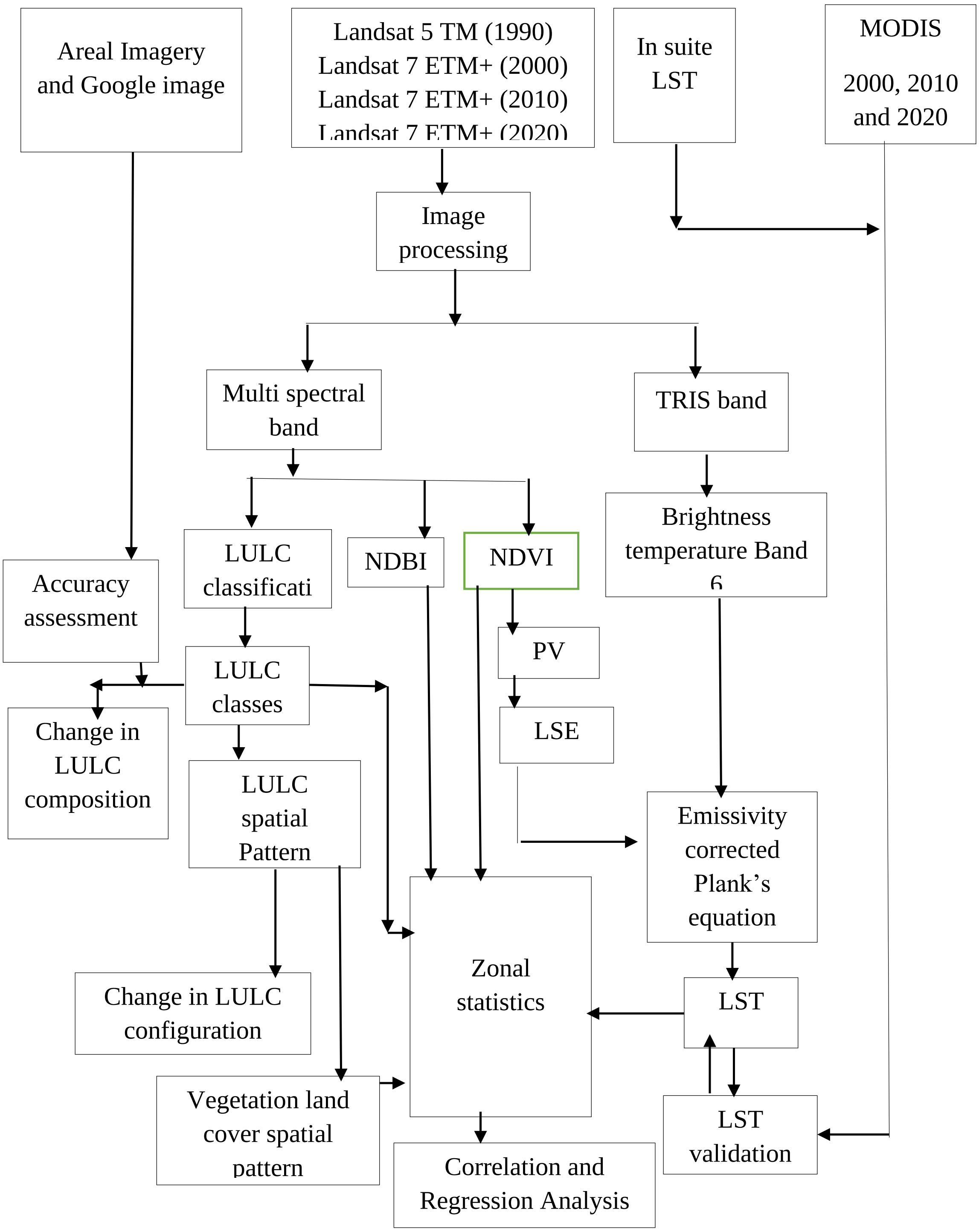

Figure 3.18 Schematic methodology flowchart of the present study

CHAPTER 4: RESULT AND DISCUSSION

4.1 Dynamics of Land use land cover

4.1.1 Accuracy of Image classification

Land-use and land-cover accuracy assessment for 1990, 2000, 2010 and 2020 years produced the overall classification accuracy of 87.5%, 87.2%, 88.62% and 88.5%, respectively. The overall land-use and landcover classification Kappa statistics for the study periods were 0.8244, 0.8118, 0.8416 and 0.8431 respectively. The overall accuracy (OA) of all images exceeds 87 % which is considered as good results for remote sensing image-based analysis. (Table 4.1) presents the details of land-use and land-cover accuracy assessment of the study period

Table 4.1 Error Matrix of classification 1990 - 2020

LULC	1990		2000		2010		2020	
	Producer Accuracy (%)	User accuracy (%)	Producer Accuracy (%)	User accuracy (%)	Producer Accuracy (%)	User accuracy (%)	Producer Accuracy (%)	User accuracy (%)
Built-up	78.19	98.96	90.95	96.51	86.18	96.15	97.65	92.47
Agricultural land	85.05	86.34	86.56	86.83	89.57	83.84	82.27	92.22
Vegetation	93.43	96.6	86.3	79.73	78.41	88.21	94.76	98.91
Bare land	94.05	79.24	85.04	85.57	93.63	89.71	77.99	75.67
Overall accuracy (%)	87.5000%		87.2000%		88.6262%		88.4956%	
κ	0.8244		0.8118		0.8416		0.8431	

4.1.2 Temporal land use land cover maps

As indicated in the land-use and land-cover classification result of 1990 image (Figure 4.1 and Table 4.2), Agricultural land was the main land-use class in the study area. From the total study area, agricultural land accounted for 207.022 Km^2 (66.09%). Whereas Bare land, vegetation and Built-up accounted for 73.3653 Km^2 (23.42%), 25.9389 Km^2 (8.28%) and 6.9174 Km^2 (2.21%), respectively, furthermore, from the total LULC classes of 1990 built-up covered the smallest area. Details of each LULC class of the study area for 1990 are illustrated in (Table 4.2) and (Figures 4.1)

The LULC classification results of 2000 image (Figure 4.1) showed that agricultural land covered the largest surface in the study area again. It accounted for 218.399 Km^2 (69.72%) followed by Bare land, vegetation and Built-up accounted for 59.9634 Km^2 (19.14%), 21.8502 Km^2 (6.98%), and 13.0311 Km^2 (4.16%), respectively (Table 4.1). like in 1990, from the total LULC classes of 2000, the smallest area was covered by Built-up land cover. Details about each LULC class of the study area for 2000 are presented in (Table 4.2) and (Figures 4.1)

As observed in 1990 and 2000 classification map, Agricultural land was again the leading land-use and land-cover class in 2010 and 2020 having an area of 206.3655 Km^2 (65.88%) and 143.4384 Km^2 (45.79%) respectively, though in 2010 it has decreased by 10.233 km^2 (3.84%) from 2000. And also decreased by 62.9271 km^2 (20.09%) from 2010 Further, in 2010 and 2020 investigation indicated that from the total area of the study unlike in the previous 1990 and 2000 the smallest land is not covered by built-up land cover which signifies unceasing expansion of built-up in the study area since 1990 Details about LULC classes of the study area for 2010 and 2020 are presented in (Table 4.2) and (Figures 4.1).

To summarize the classification result of LULC in adama city from the year of 1990 to 2020, indicating major decline with respect to area coverage observed in agriculture while vegetation and Bare land shows decreasing trend then increased. The areas of built-up classes were increased since 1990 to 2020. The extent of agriculture land was reduced from 66.09% in 1990 to 45.79% in 2020 of total area. The vegetation land class was reduced from 8.28% in 1990 to 6.48% in 2010 then again rise up to 10.56% in 2020 of the total area. The share of built-up area was 2.21% in 1990 of the total area, which was increased to 15.40% in 2020. The bare-land class was decreased from 23.42% in 1990 to 19.14% in 2000 again increase to 20.34% and 28.24% in 2010 and 2020 respectively. In general, built-up areas increased significantly with enhanced urbanization while the non-built-up areas decreased with the losing of agricultural and vegetation land cover

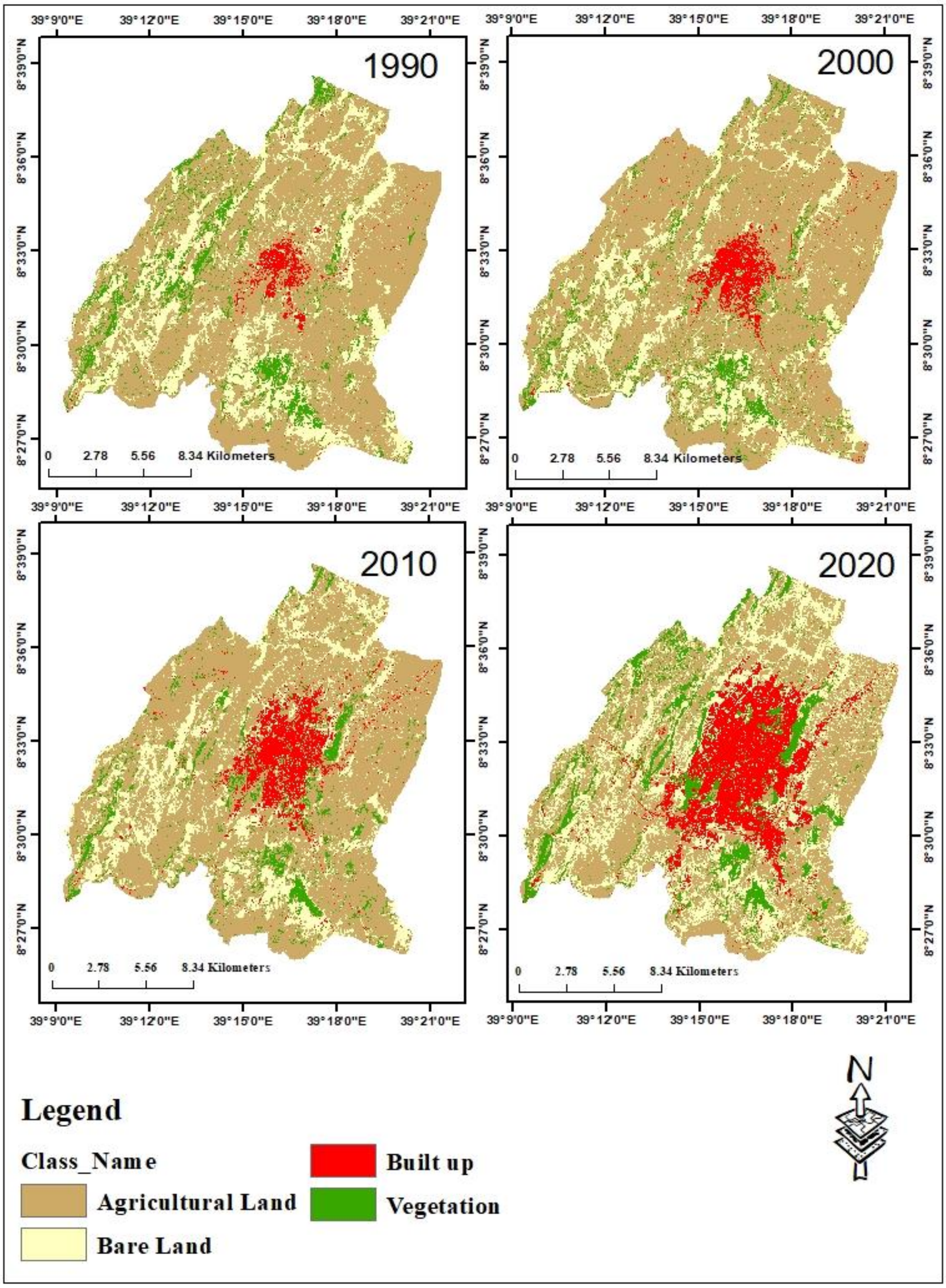

Figure 4.1 LULC Map of adama City from 1990 – 2020

Table 4.2 Area and percentage of LULC classes of Adama City from 1990 – 2020

	1990		2000		2010		2020	
Classes	Area (Km^2)							
Built up	6.9174	2.21%	13.0311	4.16%	22.8474	7.29%	48.2454	15.40%
Vegetation	25.9389	8.28%	21.8502	6.98%	20.304	6.48%	33.0858	10.56%
Agricultural Land	207.022	66.09%	218.399	69.72%	206.366	65.88%	143.438	45.79%
Bare Land	73.3653	23.42%	59.9634	19.14%	63.7263	20.34%	88.4736	28.24%
Total	313.243	100%	313.243	100%	313.243	100%	313.243	100%

4.1.3 Land use land cover Transformation

change result from 1990-2000 show that in the year 1990, the built-up area covered 6.92 km^2 of the total study area, while the agricultural land covered 207.02 km^2. In 2000, urbanized area (built-up) covered increased to 13.03 km^2 resulting in additional urbanized area of 6.1137 km^2 as 1.95 % of the total area converted to Built-up land cover, majorly at the expense of agricultural land 5.89km^2 and bare land 1.77km^2 respectively. while the agricultural land cover also increased to 218.4 km^2 at the expense of bare land 25.43km^2 and Vegetation 15.06km^2 correspondingly agricultural land also lose land cove to Built-up 5.89 km^2, Vegetation 10.86 km^2 and bare land 13.5 km^2. Likewise, Vegetation land cover decreased from 25.94 km^2 to 21.85 km^2 by losing it land cover majorly to Agricultural land 15.06 km^2 and bare land 3.93 km^2 but simultaneously vegetation land cover obtains 4.15 km^2 from bare land and 10.86 km^2 from agricultural land cover.

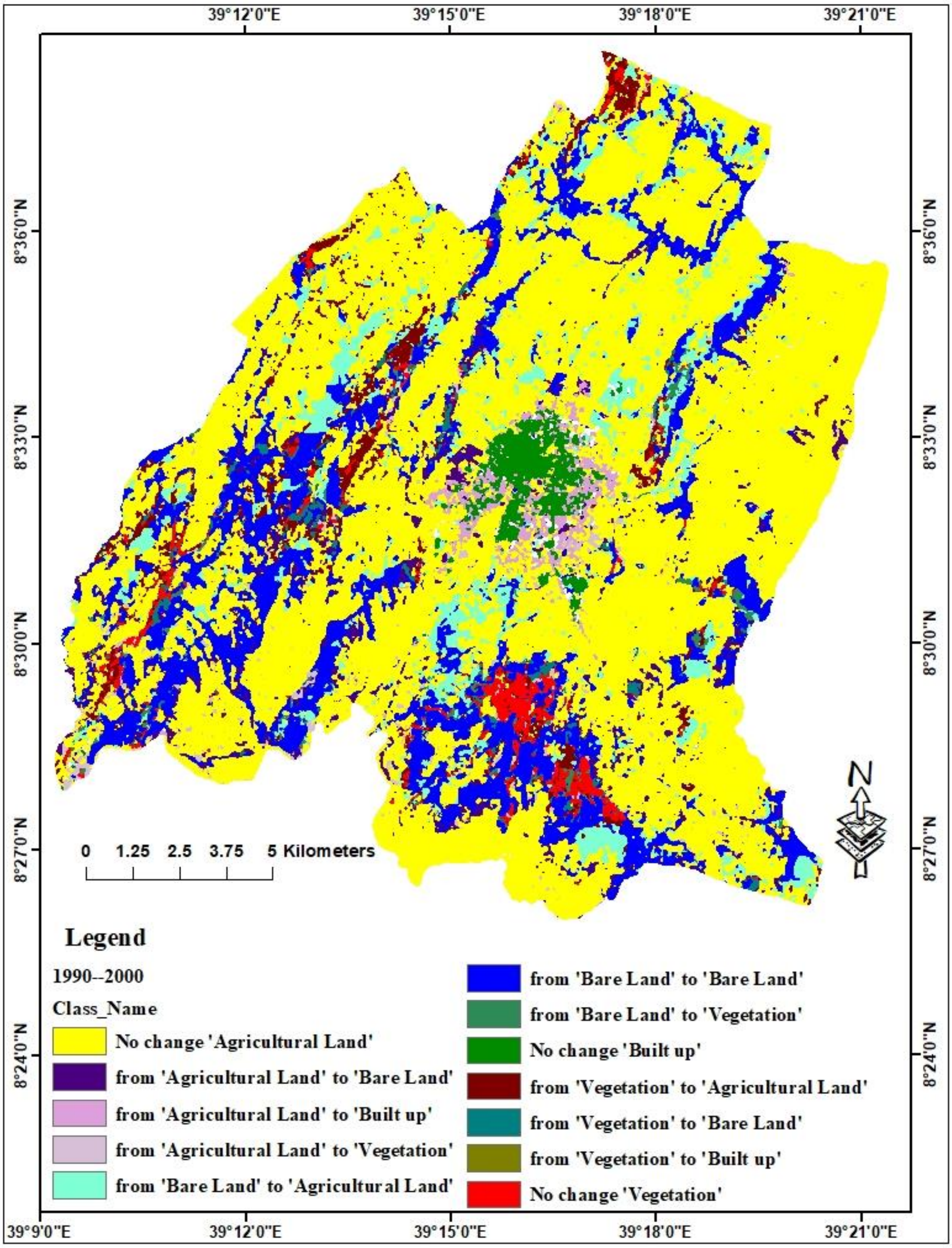

Figure 4.2 Change in LULC Map of Adama City from 1990 – 2000

Table 4.3 Area statistics and percentage of change in LULC of adama city from 1990 – 2000

Change Area (Km^2)		1990								
		Vegetation		Built up		Bare Land		Agricultural land		Class total
		Km^2	%	Km^2	%	Km^2	%	Km^2	%	
2000	Vegetation	6.81	26.245	0.03	0.481	4.15	5.650	10.86	5.248	21.85
	Built up	0.14	0.524	5.24	75.696	1.77	2.413	5.89	2.844	13.03
	Bare Land	3.93	15.156	0.51	7.351	42.02	57.276	13.5	6.522	59.96
	Agricultural land	15.06	58.076	1.14	16.472	25.43	34.66	176.77	85.385	218.4
	Class Total	25.94	100	6.92	100	73.37	100	207.02	100	
	Class Changes	19.13	73.755	1.68	24.304	31.34	42.724	30.26	14.615	
	Image Difference (**Net Gain/Loss**)	-4.09	-15.763	6.11	88.381	-13.4	-18.267	11.38	5.496	

In the year of 2010, the urban area was increased up to 22.85 km^2 (Table 4.4) at the expense of 10.78 km^2 from agricultural land and 2.08 km^2 from bare land, which means an extra net gain of 9.82 km^2 3.13% of the total study area was changed from non-built-up to built-up areas, while the extent of agriculture land was decreased to 206.3 km^2 by losing it landcover majorly to bare land 22.18 km^2, Vegetation land cover 12.24 km^2 and Built up 10.78 km^2 concurrently agricultural land gain land cover from bare land 18.24 km^2 and Vegetation 12.65 km^2 .

Table 4.4 Area statistics and percentage of change in LULC of adama city from 2000 – 2010

Change Area (Km^2)		2000								
		Vegetation		Built up		Bare Land		Agricultural land		Class total
		Km^2	%	Km^2	%	Km^2	%	Km^2	%	
2010	Vegetation	5.91	27.062	0.12	0.905	2.04	3.398	12.24	5.602	20.3
	Built up	0.39	1.763	9.59	73.624	2.08	3.475	10.78	4.938	22.85
	Bare Land	2.9	13.267	1.04	7.963	37.61	62.714	22.18	10.158	63.73
	Agricultural land	12.65	57.908	2.28	17.508	18.24	30.413	173.19	79.302	206.37
	Class Total	21.85	100	13.03	100	59.96	100	218.4	100	
	Class Changes	15.94	72.938	3.44	26.376	22.36	37.286	45.2	20.698	
	Image Difference (**Net Gain/Loss**)	-1.55	-7.076	9.82	75.33	3.76	6.275	-12.03	-5.51	

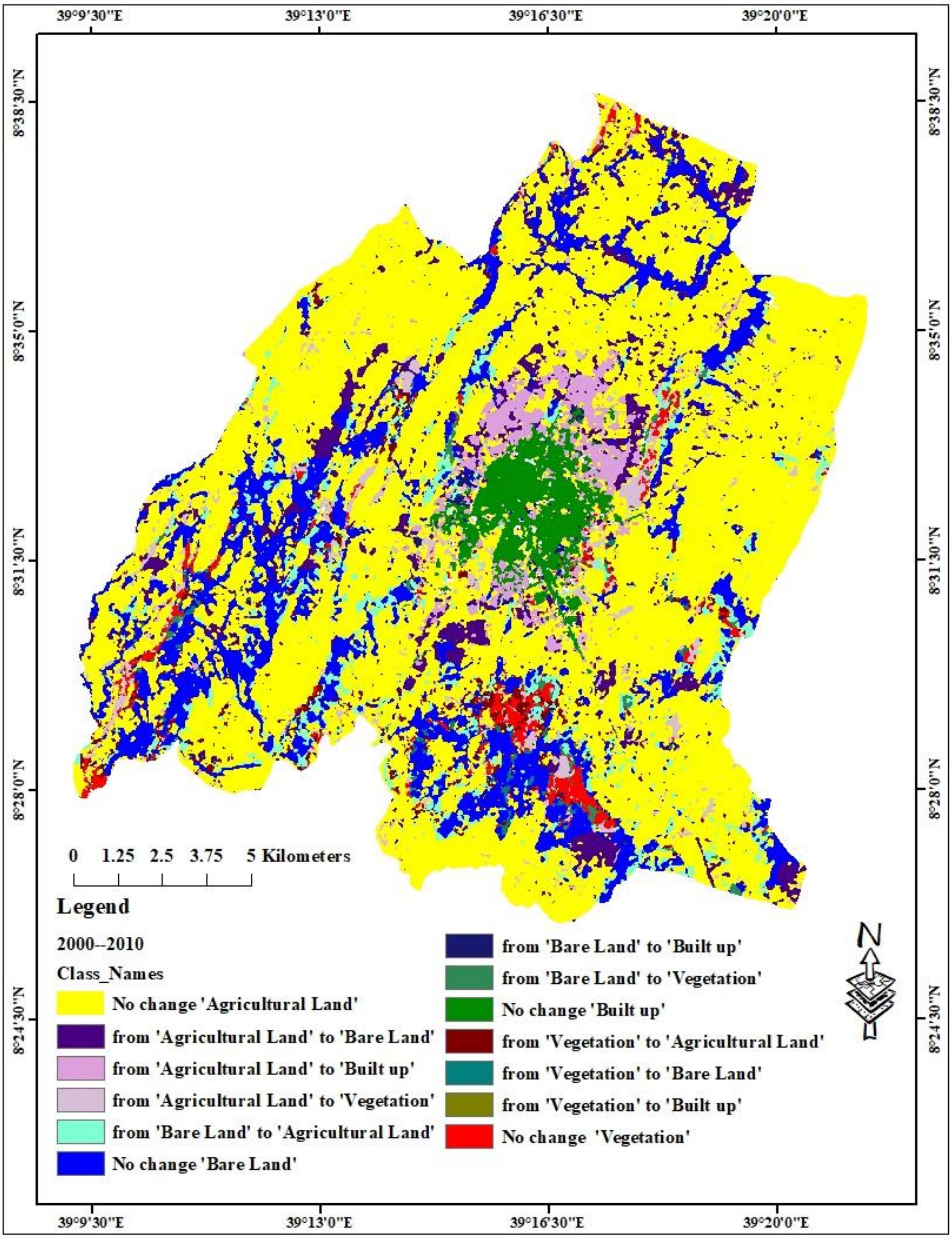

Figure 4.3 Change in LULC Map of Adama City from 2000 – 2010

Similarly, as previous in the year of 2020 urban area increased up to 48.25 km^2 (Table 4.5) an additional net gain amount of 25.4 km^2 from non-built-up area convert to built-up at the expense of agricultural land 20.9 km^2 and bare land 6.98 km^2 similarly Vegetation land cover and Bare land increase to 33.09 km^2 and 88.47 km^2 while Agricultural land decrease to 143.44 km^2 by losing its land cover to 20.9 km^2 to Built-up, 17.93 km^2 to vegetation and bare land 45.4 km^2.

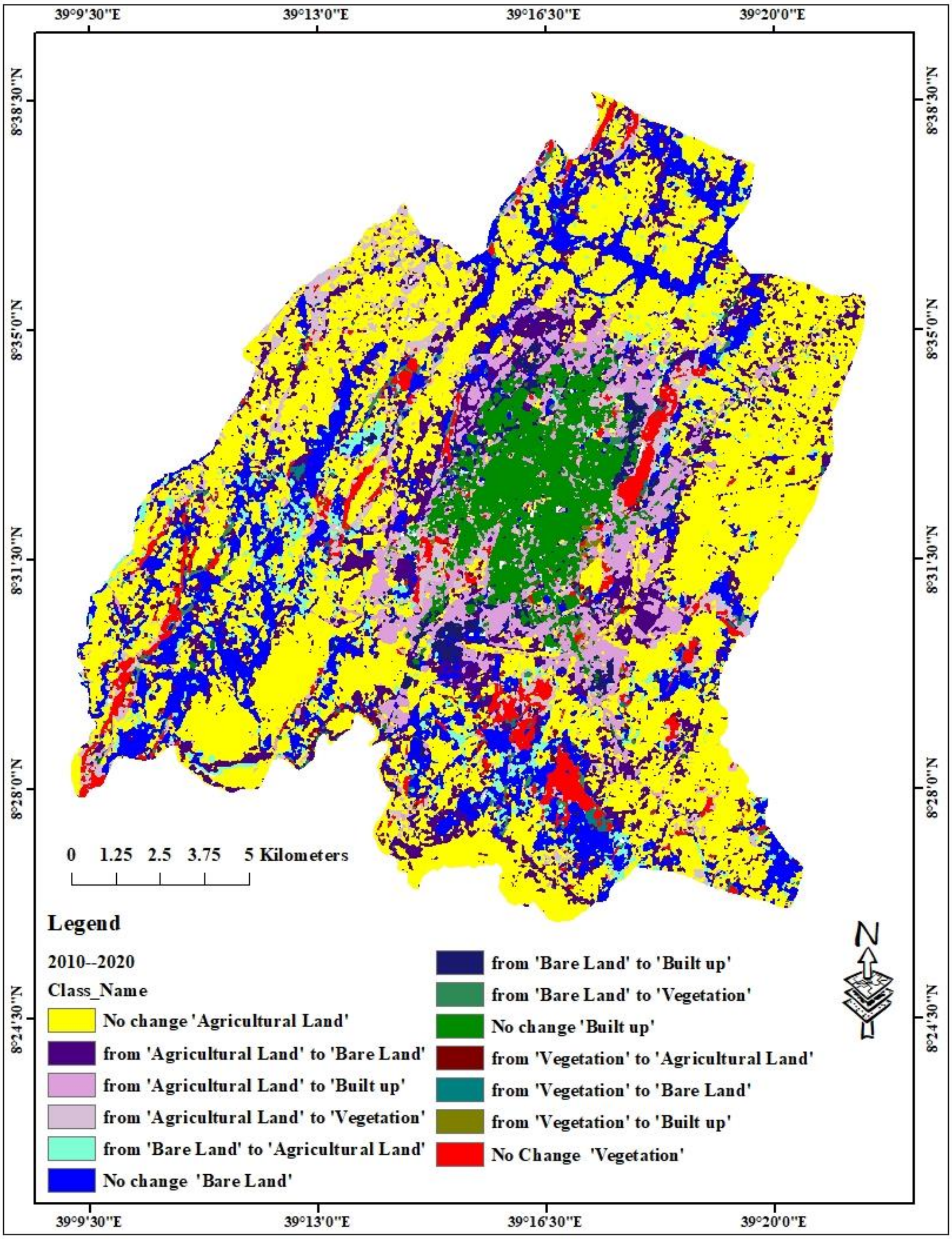

Figure 4.4 Change in LULC Map of Adama City from 2010 – 2020

Table 4.5 Area statistics and percentage of change in LULC of Adama city from 2010 – 2020

Change Area (Km^2)		2010								
		Vegetation		Built up		Agricultural land		Bare Land		Class total
		Km^2	%	Km^2	%	Km^2	%	Km^2	%	
2020	Vegetation	11.85	58.373	0.25	1.091	17.93	8.687	3.06	4.798	33.09
	Built up	1.04	5.142	19.26	84.298	20.9	10.156	6.98	10.957	48.25
	Agricultural land	4.75	23.4	1.63	7.138	122.02	59.130	15.03	23.589	143.44
	Bare Land	2.66	13.085	1.71	7.473	45.46	22.027	38.65	60.656	88.47
	Class Total	20.3	100	22.85	100	206.37	100	63.73	100	
	Class Changes	8.45	41.627	3.59	15.702	84.34	40.87	25.07	39.344	
	Image Difference (**Net Gain/Loss**)	12.78	62.952	25.4	111.164	-62.93	-30.493	24.75	38.834	

There was significant change in LULC in Adama City from 1990 to 2020. Analysis of Change detection results show a sharp increase in the Built-up class during the 30-year period (1990-2020). Meanwhile, Agricultural land had a major decline of 12.033 km^2 (3.84%) and 62.9271 km^2 (20.09%) during the two periods of 2000-2010 and 2010-2020 respectively. Agricultural land accounts half of the study area LULC and it has reduced from 207.0216 km^2 (66.09%) in 1990 to 143.4384 km^2 (45.79%) in 2020. Vegetation land cover, on the other hand, decreased in area during 1990-2010, and then increased again up-to 2020.

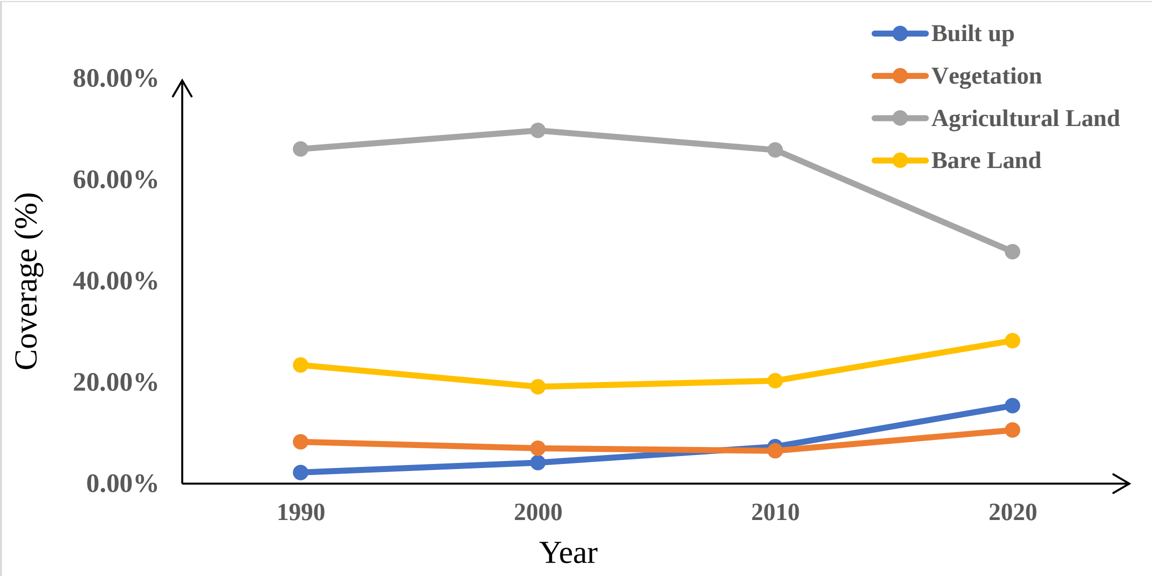

Figure 4.5 proportions of land use/land cover classes in the study area from 1990 to 2020

4.1.4 Persistence, swap and net change

1990-2000 Agricultural land shows highest Persistence followed by built-up, bare-land, and vegetation 85.385%, 75.696%, and 57.276% respectively diagonal area in (Table 4.3) and no change class in (Figure 4.2). In the meanwhile, Agricultural Land shows highest swap followed by bare land, vegetation and built up (Table 4.6) besides to this the amount of gain between 1990 to 2000 in vegetation and bare land is lower than the amount of loose between 1990 to 2000 as a result of swapping they have net loss of -4.09 Km^2 and -13.47Km^2 respectively (Table 4.6) conversely the amount of gain is higher in agricultural and built-up land cover than they lose and they have net gain +11.38 and +6.15Km^2 respectively. During the changes from 2000 to 2010 agricultural land have higher persistence followed by built-up, bare land and Vegetation 79.302%, 73.624%, 62.714% and 27.062% respectively diagonal area in table (4.4) and no change class in (Figure 4.3) Likewise, the amount of gain between 2000 to 2010 in vegetation and Agricultural land cover is lower than the amount they lose as a result of swapping and they have net loose of -1.55 and -12.03Km^2 (Table 4.6) in contrary the amount of gain between 2000-2010 in built up and bare land is higher than the amount they loose and they have net gain +9.82 and +3.77Km^2% respectively. In the third phase (2010-2020) built-up and bare land exhibit higher persistence followed by agricultural land and vegetation 84.298%, 60.656%, 59.130% and 58.373% respectively diagonal area in table (Table 4.5) and no change class in (Figure 4.4).

Table 4.6 Gain, loss and Swap in LULC of Adama City from 1990 – 2020

Area in Km^2		Gain	loss	swap	Net change (gain$^+$/loss$^-$)
1990-2000	Built up	7.83	-1.68	1.68	+6.15
	Bare land	17.94	-31.35	17.94	-13.4
	Agricultural Land	41.63	-30.25	30.25	+11.38
	Vegetation	15.05	-19.14	15.05	-4.09
2000-2010	Built up	13.26	-3.44	3.44	+9.82
	Bare land	26.12	-22.35	22.35	+3.77
	Agricultural Land	33.18	-45.21	33.18	-12.03
	Vegetation	14.4	-15.91	14.4	-1.55
2010-2020	Built up	28.99	-3.59	3.59	+25.4
	Bare land	49.82	-25.08	25.08	+24.75
	Agricultural Land	21.42	-84.35	21.42	-62.93
	Vegetation	21.24	-8.45	8.45	+12.78

The analysis confirmed that over the last three decades (1990-2020), Adama city's built-up land cover increased at the rate of 23.25% per year. The study result is similar to one conducted previously by Tesema & Abebe, (2019). This emphasized the enormous increase in the area covered by built-up areas over a 30-year period, according to (Abebe et al., 2019), Ethiopia's rapid population growth and economic progress, contribute to the growth of built-up areas.

It is widely accepted that problems like the urban heat island, flooding, and deteriorating urban environments are caused by the continual high rate of urbanization (Balzerek, 2003 and Ujoh et al., 2010). Similarly, the reduction in vegetation cover and agricultural area, particularly for urbanization goals, illustrates the inadequacy of farmland protection laws and the disregard for environmental and ecological rules implemented in the urban master plan. Unfortunately, it has been demonstrated that these urban problems have an impact on the urban development process in Adama. (Tesema & Abebe, 2019), thus Sustainable land use planning and management and sustainable urban development are the only viable solutions. because the causes of issues are unregulated urban growth. In other words, controlling uncontrolled urban expansion is considered to be crucial for countries whose economic viability and environmental sustainability are increasingly imperiled (Worku et al., 2017).

4.2 Dynamics of Landscape Structure and its pattern

4.2.1 Change in Land cover composition and configuration

The temporal changes evident in the landscape pattern metrics for each LULC class are shown in (Table 4.7). The NP at the landscape level indicated that Adama city had undergone considerable fragmentation during the study period and its trend of increasing from 3248 in 1990 to 3414 in 2010 and 4807 in 2020 indicating more uniform trend of change in landscape configuration in the city until 2010.

PAFRAC

In all land use land cover, there has been slight change in the value of perimeter area fractal dimension (PAFRAC) between 1990 and 2020. For vegetation cover decreased from 1.5792 in 2000 to 1.4797in 2010 and 1.4441 in 2020, for agricultural land 1.4743 in 1990 increased to 1.5281 in 2020, Overall, the relative shape complexity decreased for Vegetation, and Built-up land cover, while it increased for the bare-land and Agricultural land cover categories during 1990-2020. The total change of shape irregularity was highest for Bare-land 0.0866 (6.03%) and lowest for Built-up 0.0063 (0.429%) during 1990-2020 (Table 4.7).

NP

From 1990 to 2020 number of patches at the class level for bare land and built-up and agricultural land cover shows gradual increment while vegetation land cover has consistently declined between 2000 and 2020. It reveals a trend of increase in new built-up development in the outer territory of old built-up land cover, this implies that adama city had significant development of urban sprawl and emergence of numerous disconnected or fragmented Built-up land cover. and fragmentation for bare land and Agricultural land cover, while vegetation land cover evolving to merger of patches and lower degree of fragmentation in the past 30 years

CAI_MN

The mean core area index of built-up land cover increased from 0.4078 in 2000 to 1.8364 in 2020 similarly Vegetation land cover increased from 0.8024 1990 to 2.994 in 2020. The increase in mean core area index was maximum between 2010 and 2020 for Built up and 2000 and 2010 for vegetation. While agricultural land and bare land shows continuous decrement in mean core area index from 2.6814 in 1990 to 1.6057 in 2020, and from 3.4942 in 1990 to 2.0377 in 2020 respectively this indicates in the past two decades besides to development of new built-up in outer old built-up territory there was infill development inside the city and finding for vegetation land cover again strengthens that in adama city vegetation land cover was developing as a compact large patch structure between 1990 and 2020. While agricultural land and bare-land was evolving to fragmented more and more in the past 30 years which support the previous result increase in number of patches.

FRAC_MN

FRAC_MN indicates patch shape complexity. The computed FRAC MN are below 1.1, as indicated in (Table 4.7). According to Cabral et al., (2005) values greater than 1 in a fractal dimension indicate an increase in shape complexity. The simplest patch shape found was 1.02, 1.04, 1.03, and 1.04 respectively in built-up, agricultural land, vegetation, and bare terrain. Between 1990 and 2020, the rate of change was constant across all categories of land cover. Overall, there was no significant change in the relative form complexity.

PLAND

In the last three decades the PLAND of built-up Land cover increased in two-fold in each epoch from 2.2083 in 1990 to 15.4019 in 2020 while vegetation shows decrement until 2010 in the contrary agricultural land shows decrement trend after 2000. Over all, In the last three decades, built-up area has rapidly increased both with-inside the old bult-up territory and in the periphery and this has increased the mean core area index of Built-up land cover by aggregation of patch into a single large patch through the process of coalescence of smaller patches and contiguous development of new built-up area. Thus, built-up area in adama city in 2020 is much less dispersed and has evolved into a compact patch with much increase in new built-up areas Moreover, configuration metrics suggests that vegetation land cover in adama city was much less fragmented in 2020 in comparison to 1990 and 2000.

Aggregation Index

AI depicts how LULC is physically connected. The AI for barren land, Agricultural land, share a similar trend as it decreased continually during 1990-2020. Built-up AI increased during the first three period and then decreased in 2020 Vegetation land cover decreased in the first phase then increased continuously until 2020. AI for Agricultural land showed highest increase (37.76%) during 1990- 2020 as compared to other LULC types. Moreover, vegetation and built-up land have relatively have increasing trend of AI than Agricultural land and bare-land cover.

Table 4.7 Landscape dynamics in Adama City from 1990 – 2020

	TYPE	PLAND	NP		FRAC_MN	PAFRAC	CAI_MN	PD	ED	AI
1990			Class	Landscape						
1	Vegetation	8.2808	1336	3248	1.0345	1.5283	0.8024	4.36	34.91	61.86
2	Bare-land	23.4212	1179		1.0436	1.4354	3.4942	3.85	53.74	81.08
3	Agri_land	66.0897	530		1.0402	1.4743	2.6814	1.73	72.54	89.84
4	Built up	2.2083	203		1.0250	1.4653	1.0030	0.66	6.83	71.94
2000										

1	Vegetation	6.9755	1502	3335	1.0309	1.5792	0.3811	4.94	33.43	51.21
2	Bare-land	19.1428	1033		1.0402	1.4529	2.9381	3.40	46.71	79.18
3	Agri_land	69.7217	454		1.0419	1.4947	2.2529	1.49	69.50	89.86
4	Built up	4.1601	346		1.0271	1.5258	0.4078	1.14	10.76	75.71
2010										
1	Vegetation	6.4819	960	3415	1.0370	1.4797	1.5611	3.14	25.59	66.27
2	Bare-land	20.344	1444		1.0395	1.4542	2.6067	4.72	56.36	76.97
3	Agri_land	65.8803	558		1.0416	1.4704	2.1383	1.82	80.61	88.91
4	Built up	7.2938	453		1.0272	1.4848	0.9050	1.48	16.99	78.43
2020										
1	Vegetation	10.5623	439	4807	1.0429	1.4441	2.9940	1.44	24.19	85.22
2	Bare-land	28.2444	2158		1.0452	1.5220	2.0377	7.10	100.38	70.42
3	Agri_land	45.7914	1229		1.0380	1.5281	1.6057	4.04	106.04	80.07
4	Built up	15.4019	981		1.0323	1.4716	1.8364	3.23	30.74	75.23

Nearest distance (ND)

The mean nearest distance between 100 random point and nearest available vegetation patch increased (Figure 4.5-Nearest distance) from 166.0408m in 1990 to 201.079 in 2020 in the meantime PLAND of vegetation cover decreased from 8.2808% in 1990 to 6.4819% in 2010 then rise again to 10.5623% in 2020 this indicates while during in decreasing and increasing in PLAND vegetation land cover shows increase in configuration in adama city in the past 30 years. As we can see from the (Figure 4.5-vegetation) as the number of patches decreases the fragmentation of Vegetation land cover class became decreased this in turn increase the mean core area index of the vegetation land cover but, in the case of built-up in (Figure 4.5-Built-up) as the Number of Patch increases in adama city concurrently mean core area index also increased which indicates adama city is not only growing into compacted (big single patch) or infill development structure but also new built-up areas was increased along the existed built-up periphery in the past three decades.

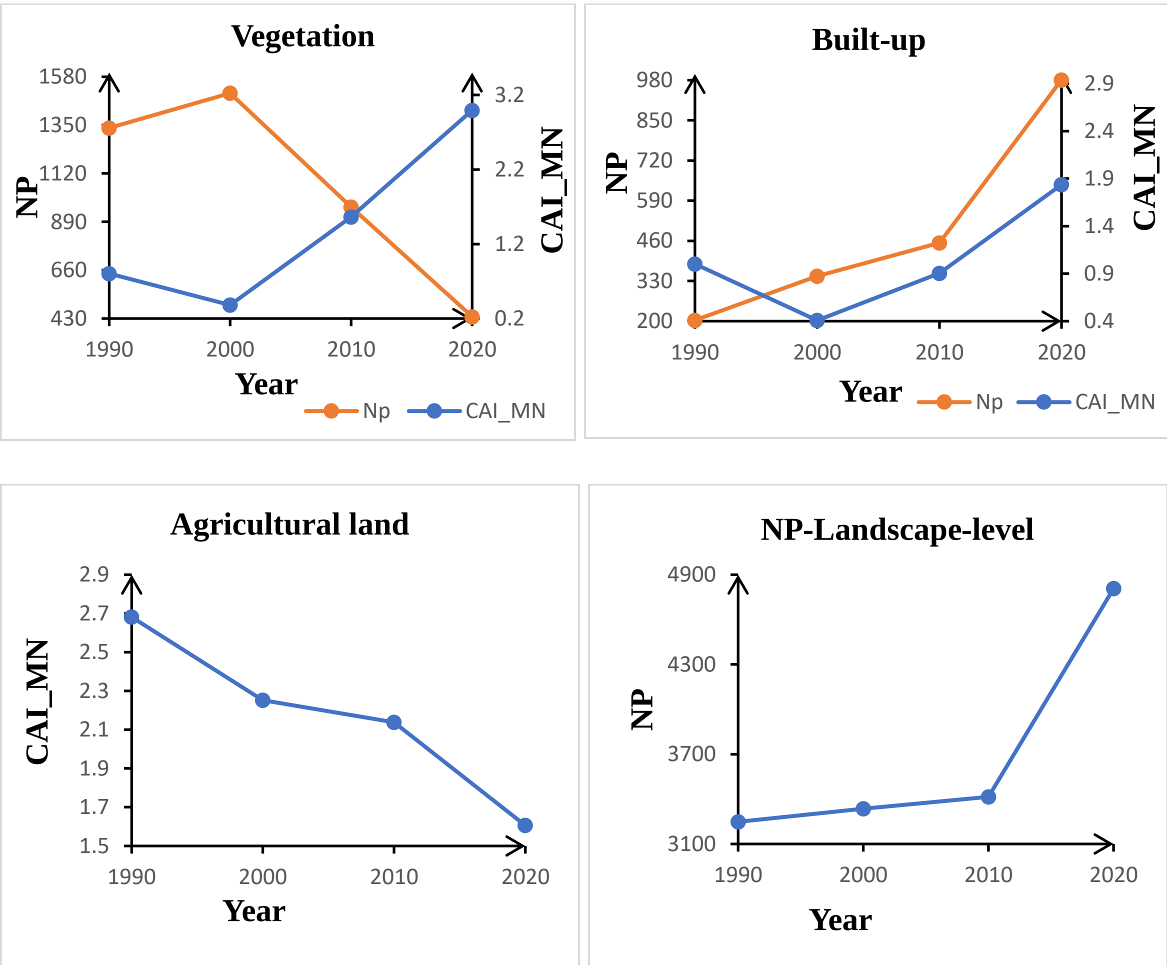

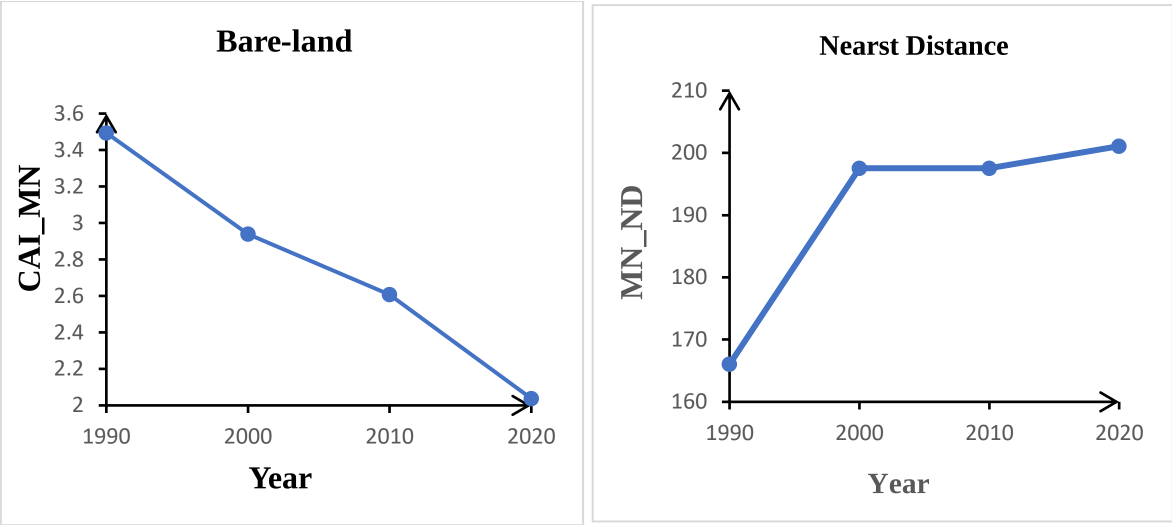

Figure 4.6 LULC spatial Pattern dynamics in Adama City from 1990 - 2020

The change in the landscape pattern during the study period underlies the fact that fragmentation of the landscape tended to strengthen in Adama city in the past three decades. Moreover, the landscape pattern structure became more fragmented, as demonstrated by changes in the number of patches at the landscape level from 3248 in 1990 to 4807 in 2020. The increased in PLAND, NP and PD of the built-up area indicate increasing urbanization and aggregation with economic development. PLAND of built-up area increased from 2.2083 % in 1990 to 15.4019 % in 2020. The AI value of build-up land increased from 71.94 in 1990 to 78.43 in 2010 then decreased to 75.23 in 2020 indicating increased connectedness of built-up area patches. With the process of urbanization, this may be due to aggregation of sub-urban residential area, industrial developed area, and urban area into a small area of clumped built-up land patches

There was a drastic change in agricultural land cover PLAND of agricultural land cover decreased significantly from 66.0897 % in 1990 to 45.7914 in 2020 %; AI also decreased over the study period however, NP, PD and ED shows decrement in the first period then continually increased until 2020. The increments of PD, ED, and NP and decrement in AI and PLAND indicates the increase in fragmentation of agricultural land cover. Mean fractal dimension index (FRAC_MN) and fractal dimension index (PAFRAC) of all land cover showed a very slight increase in the study period (1990–2020) This indicates that less change in shape complexity over the study period.

Adama city is dominated by agricultural land and bare land which together accounted for 89.5109 %, 88.8645 %, 86.2243 %, and 74.0358 % in 1990, 2000, 2010 and 2020, respectively (Table 4.7). In contrast, built-up land area covered only 2.2 % in 1990, 4.2 %

in 2000, 7.3 % in 2010 and 15.4 % in 2020. This indicates that adama city was still dominated by agriculture and bare land, however urbanization rate was increasing higher and higher consequently Sustainable land use planning and management are required. in conclusion, the landscape metrics analysis revealed major changes in land-use structure between 1990 and 2020. Urbanization also increased quickly, nearly doubling in each epoch relative to the previous one.

4.2.2 Spatial pattern of vegetation Land cover

Figure (4.6) shows the spatial pattern of vegetation land cover in adama city for the year of 2020. According to the figure most of the vegetation cover patches are located in the north west, south east and south east of adama city and less amount of this class is in the center and north east part of the city.

AI metrics shows the aggregation of vegetation land cover patch Therefore, based on visual interpretation, higher amount of vegetation aggregated pattern, mostly concentrated in north west, south east and south east of adama city. The PD metric shows the patch density of Vegetation land cover. The maximum PD is gained when every cell is a separate patch. This metric (Figure 4.6) shows that the northern easter parts of adama city have the highest density of patches and the South western and central and North eastern areas have the lowest density. Similarly, ED metrics shows vegetation cover in the North-western and south-eastern part of the city have edge density and Vegetation cover in the north-eastern part of the city have lower edge density

The FRAC_MN metric (Figure 4.6) measures the irregularities in the shape of patches and increases as landscape shape becomes more irregular. This index shows that the highest FRAC_MN value in adama city is 1.24 which is near to the neutral value 1.5 Vegetation cover in most part of the city has more regular (Square) patch structure.

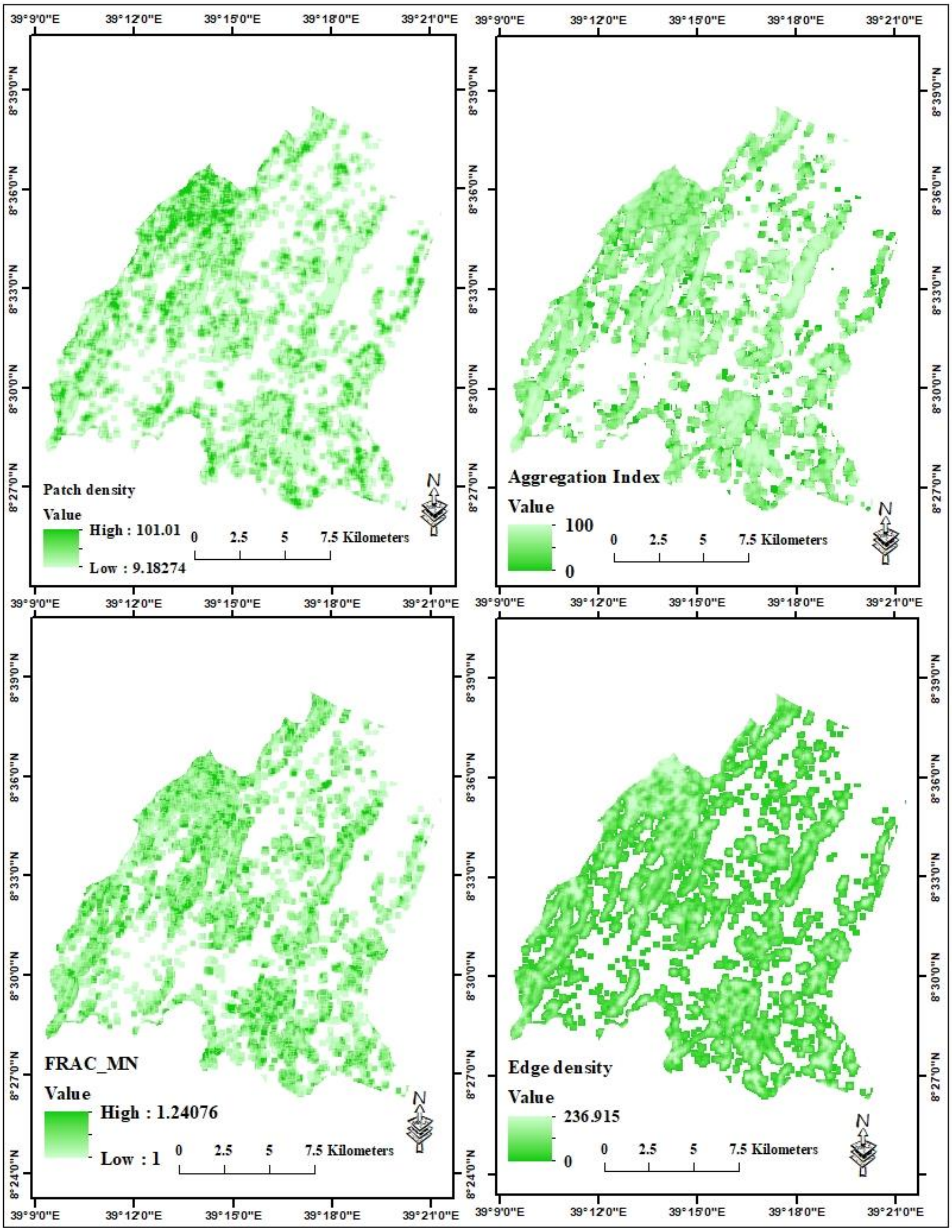

Figure 4.7 Vegetation land cover configuration Map of adama City 2020

4.2.3 Spatial distribution of Normalized differential vegetation index

The result of this study indicates that the spatial extent of vegetation cover was high in 1990 and 2020 than 2000 and 2010 in the study area. Hence, NDVI values were higher in 1990 with its maximum of 0.61 than 2000 which was 0.55 and 2010 which was 0.46 This indicates that there was high healthy vegetation cover in 1990 than in 2000 and 2010. In 2020, vegetation cover was highly increased and this made the NDVI value to increase from 0.46 to 0.67 (Table 4.8).

Table 4.8 Normalized difference vegetation index results from 1990 - 2020

Year	1990	2000	2010	2020
Min	-0.470707	-0.350676	-0.363636	-0.384254
Max	0.634271	0.540495	0.461622	0.670495
Mean	0.326733	0.26885	0.195364	0.372912
St_div	0.142715	0.224102	0.137938	0.139635

However, NDVI value in 2020 has somewhat increased as compared to that of the year 2010 due to the expansion of plantation and green spaces. Therefore, some areas in the northeast and South and south-west of the city and south-eastern part of Adama City had exceptionally high NDVI values. Besides, central, eastern and Northern parts of the city had relatively had high NDVI value than in 2010 (Figure 4.7)

(Figure 4.7) illustrated that place along-with the sideway of awash river and its neighboring areas and, some kebeles in the West and northwest like qechema, the easter tip of Adama city have higher NDVI values. However, most parts of the south, southeast of the city had low NDVI values. Central parts of Adama city where there were more settlement areas have low NDVI values.

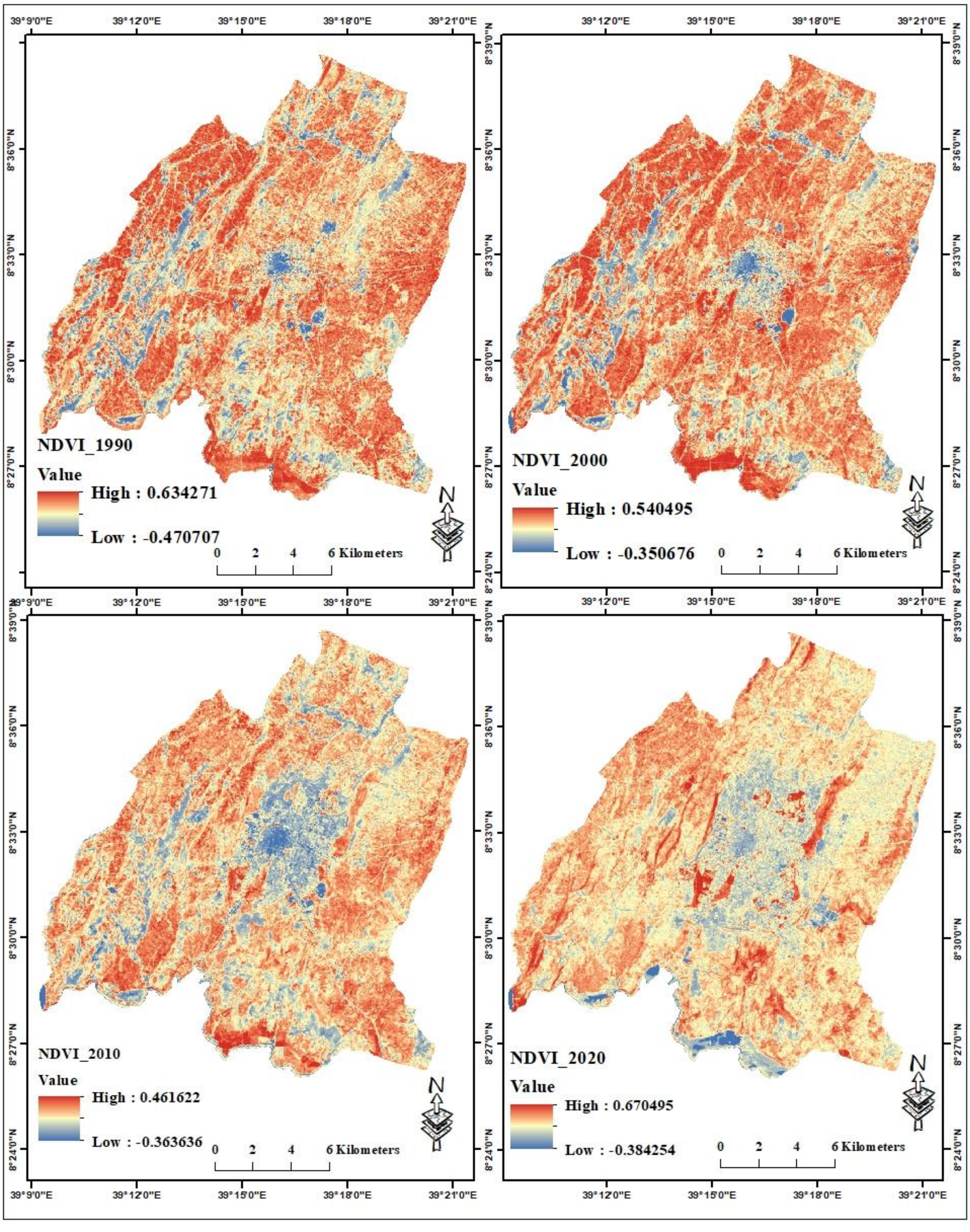

Figure 4.8 NDVI Map of Adama City from 1990 - 2020

4.2.4 spatial distribution of Normalized differential Built-up index

Another important urban climate indicator is the Normal Difference Built-up Index (NDBI) It varies from −1 to +1, where negative values specify water bodies and vegetation, positive value indicates the built-up area, and low positive value specifies types of bare soils. It represents information about the imperviousness of the landscape.

Table 4.9 Normalized difference Built-up index results from 1990 - 2020

Year	1990	2000	2010	2020
Min	-0.520291	-0.539838	-0.507813	-0.490424
Max	0.371904	0.343518	0.396215	0.433531
Mean	-0.208065	-0.190175	-0.150746	-0.145991
St_div	0.129598	0.132039	0.121771	0.107085

Mean NDBI value was −0.208 in 1990, and increased to -0.15 and -0.14 in 2010 and 2020 respectively the highest values for NDBI were in the central part of the city at each time-point because of densely built-up areas of Adama City, whereas the lowest NDBI values were in North western, south western and central and eastern parts of the city, because of the high-density Vegetation land cove (Figure 4.8)

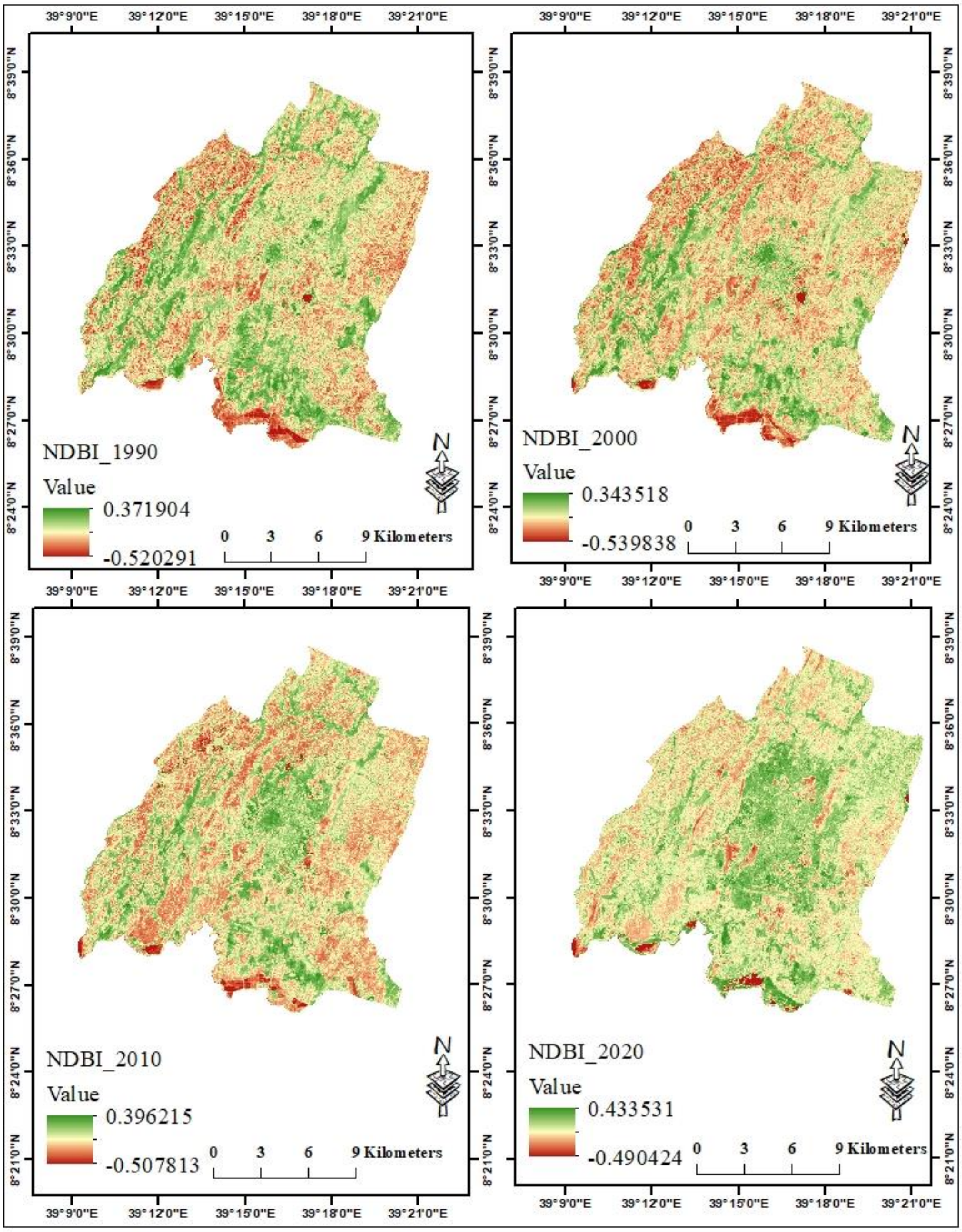

Figure 4.9 NDBI Map of Adama City from 1990 - 2020

4.3 Spatiotemporal Variation of land Surface temperature

4.3.1 Accuracy of retrieved land surface temperature

The land surface temperature extracted from Landsat thermal band of the study area for the study periods were validated based on in-suite data obtained from adama station and MODIS data that was acquired during similar period. Validation of the retrieved LST through on in-suite data obtained from adama station presented in (Table 4.10). From the table up to 17°C Variations exist between retrieved Mean LST and the ground measurements this happen due to lack of spatial representatives of collected in suite measurements besides to this surface temperature is different from ambient/environment temperature and more importantly adama/Nazareth station uses thermometer to collect ambient temperature where as to seamlessly validate the retrieved LST with in-suite measurement the instrument should be radiometer not thermometer.

Table 4.10 Mean LST retrieved from Landsat and adama station in situ LST (1990 -2020)

Year	Mean Temperature in °C	
	in situ	Landsat LST
1990	20.84	27.317909
2000	21.04	34.439978
2010	21.48	38.638761
2020	22.27	36.529768

Validation through Product from MODIS based is better for inter-comparisons. However, MODIS LST product are available since 1999 due to this satellite based intercomparison is only available for MODIS image obtained since 2000. (Figure 4.10) displays the scatterplots of Landsat LST versus MODIS. a Root mean square error (RMSE) of 0.565266 ºC, 0.91844 ºC and 1.3156 º C is obtained for the period of 2000, 2010 and 2020 RMSE tells us the average difference between the Landsat LST product and its reference (MODIS) estimate.

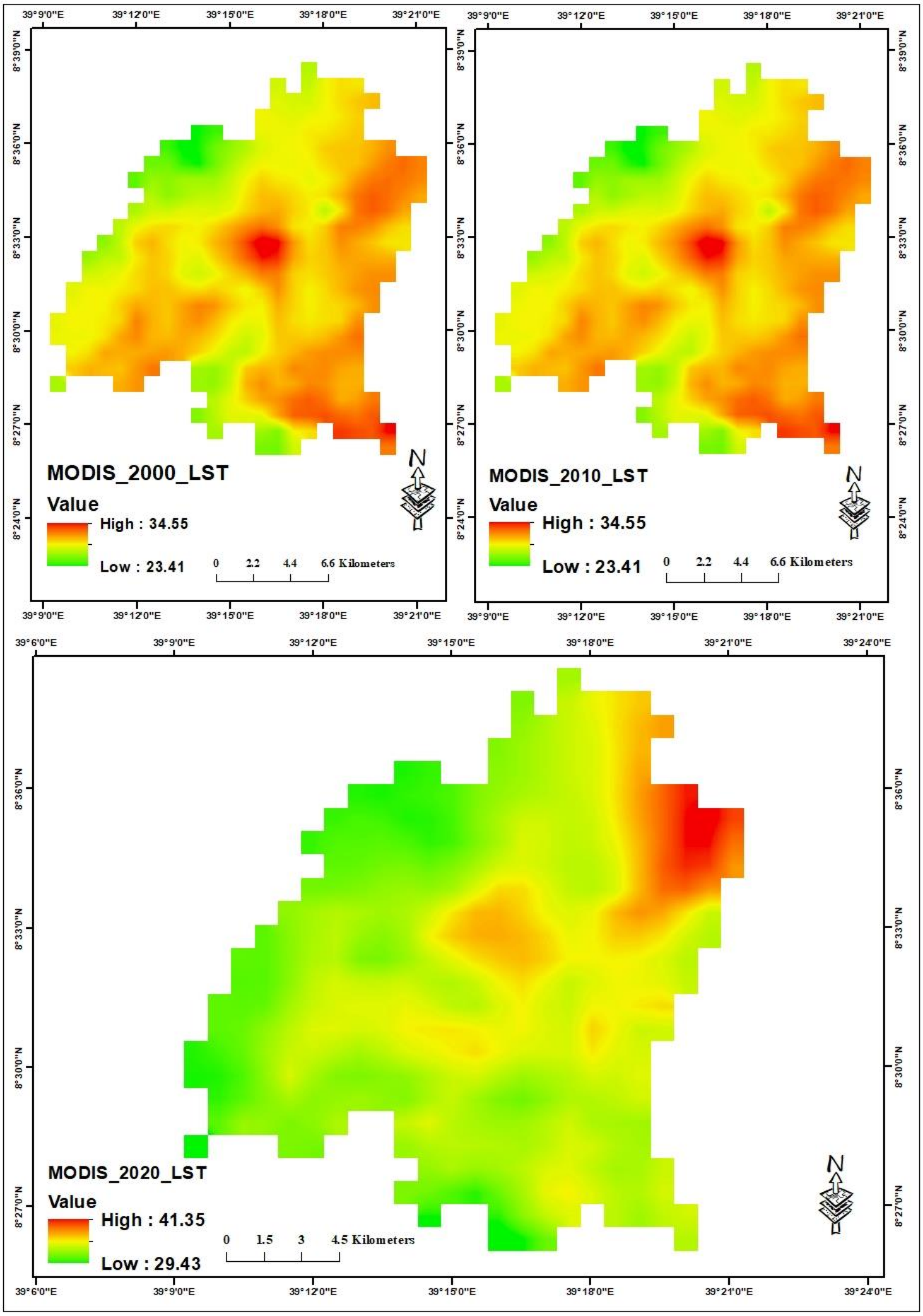

Figure 4.10 MODIS LST map of Adama City from 2000 – 2020

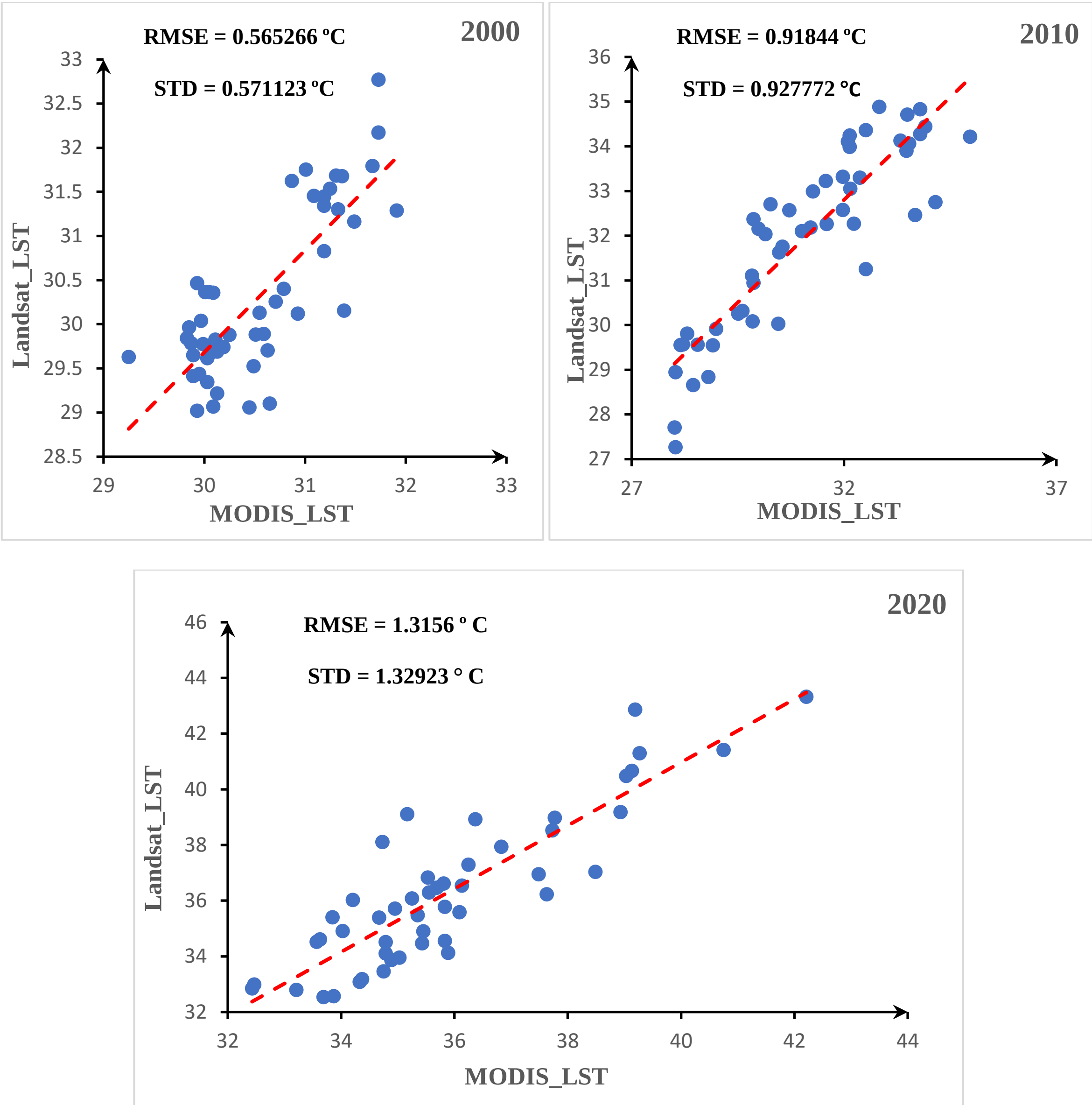

Figure 4.11 RMSE and STD between retrieved Landsat LST and MODIS LST Product (2000 – 2020)

4.3.2 Spatiotemporal distribution of Land surface temperature

The land surface temperature of the study area from 1990 to 2020 ranges from 18.56 ℃ to 47.45 ℃. In 1990, most locations in the northeast, south east and the main built-up area of adama city had higher temperature than the rest part of the city (Figure 4.11). The majority of those areas were bare-land, built-up and lower elevated areas which was exposed directly to incoming radiation. In contrary, places close to Vegetation land cover and western part of the city have a lower temperature. Spatial distribution of LST of adama city for the year of 1990 is presented in (Figure 4.11-1990). The spatial extent of LST in 2000 was higher than the year 1990 with its maximum value of 42.99. and 39.05 % of the city is covered with the range between 33.82 C°-36.54 C° (Figure 4.11) These areas were found in southwest, Northeast and southeast of the city as well as Built-up area of adama city. The land surface temperature analysis in 2010 and 2020 showed that still Northeast and southeast of the city as well as Built -up areas of adama city were warmer than place located on the Northwest and Southern tip of the city boundary Besides to these, urbanization in Northeast and southeastern part of the city and increase in industrial/Manufacturing areas in southwest contribute significantly to the warming of Adama city in 2010 and 2020 (Figure 4.11-2010 & 2020). From the figure we can perceive that Northern part of the city evolving to warm temperate environment through the past 30 years.

As the areas in the southern end (sideways to awash river) of the city Boundary which have substantial irrigation area and southern-west end surrounding Lake Koka was characterized by Lower surface temperature as indicated in the LST map of 1990-2020. However, the maximum temperature that was observed in 2020 was less than that of 2010 which signifies in 2020 surface temperature decreased in intensity as compared to the previous epoch 2010 unambiguously this resulted because of increase in Vegetation land cover in 2020 as result of plantation. Even though, the temperature of Adama city observed in 1990 were lower as compared to that of 2000, 2010 and 2020. Which shows Land surface temperature were in increasing trend in adama city in the past 30 years. areas that were represented as Built-up and bare land had exceptionally recorded high surface temperature compared to agricultural-land and vegetated areas in all.

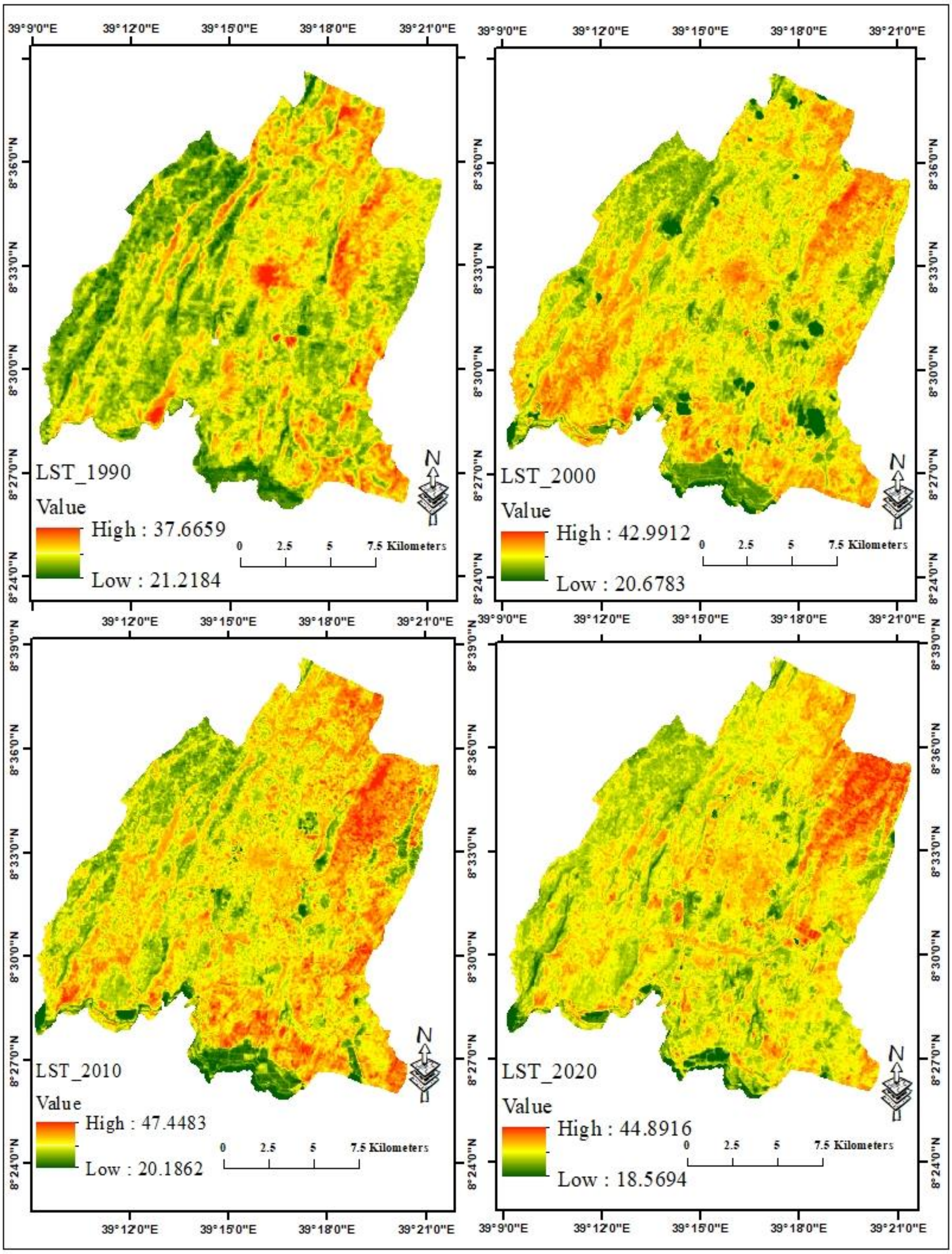

Figure 4.12 Landsat LST map of Adama City from 1990 - 2020

4.3.3 Impact of land use land cover Change on land surface temperature

Based on the results obtained from this study, it was observed that the LST has been gradually increasing from 1990 to 2020. LULC change significantly affects LST transformations between different LULC types (especially urban expansion) increase mean LST. The mean LST values associated with each LULC categories were summarized in (Table 4.11) It was observed that during 1990, 2000, 2010 and 2020 the mean temperature of Built-up land cover changed 29.524452°C, 35.819888°C, 39.421181°C and 35.959604°C respectively the mean LST of urban built-up had a 6.29 °C increased from1990 to 2000 also increased by the maximum LST difference of 5.33°C between 1990 and 2000. Similarly, from 2000 up to 2010 mean LST of Built-up increased by 3.61 °C however in 2020 mean LST of Bult up shows decrement by 3.47 °C as well the maximum LST difference from 2010 decreased by 2.55 °C this occurs due to increase in vegetation land cover in 2020. Mean LST of barren land had a 7.51 °C increase from 1990 to 2000 and by 4.4 °C from 2000 to 2010 but had decreased by 3.3 °C. The LST of vegetated areas had a 10.86 °C increased from 1990 to 2010, but decreased by 5.75 °C between 2010 and 2020. Moreover, Bare land cover has the highest average temperature, followed by Built-up, agricultural land and vegetation land cover in 1990, 2000, 2010 and 2020, Similar results were obtained in Studies done by Pu et al., (2006) and Zareie et al.,(2016) have shown that respectively the LST values of bare land are higher than the LST values of urban areas the high LST values in these areas can vary depending on the content of the soil (sand) the highest average temperatures were observed for all the LULC categories in 2010 (Table 4.11).

Table 4.11 Mean LST over each land cover classes from 1990 - 2020

Land cover		1990	2000	2010	2020
Built up	Area	691.74	1303.11	2284.74	4824.54
	mean LST in C°	29.52445	35.819888	39.421181	35.959604
Agricultural land	Area	20702.16	21839.85	20636.55	14343.84
	mean LST in C°	26.537393	33.91918	38.627665	34.952159
Bare land	Area	7336.53	5996.34	6372.63	8847.36
	mean LST in C°	28.654726	36.161227	40.569051	37.263222
Vegetation	Area	2593.89	2185.02	2030.4	3308.58
	mean LST in C°	26.850454	33.922176	37.712507	31.971338

1n 1990 56.29 % of adama city is covered by a temperature in range between 25.64 °C to 28.36 °C while in 2000, 2010 and 2020 this range decreased to 3.62 %, 1.38 % and 0.89 % of the total city Administrative boundary (Table 4.13) similarly in 2000 39.05 % of adama city is covered by temperature in range between 33.82 °C to 36.54 °C likewise in 2010 34.97 % of the city is covered by land surface temperature in range of 39.27 °C to 41.99 °C but in 2020 the 42.25 % of coverage range drops to 35.54° °C to 39.27 °C. this signifies in the last three decades distribution of temperature increased by coverage in adama city (Table 4.12)

Table 4.12 LST zones and their aerial coverage from 1990 – 2020

Temperature Range	1990		2000		2010		2020	
	Area(h)	%	Area(h)	%	Area(h)	%	Area(h)	%
<22.91	38.17	0.12	32.24	0.10	32.58	0.10	50.27	0.16
22.91 - 25.64	5479.79	17.54	315.97	1.00	43.26	0.14	50.83	0.16
25.64 - 28.36	17611.2	56.29	1133.75	3.62	432.73	1.38	280.03	0.89
28.36 - 31.09	7347.80	23.50	2582.67	8.25	620.17	1.98	1181.28	3.77
31.09 - 33.82	751.06	2.39	7464.13	23.84	1418.88	4.53	4332.58	13.84
33.82 - 36.54	38.40	0.14	12223.46	39.05	4470.11	14.28	7962.26	25.43
36.54 - 39.27	0.54	0.001	6997.70	22.35	9901.21	31.63	13226.6	42.25
39.27 - 41.99			553.11	1.77	10948.1	34.97	3682.59	11.76
41.99 - 44.72			1.01	0.003	3229.08	10.31	537.82	1.72
>44.72					208.54	0.67	0.25	0.0009

4.3.4 Urban rural gradient analysis

The analysis of the urban-to-rural gradient provides overall figures on how urbanization has been growing in adama city and Expansion of Built-up land cover by consuming different land use classes to the built-up land cover and in Adama city over the last 30 years (figure 4.12). The total reach of the Built-up cover along the urban-to-rural gradient has expanded from ∼1.8 km in 1990 to ∼5.4 km in 2020 (Figure 4.12). The highest rates of impervious cover can be found in the city center and the inner-urban ring. The increase in built-up land cover along the urban-to-rural gradient is sharper in the North-eastern, South-eastern and south-western compared to the North-western part of the city. This difference is due to Escarpment in the North-west part of the city.

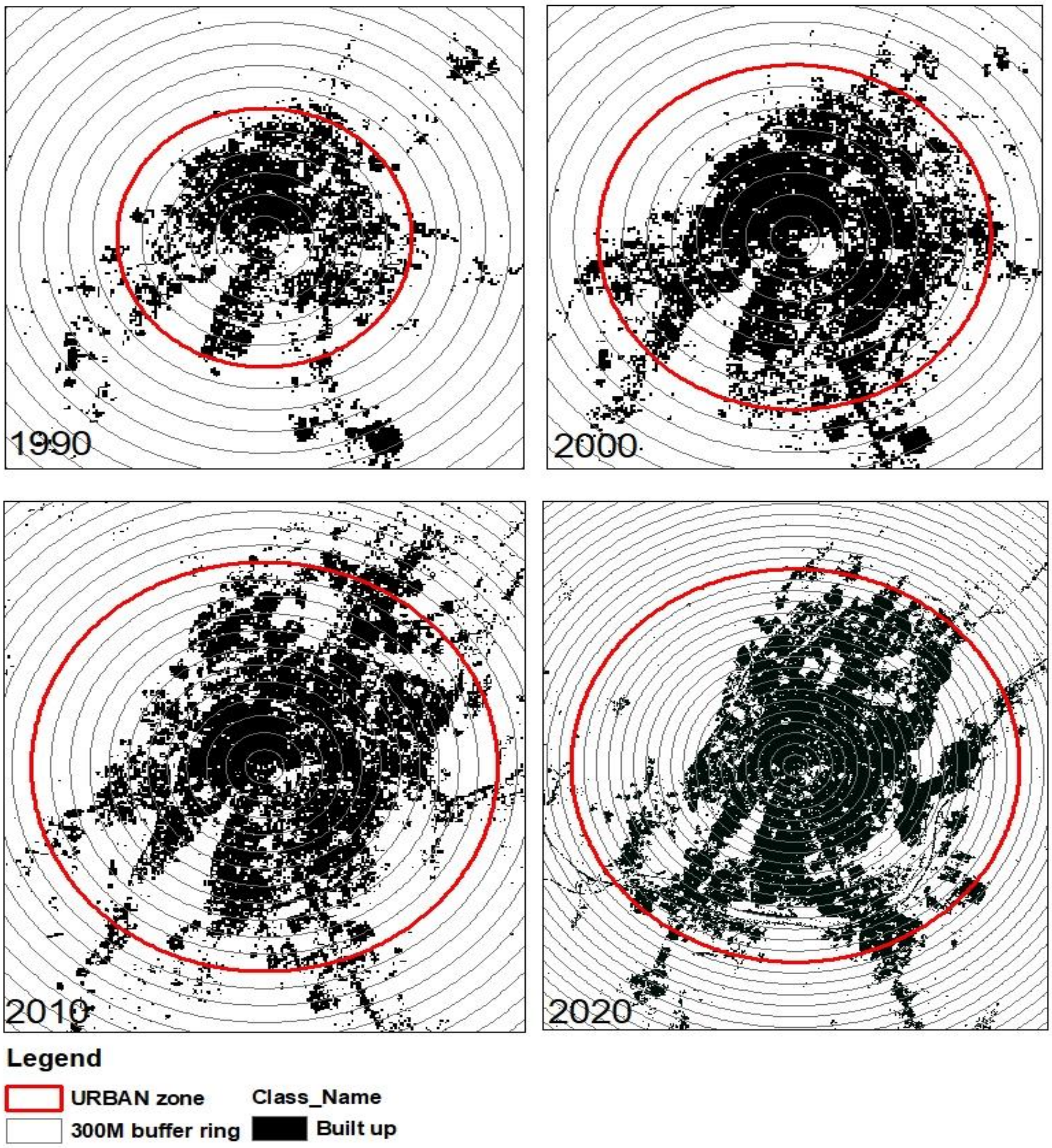

Figure 4.13 Urban Rural Zone of adama City from 1990 - 2020

4.3.5 Surface urban heat island

The study of Surface urban heat island effect in Adama City in the past three decades revealed that there was Land Surface temperatures variation between urban and outlaying rural areas. The results show the difference in average temperature in the urban and rural areas is in the range from 0.6 – 1.63 °C, the overall average temperature can be seen decreasing from 1990 to 2000 in the range of 0.56 °C and again decrease 2010 and increased in 2020 in the range of 0.56 °C from 2010 (Table 4.13). Urbanization can be seen as the prominent reason for these changes, this occurred as a result of the transformation of Agricultural and vegetation land cover into urban areas, which altered the geographical variation in temperature.

Table 4.13 Mean LST difference between urban zone and its rural surrounding from 1990 - 2020

Year	Mean LST in Urban Zone C°	Mean LST in Rural Zone C°	Variations in C°
1990	28.879606	27.253089	1.63
2000	35.444177	34.370407	1.07
2010	39.107187	38.54228	0.56
2020	35.529118	34.413173	1.12

Mean LST in the city center appeared to increase with each decadal buffer ring (Figure 4.13) in 1990 it dropped from 29.8 °C to around 27.04 °C at 3.9 km and then showed increase to 27.57 °C at about 5 km before then decreasing at the city boundary. In 2000 mean LST at the city center was higher (around 38.71 °C) and declined 33.54 °C at 2.4 km before rising again to 34.12 °C at 3.6 km before then again sharply declining 32.77 at 5.1km away from the city center. In 2010 at the center of the city, mean LST was around 40.11 °C, declining to 37.55 °C at 3.3 km then rising sharply to 39.7 °C at 6.9 km and again falling to around 38.14 °C at 11.6 km away from the city center (Figure 4.13-2010). In 2020 mean LST was highest at around 37.87 °C within 1 km of the city center rapidly declining to 34.22 °C at 3.3 km and spike again to 35.59 °C at around 4.5 km before declining again.

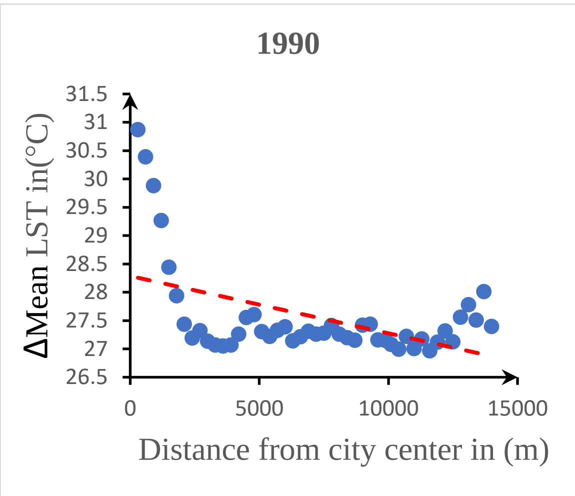

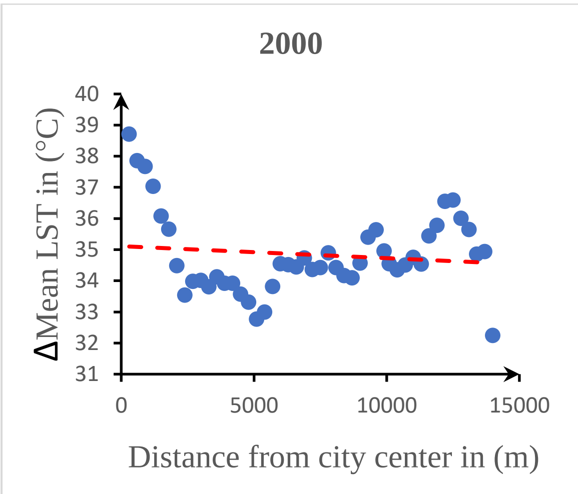

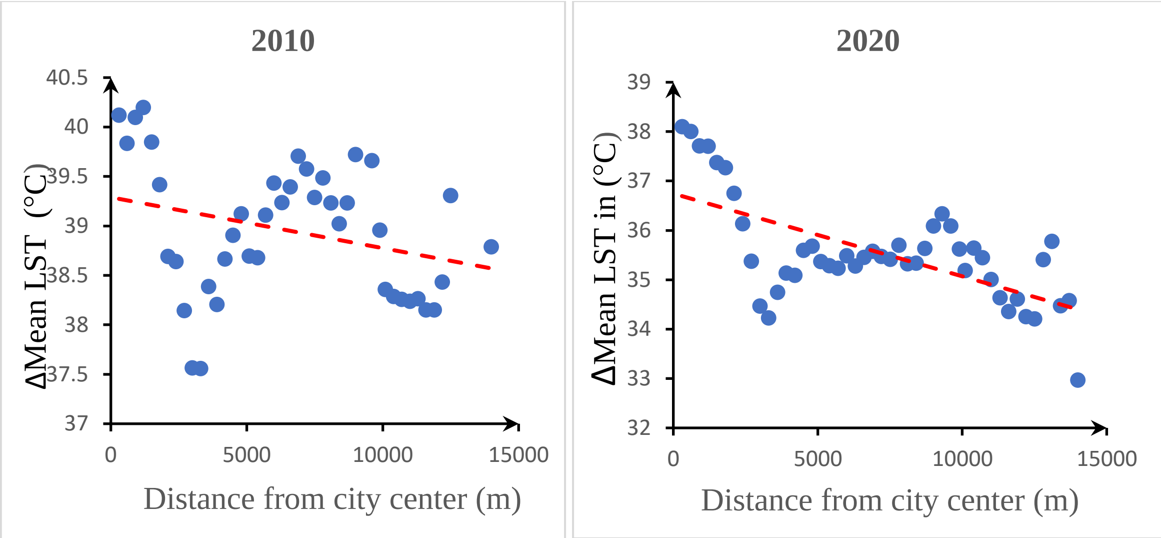

Figure 4.14 Urban heat island (Δmean LST) patterns along the urban–rural gradients of Adama City from 1990 -2020

The SUHI intensity values for the year of 1990 ranges from 0.5 °C to 2.9 °C along the urban area and reduced from 3.4 °C to 2.8 °C along the rural area. The SUHI intensity values for the year 2000 ranged from 0.8 °C to 5 °C along the urban area and also reduced from 6 °C to 2.1 °C along the rural area. SUHI intensity values for the year 2010 likewise ranged from 0.1 °C to 2.56°C along the urban area and reduced from 1.913 °C to 0.3989 °C and rise up to 1.9709 along the rural area. Correspondingly SUHI intensity values for the year of 2020 ranged from 0.1 °C to 3.6306°C and fail again to 2.4220°C along the urban area and as well reduced from 2.8714 °C to 1.7669 °C and raise up to 4°C along the rural area. the SUHI intensity results generally showed an irregular pattern of decreasing mean LST along the urban–rural gradient.

SUHII trend seen increasing and decreasing through those thirties' years. In all epoch SUHII shows constant increasing trend in urban zone in the trend of away from the city center. And decreasing trend with in the rural zone. However, in 2010 and 2020 shows fluctuating trend with in the rural zone. Previously stated continuous trend of Surface urban heat island intensity with in the urban zone signifies land surface temperature variation is also prominent with in the urban zone.

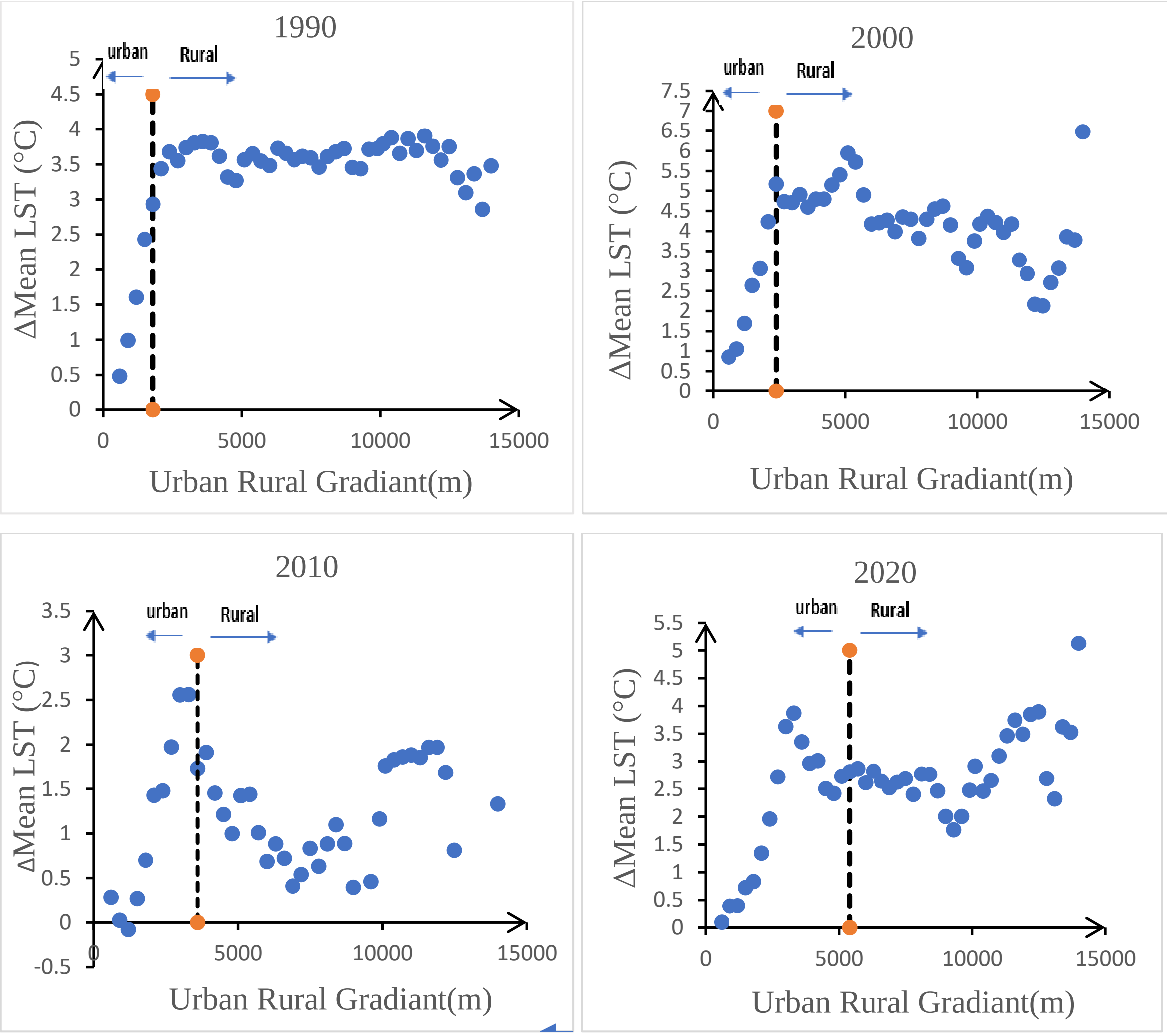

Figure 4.15 Urban heat island intensity (Δmean LST) patterns along the urban–rural gradients of Adama City from 1990 -2020

As shown on the LST computed map (Figure 4.11), temperatures rose from 1990 and 2020, with 2010 seeing higher temperatures than the rest of the epoch. In comparison to September 1990, the LST was greater in September 2020. Urban areas and bare land in all epoch had greater land surface temperatures than the surrounding areas, yet lower raised north eastern part of the city have higher land surface temperatures. The findings of the study are consistent with the findings of (Tafesse & Suryabhagavan, 2019). that LST was higher in urban areas than in the surrounding areas.

LST increases in urban is as a result of the growth in impervious surfaces, suggesting that Built-up expansions are contributing to the creation of urban heat islands (H. Li et al., 2018). LST increase in urban areas is attributed to the concentration of impervious surfaces, is also in agreement with the temperature data on (Figure 3.5) which was acquired from Adama Weather Station where the trend line is showing a slightly increasing trend of summer season temperature in adama city from 1990-2020. Albedo, thermal capacity, and heat conductivity were impacted by the conversion of natural surfaces to impermeable surfaces (Ngie et al., 2014). According to Adeyeri et al., (2017), LST is high on built-up areas and in bare surfaces whereas it is low in vegetated areas. This was consistent with the study's findings. High LSTs are experienced on bare surfaces as a result of incoming radiation that was totally absorbed.

Multidirectional and multitemporal LST profiles of adama city illustrate spatial variations of LST in the urban environment and its surroundings and it showed variation of LST with in each urban and rural buffer rings which reveals the thermal variations of LST along the urban rural gradient with in the city. The urban-rural temperature differences between the urban core and its surrounding areas show a maximum difference of 1.63 °C and minimum difference 0.56 °C This could lead to urban heat island effect in the urban areas. Vegetation has a significant impact on lowering the UHI effect, as seen by the link between LST and NDVI. Therefore, one of the most effective climate change adaptation strategies to reduce the negative effects of increased temperatures on urban area is the creation of urban green areas.

4.4 Relation between the changes in Land cover spatial pattern and LST

4.4.1 Relation between NDVI and LST

Across the study periods, the Pearson correlation analysis revealed that there was significant negative relationship between NDVI and LST for all epoch. The correlation analysis showed a strong person correlation coefficient (r) of -0.841, -0.829, -0.744 and -0.849 for the year of 1990,2000, 2010, 2020 respectively (Table 4.14), as a strong linear relationship exists between ± 0.5 and ± 1.0 at 95% level of confidence, which indicates a strong relationship between NDVI and associated LST values

Table 4.14 Pearson Correlation Between NDVI and LST

Year	Pearson correlation coefficient	Significance level
1990	-.841**	0.01(2-tailed)
2000	-.829**	0.01(2-tailed)
2010	-.744**	0.01(2-tailed)
2020	-.849**	0.01(2-tailed)

To highlight the effect of biomass on Land surface temperature, LST was represented as a function of NDVI the 1990, 2000, 2010, and 2020 analyzed result showed that NDVI and LST have inverse relationships R^2 values for the study period were 0.708, 0.687, 0.553, and 0.7215 indicating that 70%, 68%, 53% and 72% of the variations in LST were explained by NDVI in 1990, 2000, 2010 and 2020, respectively, (Figure 4.15) displays the land surface temperature and NDVI Correlation for the years 1990, 2000, 2010, and 2020 with high correlation coefficients (0.72) for the year of 2020.

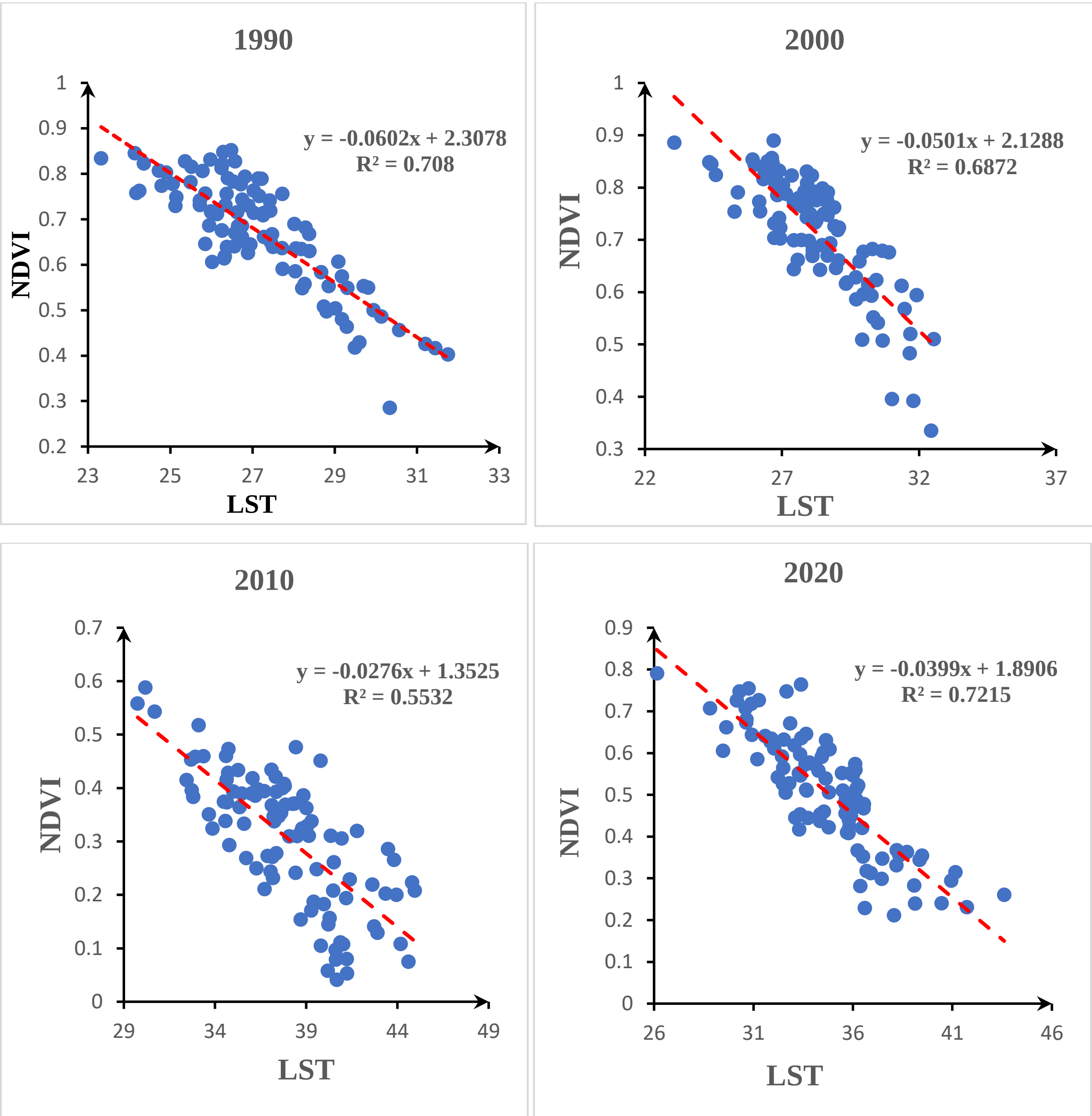

Figure 4.16 NDVI and LST correlation (1990 – 2020)

4.4.2 Relation between NDBI and LST

Pearson correlation coefficients of the bivariate correlation between NDBI and LST reveals (Table 4.15). That there is a strong positive correlation between NDBI and land surface temperature at the 0.01 level of significance for each epoch, the Pearson index was 0.639, 0.717, 0.807 and 0.762, for the year of 1990, 2000, 2010 and 2020 respectively.

Table 4.15 Pearson Correlation Between NDBI and LST

Year	Pearson correlation coefficient	Significance level
1990	.632**	0.01(2-tailed)
2000	.599**	0.01(2-tailed)
2010	.677**	0.01(2-tailed)
2020	.697**	0.01(2-tailed)

During the study period in all epoch direct relationship between NDBI and LST was found results of NDBI have shown higher surface temperature in Built-Up areas thus, the study has predicted that built-up areas or urbanization is inducing surface temperature variation in adama city. Within the study period the scatter-plot between NDBI & LST shows that NDBI have lower contribution to the variation in surface temperature but in trend of developing to more contributor i.e., R^2 = 0.3999, 0.3588, 0.4588 & 0.4864 in 1990, 2000, 2010 and 2020 respectively. The positive relationship found between NDBI and LST indicates that built-up area is generating surface temperature variations and increasing trend of its R^2 through the study period conforms that built-up expansion is one of the key contributors in surface urban heat island.

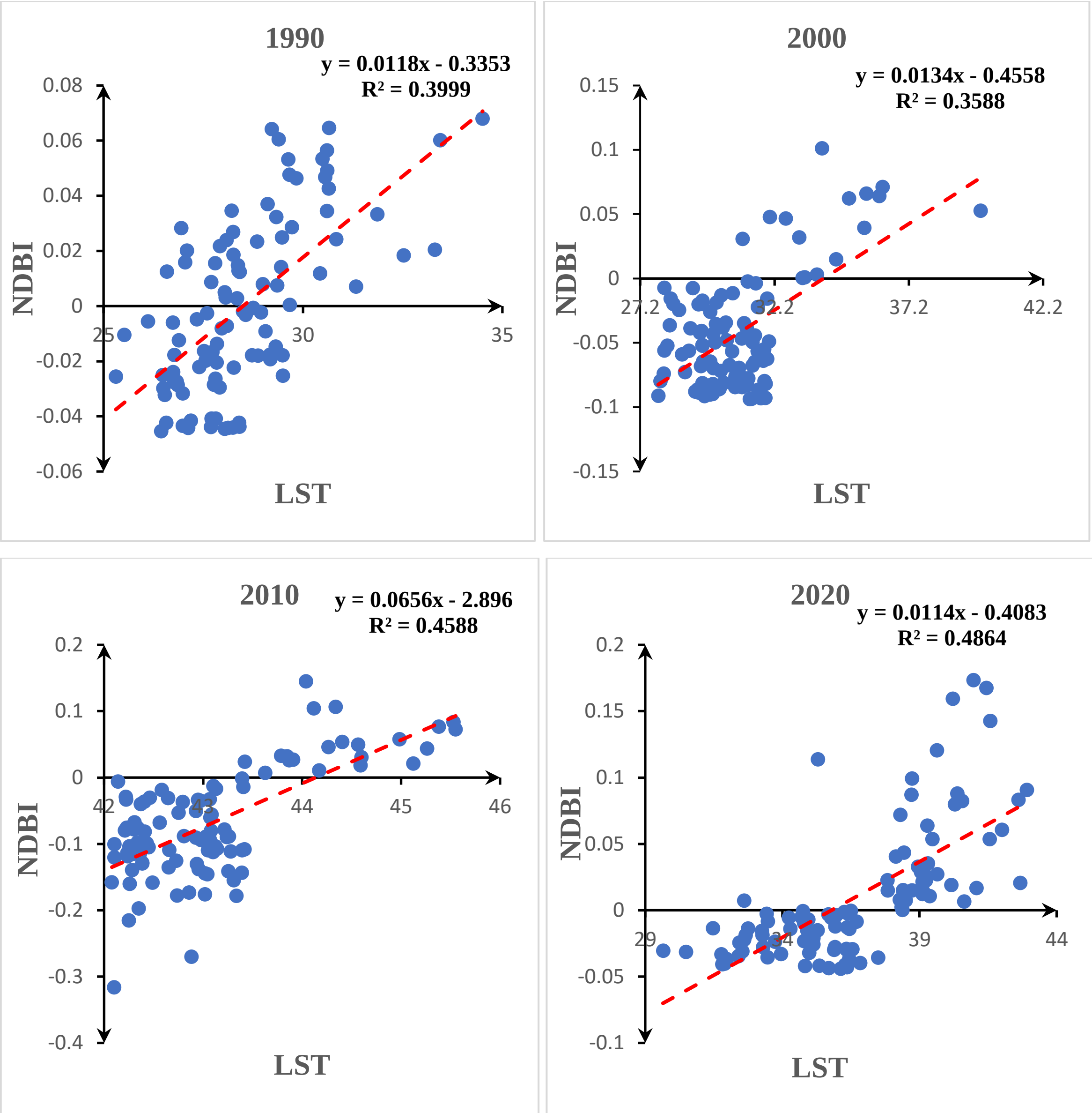

Figure 4.17 NDBI and LST correlation from (1990 – 2020)

The result reveals an inverse relationship between LST and NDVI and positive relationship between LST and NDBI. The findings of several earlier investigations (Ogashawara & Brum-Bastos, 2012; Kumar & Shekhar, 2015 and Guo et al., 2015) are extremely consistent with this observation. The study area's vegetation helps to reduce the UHI effect while the built-up area intensifies it, the impact of NDBI also has a propensity to be greater. As seen in the 1990–2020-time interval, the NDBI coefficient of R^2 increased from 0.399 to 0.486 this can be explained by analyzing the trend of rapid urbanization during this period. Besides to these the relationship between LST with NDVI and NDBI suggests that urban zone contribute for the variation in land surface temperature dynamics. However, Vegetation cover accounts the most hand for the variation in surface temperature in adama city. Therefore, NDVI and NDBI is an accurate indicator of surface UHI effects in study area.

4.4.3 Relation between vegetation cover Spatial pattern and Land surface temperature

The Pearson correlation coefficients show that all of vegetation land cover configuration metrics variables, were significantly at the 99% (2-tailed) confidence level correlated to LST. A negative coefficient for an independent variable indicates that all the variable has negative effective on LST or that LST decreases with the increase of the value of vegetation land cover configuration variable however among the four-vegetation land cover configuration metrics, only ED, PD and FRAC_MN vegetation land cover metric related closely with LST at (2-tailed) confidence level where as AI have lower negative relationship with LST. (Table 4.16)

Table 4.16 Pearson Correlation Between Vegetation land configuration Metrics and LST

Vegetation land cover configuration metrics	Pearson correlation coefficient	Significance level
PD	-.578**	0.01(2-tailed)
ED	-.615**	0.01(2-tailed)
AI	-.370**	0.01(2-tailed)
FRAC_MN	-.521**	0.01(2-tailed)

For each of the selected vegetation land cover configuration spatial metrics, except AI which have a weaker negative correlation with LST. a multi-collinearity condition with the variance inflation factor (VIF) reveal non collinearity among the configuration variable the values of VIF for each independent variable were less than 10 and tolerance higher than 0 (Table 4.17)

Table 4.17 Collinearity Test Result

Vegetation land cover configuration Metrices	Collinearity Statistics	
	Tolerance	VIF
Ed	.748	1.337
FRAC_MN	.848	1.180
PD	.739	1.352

Likewise, Normality test of configuration metrics signifies that data of the configuration metrics have symmetric distribution around the mean (all have sig value > 0.05) and less correlation between theme which states eligible for Statistical analysis (Table 4.18)

Table 4.18 Normality Test Result

Vegetation land cover configuration Metrices	Normality Statistics		
	Statistic	df	Sig.
Ed	.080	106	.094
FRAC_MN	.078	106	.123
PD	.076	106	.157

(Table 4.19) shows that the results from simple and multiple linear regression models reveals vegetation land cover spatial pattern had significant negative impacts on LST. Furthermore, all of the configuration metrics at once were the most significant indicator of LST, playing a considerably more significant role in forecasting LST relative to the other combination spatial configuration factors. Among the three-configuration metrics, disjointedly ED played more significant and negative effect in estimating LST followed by PD, in paired form ED and PD played most significant and similarly PD, ED and FRAC_MN in triple form played the most significant role than the rest combination of Metrics in predicting the variation in land surface temperature due to configuration of vegetation land cover. Approximately 57 % of the variation in LST was explained jointly by the three configuration variables.

Table 4.19 Simple and Multiple Linear regression Model Result

No	Metrics	R^2 (ANOVA)
1	PD	.334
2	ED	.379
3	FRAC_MN	.272
4	PD, ED	.492
5	PD, FRAC_MN	.459
6	ED, FRAC_MN	.491
7	PD, ED, FRAC_MN	.566

The results indicated that configuration, fragmentation, and shape complexity characteristics of vegetation cover affected LST Moreover, multiple regression result between LST and Vegetation land cover Configuration ED, PD and FRAC_MN reveals that vegetation cover configuration variables significantly predicted LST due to configuration. From the following model summary (Table 4.2) a 10% increase in PD and ED of Vegetation land cover configuration resulted approximately 0.91 °C and 0.24 °C decrease in LST respectively and Likewise 0.1 increase in FRAC_MN of Vegetation land cover configuration resulted decrease in LST by 2.58 °C

Table 4.20 Multiple Linear Regression Model Result

Model	Unstandardized Coefficients		Standardized Coefficients	Std. Error	Sig
	B	Std. Error	Beta		
Constant	65.032	6.291		10.338	.000
PD	-.091	.022	-.313	-4.200	.000
ED	-.024	.005	-.376	-5.013	.000
FRAC_MN	-25.776	6.190	-.295	-4.164	.000
Dependent Variable: Land Surface Temperature					

The results of the study's regression analysis demonstrated that not only composition of vegetation land cover but also the geographical distribution and arrangement of vegetation and land cover had a substantial impact on the magnitude of LST in Adama City. This research adds to the body of knowledge about the effects of vegetation land cover pattern on

LST in urban landscapes by explicitly characterizing the quantitative linkages of LST with the configuration of vegetation land cover characteristics. The landscape metrics of Vegetation land cover (ED, PD and FRAC_MN) clearly demonstrated a negative connection with LST, which is in line with the results of (X. Li et al., 2012; L. Yang et al., 2022; Zhou & Cao, 2020) given that green space can provide cold island effects through evapotranspiration and provide shade to prevent the surface from being directly heated by the sun, this demonstrates how an increase in Vegetation patch edge, more patches and complexity and irregular patch shape can reduce LST .

Nevertheless, vegetation land cover configuration metrics relationship with LST were different from those in the earlier investigations. For instance, there are different research that support the positive connection between PD and LST (Wesley & Brunsell, 2019; Masoudi & Tan, 2019; Keno et al., 2020), likewise ED of vegetation land cover configuration have negative correlation with LST in the study (Wesley & Brunsell, 2019; Zhou et al., 2017), but positive in (X. Li et al., 2013).

An increase in edge density may result in an increase in the amount of shadow that plants cast on nearby surfaces (Yan et al., 2019). It might also enhance the connection and flow of energy between vegetation and its surroundings. When only addressing the shading process, increasing edge density will consequently result in a reduction in LST. On the other hand, increasing edge density is mostly caused by highly disaggregated vegetation land cover configuration. According to (Masoudi & Tan, 2019), small and dispersed Vegetation land cover are warmer than aggregated and bigger patches, which may affect the effectiveness of evapotranspiration and surface albedo.

LST was observed to decrease as Vegetation land cover shape complexity increased, likely because this resulted in a reduction in LST due to an increase in the area of shadow cast by plants (Wang, et al., 2017) the more complex the vegetation land cover patch shape, the lower the LST. The reason for this is that complex vegetation land cover has more surfaces to exchange energy with the outside, which reduces the temperature of the external environment. However, the result is inconsistence with results of Keno et al., (2020) UGS with simpler and regular patches leads to reduced LST, the conflicting configuration metric findings observed by various studies are most likely caused by variation in season and spatial resolution of the thermal image, and scale of investigations in this study study's daytime thermal imaging was taken in the summer, whereas the prior studies were taken in the dry season, February (Keno et al., 2020) Seasonal variations in the link between LST and urban land cover features have been demonstrated in earlier research (Hamada & Ohta, 2010) and further research showed that the relationship between the configuration and LST changes across the scale (Chakraborti et al., 2019).

CHAPTER 5: CONCLUSION AND RECOMMENDATION

5.1 Conclusion

LUCC analysis is vital for revealing information on landscape changes. The outcomes of the analysis of LULC are important for decision-makers to work towards sustainable environmental management and development. The study employed 30 years decadal interval Landsat imageries as a main data source to analyze the dynamics of landscape composition and configuration and investigated the evolution and spatial distribution of SUHI in Adama city, further the study explored how the underlying (configuration) characteristics of vegetation land cover affect land surface temperature using simple linear and multiple regression analysis. The following significant and conclusive findings were reached.

- In the last three decades, the LULC of Adama city has changed in the main the city has experienced rapid built-up expansion. The reason for the change is the rapid urbanization and population growth. Agricultural land cover is till the predominant land cover type, but it continuously decreases. On the other hand, the urbanized area showed a significant increase with annual growth of 23.25% at the expense of agricultural land and bare land. About the rate of Built-up expansion in difference periods (1990–2000, 2000–2010, & 2010–2020), the highest city expansion occurred in 2010–2020 by 2539.8 ha.

- The city expansion was mainly distributed along the north, and southeastern part the finding of this study showed that the LST of Adama city has been increasing since 1990 and there is a significant spatial variation of LST in the city places found in the Northeast and southeast of the city, as well as Built-up areas of Adama city, were characterized by high LST than places located on the Northwest and Southern tip of the city boundary Besides to these, urbanization in the Northeast and southeastern part of the city and increase in industrial/Manufacturing areas in southwest contribute significantly to the warming of Adama city.

- The characteristic of land use types from the highest temperature in the sequence is Bare-land, Built-up, agricultural land, and vegetated land cover. It indicated that the urban area is warmer than the suburban area because the urban area is mainly covered by built-up area. Over the past 30 years, the surface UHI expanded from the inner city towards the suburban area the temperature difference between urban and suburban due to built-up expansion was 1.63 ◦C in 1990, 1.07 ◦C in 2000, 0.56 ◦C in 2010, and 1.12 ◦C in 2020. Further, these variations in land surface temperature between urban and rural zone were more elaborated by surface urban heat island intensity and revealed SUHII trend can be seen increasing and decreasing through those thirties' years. In all epochs SUHII have a constant increase in the urban zone in the trend away from the city center and decreasing trends within the rural zone, However, 2010 and 2020 show a fluctuating trend in the rural zone. as previously stated, continuous trend of Surface urban heat island intensity in the urban zone signifies land surface temperature variation is also prominent within the urban zone.

- Finally, Simple linear and multiple regression was used to quantify the relationship between LST and vegetation land cover spatial metrics including (FRAC-MN), edge density (ED), and patch density the study investigated that vegetation land cover configuration spatial metrics had a significant negative influence on the LST and found that all the three-vegetation land cover configuration variable (PD, ED, and FRAC-MN) had the most significant impact on the LST the joint effect differed in magnitude from the unique effect of the configuration of the vegetation land cover on the LST generally speaking, the joint effect of vegetation land cover configuration had a stronger influence on the LST than the unique effect of each configuration variable, optimizing the configuration of vegetation land cover which increases the PD, FRAC-MN and ED should be prioritized in sustainable urban planning and development to mitigate urban heat island effects. The study results revealed that besides to composition, underlying factor(configuration) of vegetation land cover has an impact on the LST of Adama city moreover, by increasing patch and edge density and complexity of the vegetation land cover, the thermal environment of Adama city can be improved

5.2 Recommendation

This study has harnessed wet season remote sensing imagery from both Landsat and MODIS, and examined the impact of urbanization-induced land use/ cover dynamics and vegetation land cover configuration on land surface temperature in Adama City. This was accompanied with correlation and regression analysis on the associations between different land use/ cover indices and vegetation land cover configuration spatial metrics with LST, and effect of urbanization-induced land use land cover change on LST was assessed using the urban-rural gradient analysis generated from the multi-buffer ring. This study discovered that urbanization-induced LULC transformation was one of the key factors influencing LST variation. As a result of the study's findings, the following recommendations have been made.

- The implementation of emissivity corrected Inverted Planks Equation and support vector machine supervised classification methods in Landsat imageries has proven to be an effective and simple process for LST retrieval and LULC creation. Additionally, spatial metrics were helpful in spatial analysis and as well as in illustrating the dynamics of changing the land cover configuration. Future research should incorporate spatial metrics like composition and configuration for all land use/cover categories to determine how closely LST and LULC (composition and configurations) are related, as well as the impact of season on spatial analysis. The outcomes enable the identification of the effects that LULC has on LST, which is essential for addressing the implications impacting the city climatic balance. Through the enhancement of land use planning systems, moreover this kind of analysis is helpful to enhance climate change mitigation strategies.

- This study discovered significant LULC changes caused by rapid urbanization, with Vegetation cover declining until 2010 and rising again in 2020 this study demonstrates that forestry activities in Adama City persisted after 2010, and residents and administrative of the city should continue to prioritize this work.

- Corresponds to the rising in land surface temperature in Adama City during the last three decades a sensible strategy for addressing climate change is to increase the composition of vegetation land cover however, it could clash with other socioeconomic interests that require a certain amount of area. Therefore, rather than creating new, smaller ones, urban planners should focus on increasing the complexity, edge density and patch density of current vegetation land cover to strike a balance between sustainable growth and the rise in vegetation cover. Furthermore, to reduce LST in the city and the environment, urban green zones and plantations should increase along critical roads, parking lots and buildings because these sites have considerable heating.

REFERENCE

Abbas, Z., & Jaber, H. S. (2020). Accuracy assessment of supervised classification methods for extraction land use maps using remote sensing and GIS techniques. *IOP Conference Series: Materials Science and Engineering*, *745*(1). https://doi.org/10.1088/1757-899X/745/1/012166

Abdul Athick, A. S. M., & Shankar, K. (2019). Data on land use and land cover changes in Adama Wereda, Ethiopia, on ETM+, TM and OLI- TIRS landsat sensor using PCC and CDM techniques. *Data in Brief*, *24*(March), 103880. https://doi.org/10.1016/j.dib.2019.103880

Abebe, M. S., Derebew, K. T., & Gemeda, D. O. (2019). Exploiting temporal-spatial patterns of informal settlements using GIS and remote sensing technique: a case study of Jimma city, Southwestern Ethiopia. *Environmental Systems Research*, *8*(1). https://doi.org/10.1186/s40068-019-0133-5

Abel, B. (2018). *Impacts of Land-Use and Land-Cover Changes on Land Surface Temperature Distribution in Bahir Dar Town and Its Surroundings Using Remote Sensing*. *June*.

Adeyeri, O. E., Akinsanola, A. A., & Ishola, K. A. (2017). Investigating surface urban heat island characteristics over Abuja, Nigeria: Relationship between land surface temperature and multiple vegetation indices. *Remote Sensing Applications: Society and Environment*, *7*, 57–68. https://doi.org/10.1016/J.RSASE.2017.06.005

Ae, M. J. M., & Hahs, A. K. (2007). *The use of gradient analysis studies in advancing our understanding of the ecology of urbanizing landscapes: current status and future directions*. https://doi.org/10.1007/s10980-008-9253-4

Agarwal, C., Green, G. M., Grove, M., Evans, T. P., & Schweik, C. (2002). *A Review and Assessment of Land-Use Change Models.Dynamics of Space, Time, and Human Choice*.

Aguilera, F., Valenzuela, L. M., & Botequilha-Leitão, A. (2011). Landscape metrics in the analysis of urban land use patterns: A case study in a Spanish metropolitan area. *Landscape and Urban Planning*, *99*(3–4), 226–238. https://doi.org/10.1016/J.LANDURBPLAN.2010.10.004

Akbari, H., Cartalis, C., Kolokotsa, D., Muscio, A., Pisello, A. L., Rossi, F., Santamouris, M., Synnefa, A., Wong, N. H., & Zinzi, M. (2016). Local climate change and urban heat island mitigation techniques – the state of the art. *Journal of Civil Engineering and Management*, *22*(1), 1–16. https://doi.org/10.3846/13923730.2015.1111934

Angel, S., Sheppard, S., & Civco, D. (2005). *The Dynamics of Global Urban Expansion. Transport and Urban Development Department*.

Arnfield, A. (2003). Two decades of urban climate research: A review of turbulence, exchanges of energy and water, and the urban heat island. *International Journal of Climatology*, *23*, 1–26. https://doi.org/10.1002/joc.859

Balew, A., & Korme, T. (2020). Monitoring land surface temperature in Bahir Dar city and its surrounding using Landsat images. *The Egyptian Journal of Remote Sensing and*

Space Science, *23*. https://doi.org/10.1016/j.ejrs.2020.02.001

Balzerek, H. (2003). Man-made flood disaster in the Savanna town of Gombe/NE Nigeria. The natural hazard of gully erosion caused by urbanization dynamics and their peri-urban footprints. *Erdkunde*, *57*, 94–109. https://doi.org/10.3112/erdkunde.2003.02.02

Banzhaf, E., Grescho, V., & Kindler, A. (2009). Monitoring urban to peri-urban development with integrated remote sensing and GIS information: a Leipzig, Germany case study. *International Journal of Remote Sensing*, *30*(7), 1675–1696. https://doi.org/10.1080/01431160802642297

BECKER, F., & LI, Z.-L. (1990). Towards a local split window method over land surfaces. *International Journal of Remote Sensing*, *11*(3), 369–393. https://doi.org/10.1080/01431169008955028

Becker, F., & Li, Z. (1995). Surface temperature and emissivity at various scales: Definition, measurement and related problems. *Remote Sensing Reviews*, *12*(3–4), 225–253. https://doi.org/10.1080/02757259509532286

Becker, F., & Li, Z. L. (1990). Temperature-independent spectral indices in thermal infrared bands. *Remote Sensing of Environment*, *32*(1), 17–33. https://doi.org/10.1016/0034-4257(90)90095-4

Belete, T. (2017). *Impact of Land-Use / Land-Cover Changes on Land Surface Temperature in Adama Zuria Woreda , Ethiopia , Using Geospatial Tools*. 91.

Belete Tafesse, Suryabhagavan, K. V. (2019). Systematic modeling of impacts of land-use and land-cover changes on land surface temperature in Adama Zuria District , Ethiopia. *Modeling Earth Systems and Environment*, *0*(0), 0. https://doi.org/10.1007/s40808-018-0567-1

Bhatta, B. (2010). Analysis of Urban Growth and Sprawl from Remote Sensing Data. *Springer, Heidelberg, 172. Https://Doi.Org/10.1007/978-3-642-05299-6*.

Bosilovich, M. G. (n.d.). *A comparison of MODIS land surface temperature with in situ observations*. https://doi.org/10.1029/2006GL027519

Bufebo, B., & Elias, E. (2020). Effects of Land Use/Land Cover Changes on Selected Soil Physical and Chemical Properties in Shenkolla Watershed, South Central Ethiopia. *Advances in Agriculture*, *2020*(August), 1–8. https://doi.org/10.1155/2020/5145483

Bulti, D. T., & Assefa, T. (2019). Analyzing ecological footprint of residential building construction in Adama City, Ethiopia. *Environmental Systems Research*, *8*(1). https://doi.org/10.1186/s40068-019-0130-8

Butt, A., Shabbir, R., Ahmad, S. S., & Aziz, N. (2015). Land use change mapping and analysis using Remote Sensing and GIS: A case study of Simly watershed, Islamabad, Pakistan. *The Egyptian Journal of Remote Sensing and Space Science*, *18*(2), 251–259. https://doi.org/10.1016/J.EJRS.2015.07.003

Buyadi, S. N. A., Mohd, W. M. N. W., & Misni, A. (2013). Green Spaces Growth Impact on the Urban Microclimate. *Procedia - Social and Behavioral Sciences*, *105*, 547–557. https://doi.org/10.1016/J.SBSPRO.2013.11.058

Cabral, P., Geroyannis, H., Gilg, J.-P., & Painho, M. (2005). Analysis and modeling of land-use and land-cover change in Sintra-Cascais area. *Proceedings 2005 - The 8th AGILE International Conference on Geographic Information Science, AGILE 2005*.

Cai, Z., Han, G., & Chen, M. (2018). Do water bodies play an important role in the relationship between urban form and land surface temperature? *Sustainable Cities and Society*, *39*, 487–498. https://doi.org/10.1016/j.scs.2018.02.033

Ceccato, P., Flasse, S., Tarantola, S., Jacquemoud, S., & Grégoire, J.-M. (2001). Detecting vegetation leaf water content using reflectance in the optical domain. *Remote Sensing of Environment*, *77*, 22–33. https://doi.org/10.1016/S0034-4257(01)00191-2

Central Statistical Authority. (2021). *2021 Population Projection Ethiopia: Results for Adama City. Adama, Ethiopia.*

Chaka, D., & Oda, T. (2021). Understanding land surface temperature on rift areas to examine the spatial variation of urban heat island: the case of Hawassa, southern Ethiopia. *GeoJournal*, *86*. https://doi.org/10.1007/s10708-019-10110-5

Chakraborti, S., Banerjee, A., Sannigrahi, S., Pramanik, S., Maiti, A., & Jha, S. (2019). Assessing the dynamic relationship among land use pattern and land surface temperature: A spatial regression approach. *Asian Geographer*, *36*(2), 93–116. https://doi.org/10.1080/10225706.2019.1623054

Charney, J., Quirk, W. J., Chow, S. H., & Kornfield, J. (1977). Comparative Study of the Effects of Albedo Change on Drought in Semi-Arid Regions. In *Journal of the Atmospheric Sciences* (Vol. 34, Issue 9, pp. 1366–1385). https://doi.org/10.1175/1520-0469(1977)034<1366:ACSOTE>2.0.CO;2

Chen, F., Yang, S., Su, Z., & Wang, K. (2016). Effect of emissivity uncertainty on surface temperature retrieval over urban areas: Investigations based on spectral libraries. *ISPRS Journal of Photogrammetry and Remote Sensing*, *114*, 53–65. https://doi.org/10.1016/J.ISPRSJPRS.2016.01.007

Chen, J., Zhu, X., Vogelmann, J. E., Gao, F., & Jin, S. (2011). A simple and effective method for filling gaps in Landsat ETM+ SLC-off images. *Remote Sensing of Environment*, *115*(4), 1053–1064. https://doi.org/10.1016/J.RSE.2010.12.010

Chen, X. L., Zhao, H. M., Li, P. X., & Yin, Z. Y. (2006). Remote sensing image-based analysis of the relationship between urban heat island and land use/cover changes. *Remote Sensing of Environment*, *104*(2), 133–146. https://doi.org/10.1016/J.RSE.2005.11.016

Choudhury, D., Das, K., & Das, A. (2019). Assessment of land use land cover changes and its impact on variations of land surface temperature in Asansol-Durgapur Development Region. *The Egyptian Journal of Remote Sensing and Space Science*, *22*(2), 203–218. https://doi.org/10.1016/J.EJRS.2018.05.004

Coll, C., Caselles, V., Galve, J. M., Valor, E., Niclòs, R., Sánchez, J. M., & Rivas, R. (2005). Ground measurements for the validation of land surface temperatures derived from AATSR and MODIS data. *Remote Sensing of Environment*, *97*(3), 288–300. https://doi.org/10.1016/J.RSE.2005.05.007

Cristóbal, J., Jiménez-Muñoz, J. C., Sobrino, J. A., Ninyerola, M., & Pons, X. (2009).

Improvements in land surface temperature retrieval from the Landsat series thermal band using water vapor and air temperature. *Journal of Geophysical Research Atmospheres*, *114*(8), 1–16. https://doi.org/10.1029/2008JD010616

Dash, P., Göttsche, F.-M., Olesen, F.-S., & Fischer, H. (2001). Retrieval of land surface temperature and emissivity from satellite data: Physics, theoretical limitations and current methods. *Journal of the Indian Society of Remote Sensing*, *29*(1), 23. https://doi.org/10.1007/BF02989910

Davis, J. C., & Vernon Henderson, J. (2003). Evidence on the political economy of the urbanization process. *Journal of Urban Economics*, *53*(1), 98–125. https://doi.org/10.1016/S0094-1190(02)00504-1

Degefu, M. A., Argaw, M., Feyisa, G. L., & Degefa, S. (2021). Effects of urbanization on the relationship between greenspace patterns and evolution of regional heat island in cities of Ethiopia. *Chinese Journal of Population, Resources and Environment*, *19*(4), 330–343. https://doi.org/10.1016/J.CJPRE.2022.01.006

Dejene, Tesema, B., & Abebe. (2019). *Analyzing the impacts of urbanization on runoff characteristics in Adama city, Ethiopia*. https://doi.org/10.21203/rs.2.19418/v1

Dewan, A., Yamaguchi, Y., & Rahman, Z. (2012). Dynamics of land use/cover changes and the analysis of landscape fragmentation in Dhaka Metropolitan, Bangladesh. *GeoJournal*, 1–16. https://doi.org/10.1007/s10708-010-9399-x

Dousset, B., & Gourmelon, F. (2003). Satellite multi-sensor data analysis of urban surface temperatures and landcover. *ISPRS Journal of Photogrammetry and Remote Sensing*, *58*(1–2), 43–54. https://doi.org/10.1016/S0924-2716(03)00016-9

Du, H., Cai, Y., Zhou, F., Jiang, H., Jiang, W., & Xu, Y. (2019). Urban blue-green space planning based on thermal environment simulation: A case study of Shanghai, China. *Ecological Indicators*, *106*, 105501. https://doi.org/10.1016/J.ECOLIND.2019.105501

Dube, E., & Mulugeta, S. (2015). Analysis of the Changing Functional Structure of Major Urban Centers of Ethiopia. *Ethiopian Journal of Business and Economics (The)*, *4*, 220. https://doi.org/10.4314/ejbe.v4i2.2

Dunn. C P, Sharpe. DM, Guntensbergen. G R, Stearns F, & Y. Z. (1991). Methods for analyzingtemporal changes in landscape pattern. *Quantitative Methodsin Landscape Ecology: The Analysis and Interpretation of Landscape Heterogeneity (Pp. 173–198). NewYork: Springer Verlag*.

Effati, F., Karimi, H., & Yavari, A. (2021). *Investigating effects of land use and land cover patterns on land surface temperature using landscape metrics in the city of Tehran, Iran*. https://doi.org/10.1007/s12517-021-07433-4/Published

Ellis, E. C. (2011). Anthropogenic transformation of the terrestrial biosphere. *Philosophical Transactions of the Royal Society A: Mathematical, Physical and Engineering Sciences*, *369*(1938), 1010–1035. https://doi.org/10.1098/rsta.2010.0331

Elvidge, C. D., Dietz, J. B., Berkelmans, R., Andréfouët, S., Skirving, W., Strong, A. E., & Tuttle, B. T. (2004). Satellite observation of Keppel Islands (Great Barrier Reef) 2002 coral bleaching using IKONOS data. *Coral Reefs*, *23*(1), 123–132.

https://doi.org/10.1007/s00338-003-0364-8

Erell, E., Pearlmutter, D., & Williamson, T. (2011). *Urban Microclimate – Designing the Spaces Between Buildings*.

Ermida, S. L., Trigo, I. F., DaCamara, C. C., Göttsche, F. M., Olesen, F. S., & Hulley, G. (2014). Validation of remotely sensed surface temperature over an oak woodland landscape — The problem of viewing and illumination geometries. *Remote Sensing of Environment*, *148*, 16–27. https://doi.org/10.1016/J.RSE.2014.03.016

Estoque, R., Murayama, Y., & Myint, S. (2016). Effects of landscape composition and pattern on land surface temperature: An urban heat island study in the megacities of Southeast Asia. *Science of The Total Environment*, *577*. https://doi.org/10.1016/j.scitotenv.2016.10.195

Fahrig, L. (2001). How much habitat is enough? *Biological Conservation*, *100*(1), 65–74. https://doi.org/10.1016/S0006-3207(00)00208-1

Fahrig, L. (2003). Fahrig L.. Effects of Habitat Fragmentation on Biodiversity. Annu Rev Ecol Evol Syst 34: 487-515. *Annual Review of Ecology, Evolution, and Systematics*, *34*, 487–515. https://doi.org/10.1146/annurev.ecolsys.34.011802.132419

Faqe Ibrahim, G. R. (2017). Urban Land Use Land Cover Changes and Their Effect on Land Surface Temperature: Case Study Using Dohuk City in the Kurdistan Region of Iraq. In *Climate* (Vol. 5, Issue 1). https://doi.org/10.3390/cli5010013

Federico Moran, E. (n.d.). *Land Cover Classification in a Complex Urban-Rural Landscape with Quickbird Imagery*.

Ferdissa, D. (2019). Ethnic Decentralization and Negotiating Statehood in Urban Ethiopia. *Philosophisch-Historische Fakultät Der Universität Basel*, *2019*.

Feyisa, G. L., Dons, K., & Meilby, H. (2014). Efficiency of parks in mitigating urban heat island effect: An example from Addis Ababa. *Landscape and Urban Planning*, *123*, 87–95. https://doi.org/10.1016/J.LANDURBPLAN.2013.12.008

Fletcher. (2017). Inconsistent effects of landscape heterogeneity and land-use on animal diversity in an agricultural mosaic: a multi-scale and multi-taxon investigation. *Landscape Ecology*, *33*. https://doi.org/10.1007/s10980-017-0595-7

Foley, J. A., DeFries, R., Asner, G. P., Barford, C., Bonan, G., Carpenter, S. R., Chapin, F. S., Coe, M. T., Daily, G. C., Gibbs, H. K., Helkowski, J. H., Holloway, T., Howard, E. A., Kucharik, C. J., Monfreda, C., Patz, J. A., Prentice, I. C., Ramankutty, N., & Snyder, P. K. (2005). Global consequences of land use. *Science*, *309*(5734), 570–574. https://doi.org/10.1126/science.1111772

Frenkel, A., & Ashkenazi, M. (2008). Measuring Urban Sprawl: How Can We Deal with It? *Environment and Planning B: Planning and Design*, *35*, 56–79. https://doi.org/10.1068/b32155

Furberg, D. (2014). Satellite Monitoring of Urban Growth and Indicator-based Assessment of Environmental Impact. In *Royal Institute of Technology (KTH) Department of Urban Planning and Environment*.

G/Michael, H. (2021). *Land use /Land cover change and its implications on Land Surface Temperature change in Addis Ababa and its surrounding area, Ethiopia*. *February*.

Gandhi, G. M., Parthiban, S., Thummalu, N., & Christy, A. (2015). Ndvi: Vegetation Change Detection Using Remote Sensing and Gis – A Case Study of Vellore District. *Procedia Computer Science*, *57*, 1199–1210. https://doi.org/10.1016/J.PROCS.2015.07.415

Gao, B. C. (1996). NDWI—A normalized difference water index for remote sensing of vegetation liquid water from space. *Remote Sensing of Environment*, *58*(3), 257–266. https://doi.org/10.1016/S0034-4257(96)00067-3

Garg, V., Nikam, B. R., Thakur, P. K., Aggarwal, S. P., Gupta, P. K., & Srivastav, S. K. (2019). Human-induced land use land cover change and its impact on hydrology. *HydroResearch*, *1*, 48–56. https://doi.org/10.1016/J.HYDRES.2019.06.001

Gashu, K., & Gebre-Egziabher, T. (2018). Spatiotemporal trends of urban land use/land cover and green infrastructure change in two Ethiopian cities: Bahir Dar and Hawassa. *Environmental Systems Research*, *7*. https://doi.org/10.1186/s40068-018-0111-3

Gebrekristos Mezgebo, T. (2021). *Urbanization and Development in Ethiopia: Policy Issues, Trends and Prospects*.

Gillespie, A. (1996). LAND SURFACE EMISSIVITY. *Department of Earth and Space Sciences, University of Washington, Seattle, WA, USA.*

Gillespie, A., Rokugawa, S., Matsunaga, T., Cothern, J. S., Hook, S., & Kahle, A. B. (1998). A temperature and emissivity separation algorithm for Advanced Spaceborne Thermal Emission and Reflection Radiometer (ASTER) images. *IEEE Transactions on Geoscience and Remote Sensing*, *36*(4), 1113–1126. https://doi.org/10.1109/36.700995

GORMUS, S., OĞUZ, D., EŞBAH TUNÇAY, H., & CENGİZ, S. (2021). Using Landscape Character Analysis To Assess The Relationship Between Protected and Nonprotected Areas: The Case of The Küre Mountains National Park. *Tarım Bilimleri Dergisi*, *February*. https://doi.org/10.15832/ankutbd.640159

Göttsche, F.-M., Olesen, F.-S., Trigo, I. F., Bork-Unkelbach, A., & Martin, M. A. (2016). *remote sensing Long Term Validation of Land Surface Temperature Retrieved from MSG/SEVIRI with Continuous in-Situ Measurements in Africa*. https://doi.org/10.3390/rs8050410

Guillevic, P. C., Biard, J. C., Hulley, G. C., Privette, J. L., Hook, S. J., Olioso, A., Göttsche, F. M., Radocinski, R., Román, M. O., Yu, Y., & Csiszar, I. (2014). Validation of Land Surface Temperature products derived from the Visible Infrared Imaging Radiometer Suite (VIIRS) using ground-based and heritage satellite measurements. *Remote Sensing of Environment*, *154*, 19–37. https://doi.org/10.1016/J.RSE.2014.08.013

Guillevic, P. C., Bork-Unkelbach, A., Göttsche, F. M., Hulley, G., Gastellu-Etchegorry, J.-P., Olesen, F. S., & Privette, J. L. (2013). Directional Viewing Effects on Satellite Land Surface Temperature Products Over Sparse Vegetation Canopies—A

Multisensor Analysis. *IEEE Geoscience and Remote Sensing Letters*, *10*(6), 1464–1468. https://doi.org/10.1109/LGRS.2013.2260319

Guo, W., Lu, D., Wu, Y., & Zhang, J. (2015). Mapping Impervious Surface Distribution with Integration of SNNP VIIRS-DNB and MODIS NDVI Data. In *Remote Sensing* (Vol. 7, Issue 9, pp. 12459–12477). https://doi.org/10.3390/rs70912459

Gupta, R. (2018). Remote Sensing Geology. In *Remote Sensing Geology: Third Edition*. https://doi.org/10.1007/978-3-662-55876-8

Gustafson, E. (1998). Quantifying Landscape Spatial Pattern: What Is the State of the Art? *Ecosystems*, *1*, 143–156. https://doi.org/10.1007/s100219900011

Hagen-Zanker, A. (2016). A computational framework for generalized moving windows and its application to landscape pattern analysis. *International Journal of Applied Earth Observation and Geoinformation*, *44*, 205–216. https://doi.org/10.1016/J.JAG.2015.09.010

Hamada, S., & Ohta, T. (2010). Seasonal variations in the cooling effect of urban green areas on surrounding urban areas. *Urban Forestry & Urban Greening*, *9*(1), 15–24. https://doi.org/10.1016/J.UFUG.2009.10.002

Hardin, P. J. (2000). Neural networks versus nonparametric neighbor-based classifiers for semisupervised classification of Landsat Thematic Mapper imagery. *Optical Engineering*, *39*(7), 1898. https://doi.org/10.1117/1.602574

Haylemariyam, M. B. (2018). Detection of Land Surface Temperature in Relation to Land Use Land Cover Change: Dire Dawa City, Ethiopia. *Journal of Remote Sensing & GIS*, *07*(03). https://doi.org/10.4172/2469-4134.1000245

Hereher, M. E. (2017). Effect of land use/cover change on land surface temperatures - The Nile Delta, Egypt. *Journal of African Earth Sciences*, *126*, 75–83. https://doi.org/10.1016/J.JAFREARSCI.2016.11.027

Herold, M., Couclelis, H., & Clarke, K. (2005). “The Role of Spatial Metrics in the Analysis and Modeling of Urban Land Use Change.” *Computers Environment and Urban Systems*, 369–399. https://doi.org/10.1016/j.compenvurbsys.2003.12.001

Herold, M., Liu, X., & Clarke, K. (2003). Spatial Metrics and Image Texture for Mapping Urban Land Use. *Photogrammetric Engineering and Remote Sensing*, *69*, 991–1001. https://doi.org/10.14358/PERS.69.9.991

Hester, E., & Bauman, K. (2013). Stream and Retention Pond Thermal Response to Heated Summer Runoff From Urban Impervious Surfaces1. *JAWRA Journal of the American Water Ldots*, *49*. https://doi.org/10.1111/jawr.12019

How Jin Aik, D., Ismail, M. H., & Muharam, F. M. (2020). Land Use/Land Cover Changes and the Relationship with Land Surface Temperature Using Landsat and MODIS Imageries in Cameron Highlands, Malaysia. In *Land* (Vol. 9, Issue 10). https://doi.org/10.3390/land9100372

Hulley, G. C., & Hook, S. J. (2009). Intercomparison of versions 4, 4.1 and 5 of the MODIS Land Surface Temperature and Emissivity products and validation with laboratory measurements of sand samples from the Namib desert, Namibia. *Remote*

Sensing of Environment, *113*(6), 1313–1318. https://doi.org/10.1016/J.RSE.2009.02.018

Isikdag, U., Zlatanova, S., & Underwood, J. (2011). An opportunity analysis on the future role of BIMs in urban data management. In *Urban and Regional Data Management: UDMS Annual 2011* (pp. 25–36).

Jat, M. K., Garg, P. K., & Khare, D. (2008). Monitoring and modelling of urban sprawl using remote sensing and GIS techniques. *International Journal of Applied Earth Observation and Geoinformation*, *10*(1), 26–43. https://doi.org/10.1016/J.JAG.2007.04.002

Jeevalakshmi, D., Narayana Reddy, S., & Manikiam, B. (2017). Land surface temperature retrieval from LANDSAT data using emissivity estimation. *International Journal of Applied Engineering Research*, *12*(20), 9679–9687.

Jimenez-Munoz, J.-C., Cristóbal Rosselló, J., Sobrino, J., Sòria Barres, G., Ninyerola, M., & Pons, X. (2009). Revision of the Single-Channel Algorithm for Land Surface Temperature Retrieval From Landsat Thermal-Infrared Data. *Geoscience and Remote Sensing, IEEE Transactions On*, *47*, 339–349. https://doi.org/10.1109/TGRS.2008.2007125

Jiménez-Munoz, J. C., & Sobrino, J. A. (2003). A generalized single-channel method for retrieving land surface temperature from remote sensing data. *Journal of Geophysical Research: Atmospheres*, *108*(22). https://doi.org/10.1029/2003jd003480

Jiménez-Muñoz, J. C., & Sobrino, J. A. (2010). A single-channel algorithm for land-surface temperature retrieval from ASTER data. *IEEE Geoscience and Remote Sensing Letters*, *7*(1), 176–179. https://doi.org/10.1109/LGRS.2009.2029534

Jin, M., Li, J., Wang, C., & Shang, R. (2015). A Practical Split-Window Algorithm for Retrieving Land Surface Temperature from Landsat-8 Data and a Case Study of an Urban Area in China. In *Remote Sensing* (Vol. 7, Issue 4, pp. 4371–4390). https://doi.org/10.3390/rs70404371

Kabsch, E., Olesen, F., & Prata, F. (2008). Initial results of the land surface temperature (LST) validation with the Evora, Portugal ground-truth station measurements. *International Journal of Remote Sensing - INT J REMOTE SENS*, *29*, 5329–5345. https://doi.org/10.1080/01431160802036326

Kaur, A. S. S. (2015). Reproduction of Remote Sensed Images Using Artificial Neural Network. *International Journal of Science and Research (IJSR)*, *4*(6), 3042–3047. https://www.ijsr.net/archive/v4i6/SUB156194.pdf

Keno, B., Chen, N., Xiang, Z., & Niyogi, D. (2020). Spatial Configuration and Extent Explains the Urban Heat Mitigation Potential due to Green Spaces: Analysis over Addis Ababa, Ethiopia. *Remote Sensing*, *12*, 2876. https://doi.org/10.3390/rs12182876

Kidanewald, K. (2018). *URBAN LAND USE LAND COVER CHANGE AND ITS EFFECTS ON LAND SURFACE TEMPERATURE : THE CASE OF YEKA , BOLE AND AKAKI-KALITY SUB CITIES*.

Kuemmerle, T., Müller, D., Griffiths, P., & Rusu, M. (2009). Land use change in Southern

Romania after the collapse of socialism. *Regional Environmental Change*, *9*(1), 1–12. https://doi.org/10.1007/s10113-008-0050-z

Kullo, E. D., Forkuo, E. K., Biney, E., Harris, E., & Quaye-Ballard, J. A. (2021). The impact of land use and land cover changes on socioeconomic factors and livelihood in the Atwima Nwabiagya district of the Ashanti region, Ghana. *Environmental Challenges*, *5*(May), 100226. https://doi.org/10.1016/j.envc.2021.100226

Kumar, D., & Shekhar, S. (2015). Statistical analysis of land surface temperature–vegetation indexes relationship through thermal remote sensing. *Ecotoxicology and Environmental Safety*, *121*, 39–44. https://doi.org/10.1016/J.ECOENV.2015.07.004

Landsat 7 Data Users Handbook. (2019).

Latif, M. S. (2014). Land Surface Temperature Retrival of Landsat-8 Data Using Split Window Algorithm- A Case Study of Ranchi District. *Internal Journal of Engineering Development and Research*, *2*(4), 3840–3849.

Levermore, G., Parkinson, J., Lee, K., Laycock, P., & Lindley, S. (2018). The increasing trend of the urban heat island intensity. *Urban Climate*, *24*, 360–368. https://doi.org/10.1016/J.UCLIM.2017.02.004

Li, F., Jackson, T. J., Kustas, W. P., Schmugge, T. J., French, A. N., Cosh, M. H., & Bindlish, R. (2004). Deriving land surface temperature from Landsat 5 and 7 during SMEX02/SMACEX. *Remote Sensing of Environment*, *92*(4), 521–534. https://doi.org/10.1016/J.RSE.2004.02.018

Li, H., Meier, F., Lee, X., Chakraborty, T., Liu, J., Schaap, M., & Sodoudi, S. (2018). Interaction between urban heat island and urban pollution island during summer in Berlin. *Science of The Total Environment*, *636*, 818–828. https://doi.org/10.1016/J.SCITOTENV.2018.04.254

Li, X., Zhou, • Weiqi, Ouyang, Z., Xu, W., & Zheng, H. (2012). *Spatial pattern of greenspace affects land surface temperature: evidence from the heavily urbanized Beijing metropolitan area, China*. https://doi.org/10.1007/s10980-012-9731-6

Li, X., Zhou, W., & Ouyang, Z. (2013). Relationship between land surface temperature and spatial pattern of greenspace: What are the effects of spatial resolution? *Landscape and Urban Planning*, *114*, 1–8. https://doi.org/10.1016/J.LANDURBPLAN.2013.02.005

Li, X., Zhou, Y., Yu, S., Jia, G., Li, H., & Li, W. (2019). Urban heat island impacts on building energy consumption: A review of approaches and findings. *Energy*, *174*, 407–419. https://doi.org/10.1016/J.ENERGY.2019.02.183

Li, Z. L., & Duan, S. B. (2018). Land Surface Temperature. *Comprehensive Remote Sensing*, *1–9*, 264–283. https://doi.org/10.1016/B978-0-12-409548-9.10375-6

Liao, W., Liu, X., Wang, D., & Sheng, Y. (2017). The Impact of Energy Consumption on the Surface Urban Heat Island in China’s 32 Major Cities. *Remote Sensing*, *9*, 250. https://doi.org/10.3390/rs9030250

Liu, J., Heiskanen, J., Betemariam, E., & Pellikka, P. (2015). Seasonal variation of land cover classification accuracy of Landsat 8 images in Burkina Faso. *ISPRS -*